University of Genova
Doctoral School in Science and Technology of Chemistry and Materials
(*XXXIII cycle*)

# Development of novel formulations based on biopolymers

**A dissertation for doctor's degree**

Kun Li

**Tutor: Orietta monticelli**

**Co-tutor: Alberto Fina**

# Table of contents

# List of figures

# List of tables

# Abstract

Biopolymers, generally prepared from renewable sources, have attracted increasing attention due to their unique properties, such as nontoxicity, biodegradability and biocompatibility. Indeed, the above materials have been widely applied in the biomedical field, in the development of electronic devices as well as in the food packaging. Two of the most extensively studied and exploited biopolymers are poly(lactic acid) (PLA) and polycaprolactone (PCL), which have been the objects of the present work. Despite the significant interest in these polymers, for large-scale exploitation of both PLA and PCL, it is necessary to take into account some specific issues concerning their properties. In this regards, it is relevant to underline that the methods, which can be applied for improving their characteristics or those used for disclosing new features, have to take into account the economic impact and the "bio" nature of the material, which should be maintained in the final formulation. In particular, in the case of PLA, one of the major issues, which reduces its exploitation in durable applications, is its low hydrolytic stability, compared with other similar materials. Moreover, in the applications requiring high gas barrier, the use of PLA is critical and needs a further reduction of its gas permeability. Furthermore, concerning exploitations, where electrical and thermal conductivity is demanded, the insulating nature of the above biopolymers, requires the applications of proper conductive fillers. As such, the main aim of the thesis work has been the improvement of the two biopolymer properties, developing novel formulations, whose design has taken into account all the mentioned issues.

In the case of PLA, the barrier properties, the resistance to hydrolytic degradation as well as the antistatic features have been improved by modifying the material surface by means of the application of methods based on the chemical grafting or the Layer by Layer deposition and on the use of proper fillers, such as Polyhedral Oligomeric Silsesquioxane (POSS) and graphene oxide (GO). In addition, formulations capable of imparting thermal conductivity to PCL have been studied, combining the biopolymer with graphite nanoplatelets (GNP).

# Outline of the thesis

Chapter 1 is dedicated to the description of biopolymers and biopolymer-based composites. In particular, classification, advantages and applications of biopolymers and their composites are reported. Moreover, the synthesis, properties, applications and modification of poly(lactic acid) (PLA) and polycaprolactone (PCL), which are the objects of this thesis, are emphatically introduced as well as the frequently used carbon-based nanofillers.

Chapter 2 is focused on a novel method to enhance polylactide hydrolysis resistance based on polyhedral oligomeric silsesquioxane (POSS) grafting on the surface of poly(L-lactide) (PLLA) films. The occurrence of the reaction between an amino-POSS /POSS-$NH_2$) and PLLA films at mild conditions (40°C or 60°C) are verified by IR measurements. The stability of both neat PLLA film and POSS-$NH_2$-grafted films are tested by putting them in contact with water at 50 °C for several weeks. Indeed, the neat PLLA film are found to break into small pieces after 4 weeks contact with water while the POSS grafted PLLA films kept their relatively high integrity. This relevant improvement in hydrolysis resistance is believed to be caused by presence of super-hydrophobic POSS molecules on the surface of PLLA films, which acting as a barrier, protect PLLA films from contact with water directly, thus enhancing their hydrolysis resistance.

Chapter 3 describes the application of Layer-by-Layer (LbL) assembly method in modifying the surface properties of PLLA films. The positively charged chitosan (CH) and branched polyethylenimine (BPEI) solutions are used to couple with negatively charged graphite oxide (GO) to create bi-layers of GO on the surface of PLLA films, following a very simple dipping, washing and drying procedure. The growth of the GO on PLLA surface is simulated using Si wafers as substrates and it is monitored by IR. BPEI is found to have much better combination result with GO compared to CH due to the dependence of ionization degree of GO carboxyl groups on pH. The $O_2$ permeability of PLLA LbL-treated films is found to decrease compared to neat PLLA films. The reduction of GO deposited on the PLLA films is performed by using

sodium borohydride ($NaBH_4$), and the resulted systems are found to have promising antistatic properties.

Chapter 4 is focused on the preparation of nanopapers based on PCL and graphite nanoplatelets (GNP) with the aim at achieving both high thermal conductivity and mechanical properties. The PCL-GNP nanopapers are prepared by simply solution blending, sonication, filtration, drying and pressing. Nanopapers with different PCL content (from ca.5 wt.% to 20 wt.%) are obtained by adjusting the initial ratio between PCL and GNP in the suspensions. The crystallization temperature of PCL when added in the GNP nanopapers is found to increase by ca. 20 ºC with respect to the neat polymer. Moreover, extra melting peaks at relatively high temperatures are found for all the composite nanopapers, which to the best our knowledge were never reported in the literatures. It is relevant to underline that some of the peaks at high temperatures are found to be related to the structuring of PCL chains in the galleries of GNP. Concerning the thermal conductivities of the nanopapers, the insertion of PCL chains leads to a slight decrease of thermal diffusivity. Nevertheless, the nanopapers prepared by the combination of GNP and limited amount of PCL, can maintain high thermal conductivity (ca. 160 $Wm^{-1}K^{-1}$ for nanopaper with ca. 8wt.% of PCL). Moreover, the prepared systems show good mechanical properties, as evidenced by the DMTA temperature sweep measurements.

# 1 State of art

## 1.1 Biopolymers

Polymers are a class of “giant” molecules with long chains that are consisted of discrete building blocks linked together. The simple building blocks are usually called monomers, while for building blocks with complicate structures are sometimes referred as “repeat units”. Since the first synthetic plastic was produced by John Wesley Hyatt in 1869, petroleum-based polymer plastics have flourished due to their light weight, easy processing, excellent strength, versatility, durability, and low cost.[1] Over the past decades, polymer materials have become an indispensable part of human life, while bringing very large convenience to human beings, the fast development of petroleum-based products also caused serious pollution to the environment, which in turn affected the health of human and the survival of other species.[2] According to the latest report, approximately 350 million tons of synthetic polymers are produced over the world every year and the demand is further increasing, and most of these plastics had been abandoned after being used, which resulted in a large amount of plastic waste accumulation, causing non-negligible damage on environment and threatening the safety of biosphere.[3] In addition, the increasing demand of petroleum-based polymer materials are exacerbating the depletion of petroleum resources, it is not hard to imagine that the production of petroleum-based polymers will be hindered by limited resources and rising raw material prices in the near future.

The rising concern about escalating price of fossil fuel and their impact on environment, as well as the limited applications of fossil-based polymers have made it necessary to search for substitutes for petrochemical plastics. The development of more sustainable processes for a greener and bio-based future is the current global goal, which has led to great interests in researching in bio-based polymers, which are the most promising alternatives of fossil fuels. Biopolymers are usually referred as polymers that developed from living beings, and the name indicates that they are biodegradable polymers. The development of biopolymer-based

materials from renewable resources is an very active research area that is attracting increasing scientific and industrial attentions.[4, 5]

The first generation of bio-based polymers were dependent on the synthesis of the building blocks (monomers), including lignocellulosic biomass (starch and cellulose), fatty acids, and organic waste. The term “Biodegradable” describes the functionality of a polymer, “biodegradability”. Polymers with biodegradability can degrade under the action of several microorganisms such as molds, fungi, and bacteria within a specific period and will not cause any damage to environment. The Japan Bioplastics Association (JBPA) defined the term “biodegradability” as the characteristic of a material that can be microbiologically degraded to the final products of carbon dioxide and water without harming the environment, which can be recycled in the nature. The biodegradability of plastics can be determined by following the ISO methods and only the plastics that meet all the rigorous criteria (e.g., contents of heavy metals, safe intermediate reaction products) can be classified as green plastics.

### 1.1.1 Classification of biopolymers

By considering the source of raw materials and the biodegradability of synthetic products, biopolymers can be divided into three categories, as presented below:

Type-A: biopolymers made from renewable raw materials (also only partially from renewable), and being biodegradable;

Type-B: biopolymers made from fossil fuels, and being biodegradable;

Type-C: biopolymers made from renewable raw materials (also only partially from renewable), and not being biodegradable.

The biopolymers of type-A can be produced under biological systems or chemically synthesized from bio-based raw materials (e.g., corn, sugar, starch, etc.). Biodegradable bio-based biopolymers include synthetic polymers from renewable resources such as poly (lactic acid) (PLA), as well as biopolymers produced by microorganisms, such as PHAs, and also natural occurring biopolymers, like starch and proteins. As one kind of the most promising

biopolymers, biodegradable biopolymers made from renewable raw materials are attracting global concern and will be the main direction of the polymer development in the future.

The biopolymers of type-B are produced from fossil fuel and being biodegradable, such as synthetic aliphatic polyesters made from crude oil or natural gas, and are certified biodegradable and compostable. PCL, poly (butylene succinate) (PBS), and certain "aliphatic–aromatic" co-polyesters are at least partly fossil fuel-based polymers.

The biopolymers of type-C can be produced from biomass or renewable resources and are non-biodegradable. Non-biodegradable bio-based biopolymers include (1) synthetic polymers from renewable resources such as specific polyamides from castor oil (polyamide 11), specific polyesters based on bio-propane diol, bio-polyethylene (bio-LDPE, bio-HDPE), bio-polypropylene (bio-PP), or bio-poly (vinyl chloride) (bio-PVC) based on bioethanol, etc.; (2) natural occurring biopolymers such as natural rubber or amber. A detailed classification of the most common biopolymers is shown in Table 1-1.

Table 1-1 Classification of the most common biopolymers.

| | **Biodegradable** | **Non-biodegradable** |
|---|---|---|
| **Bio-based** | CA, CAB, CAP, CN, P3HB, PHBHV, PLA, starch, chitosan | PE (LDPE), PA11, PA12, PET, PTT |
| **Partially bio-based** | PBS, PBAT, PLA blends, starch blends | PBT, PET, PTT, PVC, SBR, ABS, PU, epoxy resin |
| **Fossil fuel-based** | PBS, PBSA, PBSL, PBST, PCL, PGA, PTMAT, PVOH | PE (LDPE, HDPE), PP, PS, PVC, ABS, PBT, PET, PS, PA6, PA66, PU, epoxy resin, synthetic rubber |

*ABS, acrylonitrile-butadiene-styrene; CA, cellulose acetate; CAB, cellulose acetate butyrate; CAP, cellulose acetate propionate; CN, cellulose nitrate; HDPE, high-density polyethylene; LDPE, low-density polyethylene; P3HB, poly(3-hydroxybutyrate); PA11, aminoundecanoic acid-derived polyamide; PA12, laurolactam-derived polyamide; PA6, polyamide 6; PA66, polyamide 66; PBAT, poly(butylene adipate-coterephthalate); PBS, poly(butylene succinate); PBSA, poly(butylene succinate-co-adipate); PBSL, poly(butylene succinate-co-lactide); PBST, poly(butylene succinate-co-terephthalate); PBT, poly(butylene terephthalate); PCL, poly(ε-caprolactone); PE, polyethylene; PET, poly(ethylene terephthalate); PGA, poly(glycolic acid); PHBHV, poly(3-*

*hydroxybutyrate-co-3-hydroxyvalerate); PLA, poly(lactic acid); PP, polypropylene; PS, polystyrene; PTMAT, poly(methylene adipate-co-terephthalate); PTT, poly(trimethylene terephthalate); PU, polyurethane; PVC, poly(vinyl chloride); PVOH, poly(vinyl alcohol); SBR, styrene-butadiene rubber.*

### 1.1.2 The advantages of biopolymers

Polymer products have become widely used materials in everyday life due to their immense advantages over metals, such as low cost of production, lightweight nature, easy processing, corrosion resistance, and high impact strength, etc. Being a special classification of polymers, apart from all the advantages belonging to traditional ones, biopolymers possess many unique properties, which the traditional polymers do not have.

In contrast to fossil-based polymers that rely on the fossil resources, which are not being newly formed at any significant rate, biopolymers are mainly produced by using renewable biomass resources, such as vegetable oil, cornstarch, pea starch, algae, and so on. The stocks of these biomass resources in the nature are very huge and mainly come from plants, animals and microorganisms, being reproducible artificially from biological starting materials or under the nature procedures of biological system. The huge storage capacity and their reproducibility make biomass resources great prospect for the production of biopolymers, thus cut down the dependence on fossil resources.

Apart from limitation of the resources, the biodegradable character of biopolymers is another great advantage with respect to traditional fossil-based polymers, which can help to decrease the environmental pollution problems from synthetic polymer plastics. As previously mentioned, the increasing demand of plastic products and their extremely stable chemical properties have led to a huge accumulation of plastic wastes in the nature, causing a non-negligible impact on the environment and is also threatening the survival of many organisms, and even leading to their destruction.[6-9] Plastic wastes from biopolymers can be biodegraded by aerobic degradation or anaerobic digestion in the nature without causing any harms to the environment.[10] In the presence of microorganisms, such as bacteria and fungi, the biodegradation process starts from the broken of the polymer chains. During the aerobic

biodegradation, the biopolymer wastes can be decomposed into carbon dioxide and water and then will be cyclic utilization in biosphere. While during the anaerobic biodegradation, water and methane will be the degradation products,[10] which is also recyclable in the nature and does no harm to the environment and other creatures in the biosphere.

A third advantage of biopolymers with respect to fossil-based polymers is the non-toxicity and their biocompatibility with human body, which is already widely used in the fields of drug delivery [11-13] and tissue engineering,[14-16] as well as food packaging.[17-19]

### 1.1.3 The application of biopolymers

In the area of biomedical applications, such as those in tissue engineering,[14-16, 20] pharmaceutical carriers and medical devices,[11-13, 21] biopolymer materials have been widely used. Gelatin, a common biopolymer, was widely applied in medicine for dressing wounds.[22-24] Porous gelatin scaffolds and films were produced combined with solvents or gases, which enable the scaffolds and films to hold drugs or nutrients to the wound that needs healing.[25] Electro-spun PLGA-based scaffolds had been applied extensively in biomedical engineering, such as tissue engineering and drug delivery systems.[26]

In the field of packaging, biopolymers are used as food packaging materials, and encapsulation matrices for functional foods. Starch and PLA are potentially the most attractive types of biodegradable materials due to the balance of their properties and the fact that they are now commercially available.[27] Chitosan has shown great potential as an antimicrobial packaging agent to preserve food against a wide variety of microorganisms.[28-30] Incorporating antimicrobial compounds into edible films or coatings provides a novel way to improve the safety and shelf life of ready-to-eat foods. To be a versatile biopolymer, chitosan, can also be used in water treatment processes as flocculant and will biodegrade in the environment over periods of weeks or months.[31] Amylose, when mixed with plasticizers have excellent potential in forming thin films for various food and packaging applications.[32] Lysozyme is one of the most frequently used antimicrobial enzymes in packaging materials, since it is a naturally

occurring enzyme.[33, 34]

## 1.2 Poly (lactic acid) (PLA)

Poly (lactic acid) or polylactide known as PLA is one of the most used biopolymers in recent years. PLA is produced either by ring-opening polymerization of lactides or by condensation polymerization of the lactic acid monomers, which can be obtained from the fermentation of corn, beet-sugar, cane sugar etc.[35-37] PLA has been of significant research interest due to its biocompatibility and biodegradability that leading to applications in medical science and biotechnology. It possesses desirable characteristics include the decomposition into naturally occurring metabolites via hydrolysis or enzymatic processes.[38] Over the past decades, the degradation of PLA materials has been studied in the field of practical medical applications such as drug delivery systems, sutures, and surgical implants.[39-41] PLA has been studied for implantations including architecturally fabricated stents, which could replace conventional metallic stents. Compared to the conventional metallic or non-biodegradable polymers, the huge advantage of PLA-based biopolymers is the ease removal by the body system itself and the retention of shape during time.

Due to its biodegradation ability, PLA presents a major advantage in entering in the natural cycle, implying its return to the biomass, which is explored to be an alternative solution to solve the ecological problem of plastic waste accumulation, with a major focus on packaging.[42-45] PLA can be used to produce various commercial products through different production processes. These products made of PLA, after being discarded, could be completely biodegradable and can be converted into carbon dioxide and water, which can be recycled by the biosphere without leading any damage to the environment. The sustainable life cycle of PLA-based products in nature is shown in Figure 1.1.

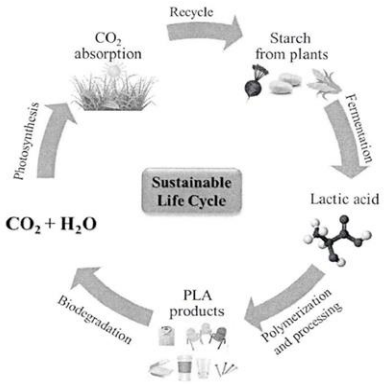


Figure 1.1 Sustainable life cycle of PLA in nature.[38]

Furthermore, PLA has been proposed as a renewable and degradable plastic for uses in service ware, waste-composting bags, mulch films, controlled release matrices for fertilizers, pesticides, and herbicides.[46] All these attributes of PLA lead to the great development of green packaging materials, which is currently the focus of research and demand from common people to environmentalists throughout the world.

### 1.2.1 Synthesis and classification of PLA

PLA is a biodegradable thermoplastic derived from lactic acid or lactide. Both polylactide and poly(lactic acid) with the abbreviation of PLA are the same chemical products; only they differ from each other in means of production monomers. Because of chirality, lactic acid (LA) has two optical isomers: L-lactic acid and D-lactic acid. These two different optical isomers correspond to three different isomers of the cyclic dimers, namely L-lactide, D-lactide, and meso-lactide respectively, as shown in Figure 1.2, and the D-, L- or meso-form is optically inactive. L-lactic acid is the natural and biologically important isomer, and D-form can be produced either by microorganisms or by racemization. Lactic acid was primarily found in the fermented milk products, such as yogurt, kefir, and some cottage cheeses. Lactic acid is commercially manufactured by bacterial fermentation process using various substrates like corn, potato, beet, cane sugar, dairy products and even from agricultural waste materials.[47] Fermentative production of LA can offer great advantage in producing the optically pure L- or D-LA. The optical purity of LA is an essential factor that can determine the physical properties of PLA. Polymers with high L-type LA can be used to produce crystalline product

whereas the high D-type ( > 15%) will result in an amorphous product.

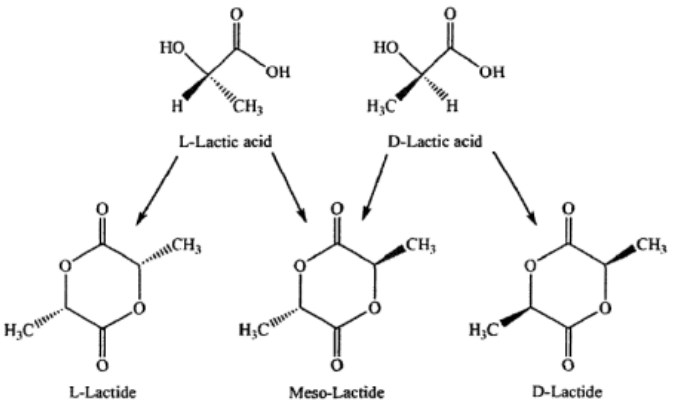


Figure 1.2 Optical isomers of lactic acid and lactide.

Poly(lactic acid) can be synthesized by using reaction starting from lactic acid (Figure 1.3a) or by ring opening polymerization of lactide monomers (Figure 1.3b). The major limitation of the direct polycondensation reaction is the low molecular weight of the produced products. The generated water during the polymerization process has to be removed continuously, and rapidly equilibrium occurs between polymerization and de-polymerization reaction. In addition, long reaction time and high temperature are needed for the direct polymerization of lactic acid. To overcome the limitation, lactic acid is initially oligomerized and catalytically dimerized to produce the cyclic lactide monomers. The high molecular weight polylactide can be produced from lactide monomers by ring opening polymerization.

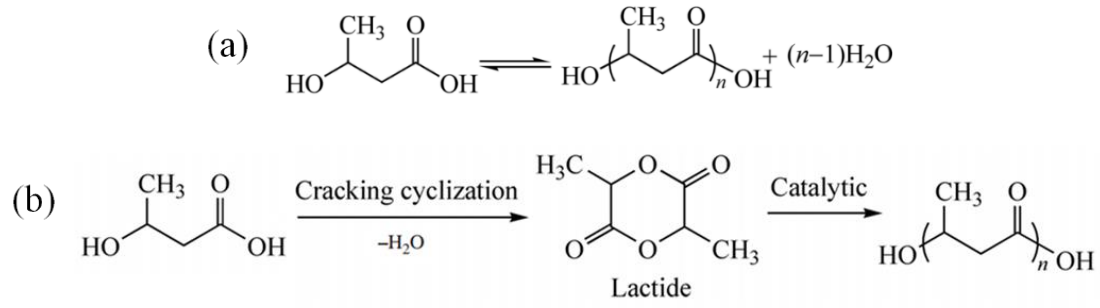


Figure 1.3 Synthetic PLA by direct polycondensation of lactic acid (a) and by ring opening polymerization of lactide monomers (b).

The stereo-chemical composition of the lactide monomer stream can determine the stereo-chemical composition of the resulting polymer since bonds to the chiral carbons will not be

broken in polymerization process. Poly(L-lactide) can be polymerized from only L-lactide and the same situation for poly(D-lactide). However, the polymerization of the mixture of 50% of D-lactide and 50% of L- lactide will produces poly (DL-lactide), which is an amorphous polymer. In addition, PLA can be produced with varying fractions of L- and D-lactide to obtain products with different crystallization properties. To get PLA products with proper mechanical properties, the unreacted lactide monomers need to be removed from the polymeric matrix after the polymerization process, as they can act as plasticizer leading to poor mechanical strength and thermal stability of PLA, thus decreasing shelf life of the products made of PLA.

### 1.2.2 Properties of PLA

As previously mentioned, because of the molecule chirality of lactic acid, PLA exists in three forms: poly (L-lactic acid), poly (D-lactic acid) and poly (meso-lactic acid). It is already well reported that the properties of PLA depend largely on the ratio and the distribution of the two isomers and the molecular weight of the final product. The glass transition temperature ($T_g$) of conventional PLA is about 50 to 70 °C, and the melting temperature ($T_m$) is between 170-190 °C. The $T_g$ and $T_m$ of PLA decrease with increasing content of D-lactic acid in the polymer. The general properties of the conventional PLA are shown in Table 1.1. PLA with high molecular weight is a thermoplastic with high rigidity, colorless and shiny appearance, possessing similar properties as polystyrene (PS). Amorphous PLA is soluble in most of the organic solvents, such as THF, chloroform, benzene, and dichloromethane; but the crystalline PLA can only be dissolved in some of the organic solvents (chloroform, benzene) at high temperature.

Table 1-2 The general properties of conventional PLA.[45, 48]

| **Properties** | **PLA** | **Properties** | **PLA** |
|---|---|---|---|
| Molecule weight | 10-30 ($\times 10^4$) | Crystallinity (%) | 10-40 |
| Glass transition T (°C) | 50-61 | Melting point (°C) | 130-215 |
| Impact strength (J/m) | 16-26 | Vicat softening T (°C) | 52-165 |
| Bending strength (MPa) | 88-106 | Distortion T (°C) | 50-55 |
| Young modulus (MPa) | 3750-3900 | Tensile strength (MPa) | 44-59 |
| Elongation at break (%) | 4-10 | Melt index (10 min)(g/min) | 0.2-2.0 |

Nature derived lactides are mostly in L-form and exhibit crystalline behavior. The crystallization behavior of polylactides depends on its thermal history,[49] amount and type of additives,[50] and stereo sequence distribution.[51] In addition, crystallization also depends upon optical purity. It was reported that at least 72% threshold optical purity in composition is required to obtain significant crystallinity of polylactides,[51, 52] otherwise, when the content of D-lactic acid is higher than 30%, PLA exists as an amorphous polymer.[53-55] Depending on the optical isomers of lactic acid or lactide, PLA can form three types of crystals with different helical conformations, namely α, β and γ-form.[56] Within all of them, α-form is the most stable crystal and can be produced by melting crystallization, cooling crystallization and solution crystallization, with a higher melting temperature, which is around 185 °C.[57] The β-form crystal, which is less stable, can be formed from the transition of α-form under high tensile stress, with a slightly lower melting point of 175 °C.[56] The γ-form crystal can be obtained by epitaxial growth on the hexamethylbenzene substrate.[57, 58] The crystallization rate and crystallinity of PLA are limited by its high glass transition temperature, and the crystallinity can have a significant effect on the properties of products made of PLA, such as melting temperature, mechanical strength, barrier properties, and degradation property.[59] The mechanical properties of PLA can be determined by the molecular weight, the higher the molecular weight, the greater the mechanical strength of PLA. Studies have shown that when the average molecular weight of PLA doubles, the tensile modulus triples, and the tensile strength increases several times.[59] Even the strong tensile strength and Young's modulus make PLA comparable with traditional plastics, such as polypropylene (PP), polyethylene (PE), and polystyrene (PS), the poor toughness and the relatively low distortion temperature are limiting its development and application in every field. Table 1.2 gives a simple comparison of the general properties between PLA and fossil-based traditional polymers.

Table 1-3 Comparison of general properties between PLA and fossil-based polymers.

| Sample | PLA | PP | PS | PET |
|---|---|---|---|---|
| Density (g/cm$^3$) | 1.26 | 0.91 | 1.05 | 1.40 |
| Tensile strength (MPa) | 53 | 31 | 45 | 54 |
| Tensile modulus (MPa) | 3.4 | 0.9 | 2.9 | 2.8 |
| Elongation at break (%) | 6 | 120 | 2.9 | 130 |
| Glass transition T (°C) | 55 | -10 | 105 | 75 |
| Distortion T (°C) | 55 | 95 | 75 | 67 |

The rich ester groups of PLA molecular chain make it easy to hydrolyze, thermal degradation can easily occur especially when PLA was processed at high temperature and humidity. Being a biodegradable polymer, the degradation rate of PLA is very slow. The degradation cycle of PLA-based products usually takes several months to several years. In the application of some disposable products area, PLA, not being able to degrade rapidly after being discarded, results in some kind of garbage accumulation. Therefore, the recycling of PLA is also very important and a large amount of research has focused on the recycling of PLA materials, of which thermo-mechanical recycling is widely studied to be a feasible recycling method for it.[60]

### 1.2.3 Applications of PLA

The interesting features of PLA, such as easy processing, good mechanical properties, transparency, biodegradability, and good biocompatibility, are making it available in a wide range of fields. While, at the beginning, when the high molecular weight PLA was firstly investigated and produced, its applications were deeply limited by the high cost of production, and it was mostly used in the biomedical field.[39-41, 61] Nowadays, with further improvement of its synthetic conditions, the production cost was largely decreased, which promoted greatly the investigation and application of PLA.

The good biocompatibility and biodegradability, as well as excellent physical and mechanical properties of PLA have made it be widely used in the field of biomedicine, mainly in non-removable surgical sutures, sustained release of drugs, orthopedic materials, infusion tool

products, etc.[62] The good biocompatibility of PLA with the human body makes it a promising material as surgical suture into human body, which can be degraded by itself after the wounds are healed. The unnecessary removal of PLA-based surgical suture can avoid the secondary injury to the patients during removal. In order to reduce or avoid damage to the organs of other parts of the body during the medical process, it is necessary to use a carrier that can regulate the precise delivery of the drug. The good biodegradability and excellent biocompatibility of PLA have been widely used in the process of drug sustained release treatment.[63, 64]

In the field of food packaging, in order to ensure the safety of the foods, the selected packaging materials should have good barrier properties, excellent optical characteristics, and being easily molded properties. In addition, as food packaging materials, they must also have good anti-migration, anti-residue characteristics, chemical stability and good heat resistance. The application of PLA in the packaging field has attracted widespread attention, not only because PLA is derived from renewable plants and being biodegradable, but also because the thermal and mechanical properties of PLA products can be regulated by adjusting the processing parameters or by adding different additives according to demand. Nowadays, PLA is mainly used in food packaging, such as the packaging of vegetables, fruits, disposable tableware, etc.[65] After being discarded, these packaging products will be naturally degraded in about 6 months in the soil, which can help avoid the accumulation of white pollutions.

Based on the micro-nano structure and super-hydrophilic construction of PLA surface, PLA microporous membrane can be used for oil-water separation, achieving efficient separation of oil-water mixture.[66-68] Meanwhile, the surface functionalized PLA microporous membrane also have anti-pollution and antibacterial properties.[67] Gu et al. used non-woven fabric of PLA to be the raw material, and functionally modify the fiber surface with dopamine, and then loaded with micron-sized polystyrene (PS) microspheres and silica nanoparticles to build an ultra-wet and multi-stage oil-water separation composites with high efficiency and high reusability.[68] The construction of environment-friendly PLA oil-water separation materials

provides an effective solution to reduce seawater pollution caused by crude oil leakage. At the same time, the use of biodegradable oil-water separation materials reduces the secondary pollution on the environment after the discard of materials, and maintains the sustainable development of the environment.

In order to alleviate the pressure on the use of petroleum energy and the intensification of the greenhouse effect, many companies have applied plastic products made of PLA materials to the electronics field to make laptop computer materials, mobile phone case materials, DVD case materials and so on. These products emit only a small amount of carbon dioxide during use and after being discarded, which is about 15% less than petroleum-based plastics. Comparative mechanical properties of PLA-based products can be achieved by either preparing PLA related composites or by adjusting the processing parameters.[69] the Nippon Electric Company (NEC) has developed a PLA plastic that can be widely used in most electronic products, this PLA product has good flame retardance and can have excellent fire prevention effects without the addition of phosphorus-based or halogen flame retardants, which has attracted extensive attention from companies of electronics field.[70]

### 1.2.4 Modification of PLA

Concerning the specific properties of PLA, it is worth mentioning that its weak toughness, low impact strength and relatively small elongation at break are limiting its applications in some fields, where toughness and impact resistance are critical. Meanwhile, the low melting point of PLA makes it unsuitable for high temperature applications. PLA has a higher permeability than other plastics, which makes moisture and oxygen go through more easily than other materials, resulting in a faster food spoilage process. Thus, PLA is not recommended for long-term food storage applications. To overcome the weakness of low toughness of PLA, different strategies had been used, such as copolymerization, plasticization, compounding and blending.[48] The impact strength has been improved by adding various fillers, which can also help decrease the permeability and increase the lifetime of PLA-based

products.[71-74] Surface functionalization of PLA film is another frequently used method to improve the barrier property of this polymer.[27, 75-78] Here, we mainly focus on the modification of PLA by using graphene-related materials (GRM) and the surface modification of PLA-based films.

As one of the most promising nanomaterials, graphene is a single atomic layer of $sp^2$ carbon atoms bonded together in hexagonal lattices.[79] It has attracted attention of the worldwide scientific community since was ever discovered owing to its outstanding electrical, thermal and mechanical properties.[80] Unfortunately, the industrial scale production of graphene still remains very challenging, even different kinds of producing techniques had been developed.[81-83] Graphene-related materials, including single layer graphene, few layered graphene (FLG), graphite nanoplatelets (GNP), graphene oxide (GO) and reduced graphene oxide (rGO), are multifunctional nanostructured building blocks with extraordinary properties, which are typically used in the field of polymer nanocomposites to improve the mechanical, thermal and electrical properties of the polymer matrix.[84-90] In recent years, PLA/GRM composites have been prepared by dispersing graphene-based nanosheets in a PLA matrix to improve the performance or give new properties to polymer matrix.. The mechanical and thermal properties as well as the crystallization behavior of PLA can be significantly improved by adding GRM into PLA matrix.[91] The generally used preparation methods for PLA/GRM composites includes solution intercalation, in-situ polymerization and melting blending method.[92]

In the case of the solution intercalation, polymers are dissolved into organic solvents to prepare solutions, in which the GRM nanoparticles can be well dispersed to get suspensions with combined polymer chains and nanoparticles. The polymer composites were finally obtained after the solvents were volatilized or removed by filtration. The composite materials prepared by solution intercalation usually have high quality due to the sufficient interaction between polymer chains and nanoparticles in the solvent. Li et al.[93] performed a comparative crystallization study on two types of PLA composites with carbon nanotubes (CNT) and

graphene nanosheets (GNS) prepared by solution coagulation. They found that both CNT and GNS could serve as heterogeneous nucleation agents, shortening the induction period of crystallization and accelerating the crystallization of PLA.

The in-situ polymerization approach is a method of preparing PLA/GRM composite materials by polymerizing the mixed GRM particles and the liquid phase monomers under the action of initiators. Li and coworkers dispersed GO in lactic acid monomers and prepared PLA/GO composites by in-situ polymerization.[93] The mechanical properties and thermal stability of the PLA/GO composites were improved with respect to the neat PLA. SEM micrographs of the PLA/GO composites showed agglomerations of GO in the PLA matrix, which was believed to be caused by the Van der Waals interaction among GO as well as the poor compatibility of GO with the polymer matrix. [93]

Melt blending is a method in which polymers and GNPs are melt blended under the action of thermal and shear stress by using processing techniques such as extrusion and injection molding. Villmow et al.[94] reported the influence of melt-mixing conditions on the dispersion of MWCNT within PLA matrix with the aim to develop a guideline for plastic manufacturers. The key-challenge was to achieve a suitable distribution and dispersion of MWCNT to ensure low percolation thresholds, combined with high mechanical performance. Wu et al.[95] investigated the effect of various functionalized MWCNT on the rheology and thermal stability of PLA nanocomposites, prepared by melt compounding. Carboxylic- and hydroxyl-functionalized as well as purified MWCNT were used as models. The above study demonstrated that the best dispersion level of MWCNT within the PLA matrix was achieved with carboxylic-functionalized MWCNT, as highlighted by rheological measurements and TEM analyses. The melt blending method is currently the most commonly used preparation process for PLA blending and modification, due to the advantages of its simple processing technology. However, in the process of melt blending, the poor mobility of PLA macromolecular chains together with its high viscosity, make difficult for GRM particles to be evenly dispersed in the PLA matrix, resulting in poor modification effects.

Apart from the mostly used modification methods mentioned above, which are mainly used to modify the bulk properties of PLA, chemically and physically surface modification is another strategy to change the surface properties of PLA films without affecting the bulk properties. Pellis et al.[96] investigated the potential for introduction of carboxylic and hydroxyl groups on surface of PLA films to improve loading ability with the chemotherapeutic drug doxorubicin via ionic interactions. They found that by tuning the extent of enzymatic hydrolysis on surface of PLA films, it is possible to tune the degree of surface hydrophilicity and roughness to PLA films. Due to the introduction of carboxylic and hydroxyl groups on PLA surface, the binding of the chemotherapeutic drug doxorubicin by electrostatic interactions was enhanced while the release of the chemotherapeutic drug doxorubicin was driven by electrostatic interactions.[96] In another work of the same group,[97] an enzymatic process for the grafting of carboxylic acids onto the surface of poly(L-lactic acid) (PLLA) films was developed using candida antarctica lipase B as a catalyst. Enzymatic hydrolysis of PLLA film, using Humicola insolens cutinase, was also reported. The grafting of hydroxyl and carboxylic groups on the surface of PLLA films resulted in a decrease of water contact angle from 74.6 to 33.1°. However, from the results of yield measurements, no significant difference was observed between functionalizing pre-hydrolyzed and non-pre-hydrolyzed films, which was believed to be caused by the rearrangement of the outer polymer chains in the hydrophobic reaction environment.[97] Guo et al.[98] introduced a two-step process to produce PLA films with an electroactive hydrophilic surface by covalent modification with aniline tetramer (AT), which was done firstly by the photo-grafting of acrylic acid and maleic anhydride onto PLA film, and subsequent coupling with conductive aniline AT. They reported that PLA films, after grafting AT, got an electrically conductive surface, and the conductivity increased with increasing AT content on the surface.[98] Different chemical modification strategies had been used to obtain various surface properties of PLA films, such as cell-adhesion properties,[99] wettability to water[100] and so on. The key aspect of the chemical modification of PLA surface is the reaction between the end functional groups of PLA chains

and the modifier, or the introduction of an intermediate molecule, which can react with both PLA and the modifier. Compared to chemical modification strategies, the physical modification of PLA surface has a much easier operation process, which mainly relies on the interaction between positive and negative charges. Layer-by-layer (LbL) assembly is one of the mostly used physical modification methods for PLA-based films, which has attracted extensive attentions in different application fields of PLA films.[101-106] The standard conventional method for LbL assembly on planar substrates is immersive assembly, whereby the substrate is sequentially immersed into polymer solutions for deposition, with rinsing steps between the deposition steps. Gong et al.[104] grafted chondroitin sulfate and collagen type I onto the surface of aminolyzed PLLA membranes and porous scaffolds by LbL assembly to enhance the cell–material interaction. According to the results of chondrocyte culture, they demonstrated that the cell attachment, viability, proliferation and morphology of the modified PLLA membranes were apparently improved in comparison with those of the untreated PLLA. Halász and coworkers produced LbL deposition of cellulose nanocrystals and chitosan onto PLA films and bottles to reduce the water vapor permeability and thus reduce the hydrolysis of PLA.[103] He et al.[105] prepared a LbL structure of PLA-PEI-GO by immersing PLA films into PEI solution and GO suspension alternately. It was found that the oxygen barrier properties was significantly improved while with unsatisfied water vapor barrier properties, which was believed to be caused by the hydrophilic functional groups of GO.

## 1.3 Polycaprolactone (PCL)

Polycaprolactone (PCL) is synthetic biodegradable polyester with good resistance to water, oil, solvent and chlorine, which can be produced from crude oil. Being one of the earliest synthesized polymers in the early 1930s, PCL has become commercially available following efforts to identify synthetic polymers that could be degraded by microorganisms. Attention was drawn to PCL and its copolymers owing to their numerous advantages over other

biopolymers in use, including the tailorable degradation kinetics, mechanical properties, ease of shaping and manufacture, and the controlled delivery of drugs. PCL is a hydrophobic, semi-crystalline polymer; having a glass transition temperature ($T_g$) of ca. − 60 °C and melting point ranging between 59 and 64 °C, enabling an easy formability process at relatively low temperatures. The number-average molecular weight of PCL samples may generally vary from 3000 to 90,000 g/mol.[107] The crystallinity of PCL tends to decrease with increasing molecular weight. The good solubility, low melting point and exceptional blend-compatibility of PCL have stimulated extensive research into potential applications in a wide range of fields, such as food packaging, medical implant, and controlled drug delivery system and so on.[12, 14, 15, 18, 22, 108]

### 1.3.1 Synthesis and properties of PCL

PCL can be prepared by either ring-opening polymerization (ROP) of cyclic monomer ε-caprolactone using a variety of catalysts or via free radical ring-opening polymerization of 2-methylene-1-3-dioxepane.[109, 110] General synthetic methods for polycaprolactone is shown in Figure 1.4. There are different mechanisms that can be used for the polymerization of PCL, which are anionic, cationic, co-ordination and radical. Each of these mechanisms can affect the resulting molecular weight, molecular weight distribution, end group composition and chemical structure of the copolymers.[107]

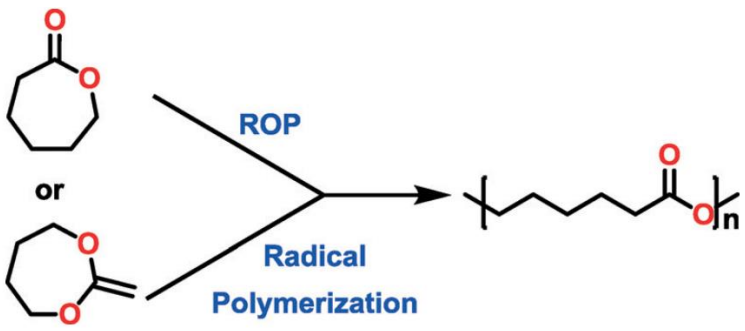


Figure 1.4 General synthetic strategies for PCL.

As a biopolymer, PCL has been identified for its potential commercial applications. In contrast to conventional plastics such as polypropylene (PP) and polyethylene (PE) and so on, which

require hundreds or even thousands of years to fully degrade, PCL biodegrades into naturally occurring products within only a few years.[15] Like many other biopolymers, PCL did not have the mechanical properties to be applied in high load bearing applications, which is currently limiting its use. Nevertheless, it possesses superior rheological and viscoelastic properties over many of its resorbable-polymer counterparts. PCL exhibits high crystallinity and is highly hydrophobic, thus having relatively lower biodegradation rate compared to other biopolymers.[111] The homo-polymer PCL has a total degradation of 2–4 years depending on the molecular weight of PCL chains used for the devices.[112-114] The rate of hydrolysis can be altered by copolymerization with other lactones, glycosides or lactides.[107] Extensive studies by some researchers concerning the in vitro and in vivo degradation of PCL scaffolds, detected no evidence of internal catalysis demonstrated by uniform molecular weight distribution over time, and cross-sectional examination of the scaffold struts over 6 months.[115] Other degradation studies using PCL in separate in vitro and in vivo conditions reported that both hydrolytic degradation rates were similar, and thus concluded that enzymatic involvement in the first stage of degradation phase was not a significant influence factor in the degradation process of PCL.[116, 117] Therefore, PCL is an interesting material for application requiring long degradation time.. To have a clear awareness of the properties of PCL, the physical-mechanical properties of several degradable polymers, (PCL, PLA, L-PLA, DL-PLA, PGA, PHB), had been summarized and compared by Van de Velde and Kiekens.[118] Some of these properties are listed in Table 1-4, which included the polymer density ρ, the tensile strength σ, the tensile modulus E, the elongation at break ε, the glass transition temperature $T_g$ and melt point $T_m$.

Table 1-4 Physical properties of various biopolymers.[118]

| Properties | Type of biopolymers | | | | | |
|---|---|---|---|---|---|---|
| | PCL | PLA | L-PLA | DL-PLA | PGA | PHB |
| ρ ($gcm^{-3}$) | 1.1 | 1.2 | 1.3 | 1.3 | 1.5-1.7 | 1.2 |
| σ (MPa) | 21-42 | 20-60 | 15-150 | 28-50 | 60-100 | 40 |
| E (GPa) | 0.2-0.4 | 0.4-3.5 | 2.7-4.2 | 1.0-3.5 | 6.0-7.0 | 3.5-4.0 |
| ε (%) | 300-1000 | 3-6 | 3-10 | 2-10 | 2-20 | 5-8 |
| $T_g$ (°C) | -60- -65 | 45-60 | 55-65 | 50-60 | 35-45 | 5-15 |
| $T_m$ (°C) | 58-65 | 150-162 | 170-200 | - | 220-233 | 168-182 |

### 1.3.2 Crystallization behavior of PCL and PCL related nanocomposites

The crystallization of PCL is connected by the two basic stages of working mechanism, namely the homogeneous nucleation at a given temperature and the growth of small to large crystals, which mainly depends on temperature. The homogeneous nucleation is considered to be initiated as soon as a pertinent critical free energy barrier was overcome. The path of homogeneous nucleation may be clarified within the classical nomenclature. It starts with embryos, which need to increase the free energy for further growth in size and perfection. The embryos must move by fluctuation across the barrier of the critical nucleus, described as the saddle point in the size and perfection landscape of the free enthalpy of formation. This leads to the supercritical nucleus that can grow with a thermos-dynamically permitted decrease in the free enthalpy of formation. The actual rate of progress can be additionally determined by kinetic factors which also are size and perfection dependent, creating a much more intricate, multidimensional free enthalpy landscape.

The kinetics of nucleation and crystallization of PCL was well studied by Evgeny and coworkers,[119] using differential fast scanning calorimetry (DFSC) technique, which allows temperature control of the samples and determination of its heat capacity using super-high heating rates up to 50,000 K/s. They found that the crystal growth and nucleation cannot be fitted with a single viscosity-related term which slows the process in parallel to the bulk glass transition kinetics. Particularly the nucleation rate needs to be much faster, the local viscosity

terms as can be known from dielectric and heat capacity measurements for large-amplitude motion of molecules. Following nucleation, a growth of small to large crystals, depending on temperature, occurs as the second stage. In the past, a new growth barrier in the form of the secondary or molecular nucleation was assumed. The molecular nucleation was thought to introduce the molecular segregation on crystallization.[120, 121] However, their new data gave a hint that the segregation may have already occurred before or in the nucleation stage. Further growth of the initial crystals at a given temperature was hindered by the slow, long-range diffusion, leading ultimately to a sufficient amount of rigid-amorphous fraction with a higher glass transition temperature to stop the further growth. The melting of crystals retains nuclei that can enhance the cold crystallization behavior for low melting temperatures. For high melting temperature such nucleus retention which was called self-nucleation in the past were found to survive heating above the equilibrium melting temperature.

The crystallization behavior of PCL based nanocomposites was studied by many researchers using different PCL composites systems.[122-129] Xu et al. studied the non-isothermal crystallization behavior of the multiwall carbon nanotube (MWNT) reinforced PCL composites, prepared by using a simple melt-compounding method.[122] They claimed that the non-isothermal crystallization behavior of the PCL/MWNT nanocomposites exhibited strong dependency of crystallinity, crystallization temperature, halftime of crystallization ($t_{1/2}$) and Avrami exponent ($n$) on the MWNT content and cooling rate. The MWNT in the nanocomposites exhibited a high nucleation activity. All the crystallization activation energies ($E_a$), calculated with the Kissinger model for the composite systems, were higher than that of the neat PCL. In addition, the $E_a$ values of the nanocomposites were found to gradually decrease with increasing content.[122] Very similar results on $E_a$ in PCL/MWNT nanocomposites were obtained from the work of Wu et al.[124] Wang and coworkers studied the crystallization and mechanical properties of PCL/GO nanocomposites prepared by using in-situ polymerization method.[123] The effect of GO on crystal structure, crystallization behavior and spherulitic morphology of the PCL matrix were investigated and the results showed that

the crystallization temperature of PCL was enhanced significantly due to the presence of GO in the nanocomposite systems. However, the addition of GO did not affect the crystal structure.[123] Gu et al. prepared PCL/RGO nanocomposites by injection molding and studied the effects of RGO on the crystallization behavior of PCL matrix.[125] RGO was found to be an effective nucleation agent for PCL. Their results, obtained by wide angle X-ray diffraction and small angle X-ray scattering measurements, showed that the incorporation of RGO can enhance the orientation degree of PCL crystals in the flow direction without affecting the crystal structure of PCL. Moreover, the orientation of PCL chains was found to be enhanced with the increase of RGO content, which was believed to be attributed to the obstruction of RGO on the motion of PCL chains.[125]

### 1.3.3 Applications of PCL

As previously mentioned, due to the excellent biocompatibility, flexibility, and thermo-plasticity, PCL and PCL based composites/nanocomposites have been proposed for use in various biomedical and biomaterial applications.[12, 14, 15, 22, 112, 116]

PCL is suitable for controlled drug delivery due to a high permeability to many drugs and excellent biocompatibility. The fact that PCL degrades at a slower rate than other biopolymers such as PLA, PGA, PLGA and its copolymers makes it the most suitable materials for long-term drug delivery systems over a period of more than 1 year.[130] Drug release rates from PCL also depends on type of formulation, method of preparation, PCL content and percent of drug loaded. The ability of PCL to form compatible blends with other polymers can affect their degradation kinetics, facilitating tailoring and thus fulfill its applications. The advantages of PCL for these applications include tailorable degradation kinetics, mechanical properties, ease of shaping and manufacture, enabling appropriate pore sizes conducive to tissue in-growth, and the controlled delivery rates of drugs contained within their matrix.[107] Functional groups could also be added by chemical reactions to make the polymer more hydrophilic, adhesive, or biocompatible which enabled favorable cell responses. Pitt and co-workers undertook

several studies including degradation studies both in vitro[131] and in vivo.[132] Later on, the subdermal delivery of l-methadone within PCL microspheres was investigated.[133] And since then, PCL has been utilized as an ultra-thin film for dressing cutaneous wounds,[22, 134] release vehicle for the chemical antiseptic chlorohexidine,[135] as well as in dentistry.[22]

Tissue engineering is closely related with applications that repair or replace portions of or the whole tissue. Developments in tissue engineering have yielded numerous set of tissue replacement parts such as scaffold fabrications, bone engineering, blood vessel engineering, skin engineering, nerve engineering and so on.[107] One of the goals of bone tissue engineering is to create tissue replacements by culturing bone cells on synthetic three-dimensional porous scaffolds, which can promote new tissue formation by providing a high surface that promote the attachment, migration, proliferation, and desired differentiation of connective tissue. PCL can be used in a wide range of scaffold fabrication technologies and its relatively inexpensive production routes, compared with other aliphatic polyesters, is a huge advantage. The realization that PCL possesses superior rheological and viscoelastic properties over many of its resorbable polymer counterparts renders the ease to manufacture and manipulate into a large range of scaffolds.[107]

In food packaging, a major emphasis is on the development of high barrier properties against the diffusion of oxygen, carbon dioxide, flavor compounds, and water vapor.[136] Moreover, several nanostructures of PCL had been used to provide active and/or smart properties to food packaging systems, as exemplified by antimicrobial properties, oxygen scavenging ability, enzyme immobilization, or indication of the degree of exposure to some detrimental factors such as inadequate temperatures or oxygen levels.[136]

### 1.3.4 PCL-based nanocomposites

As previously mentioned, PCL has been attracting widespread attentions mainly in the fields of biomedicine and tissue engineering. However, the relatively poor mechanical properties of PCL are restricting its applications in the fields where high moduli are indispensable

requirements. The incorporation of nanofillers, such as graphene, graphite oxide, carbon nanotubes, layered silicate and nanoclays has provided an effective method to improve the physical-mechanical properties of PCL.[128, 137-140] Among these nanofillers, graphene and carbon-related nanomaterials are the most promising materials to enhance the properties of PCL duo to their fantastic properties.[79, 80, 141-144]

Wang et al. prepare PCL/GO nanocomposites by in situ polymerization at low GO loadings.[123] They reported that, compared to the pure PCL, the thermal stability of PCL was remarkably increased with the addition of GO nanosheets. Moreover, the tensile strength and Young's modulus of PCL with incorporation of GO were greatly improved without a significant decrease of the elongation at break. The results from SEM measurements showed not only a homogeneous dispersion of GO but also a strong interfacial adhesion between GO nanosheets and PCL matrix.[123]

Zeng and coworkers[145] prepared PCL nanocomposites with poly(sodium 4-styrenesulfonate) (PSS) functionalized graphene nanosheets (GNS) through solution coagulation with GNS loading of 0.05 to 1.0 wt.%. The results from tensile tests showed that both the tensile strength and the Young's modulus of PCL were increased gradually with increasing the loading of GNS within 0.5 wt.%, meanwhile the elongation at break of the nanocomposites increased slightly. Conversely, when the loading of GNS was higher than 1.0 wt.%, the tensile strength and elongation at break reduced considerably due to the aggregation of GNS , which phenomenon was demonstrated from their SEM results.[145]

By using the solution evaporation technique, Pan et al. fabricated PCL/MWNT composite scaffolds for bone tissue engineering application, with MWNT loading up to 2.0 wt.% in PCL matrix.[14] They claimed that the tensile and compressive modulus of the composite scaffolds were significantly increased with increasing MWNT loadings. The bone-marrow-derived stroma cells (BMSC) on the composite scaffolds differentiated down the osteogenic lineage and expressed high levels of bone marker alkaline phosphatase (ALP). The proliferation and differentiation of the BMSC of scaffolds with low MWNT loadings (0.5 wt.%) were found to

be enhanced more than that of scaffolds with the higher MWNT loadings.[14]

The effect of GO as an enforcing filler on the properties of PCL was studied by Kai et al.[146] The Young's modulus and tensile strength of PCL was increased to 1000 MPa and 26 MPa respectively, which are around 3.0 and 1.7 times of the neat PCL. Furthermore, results from WAXD measurements showed an expansion of the GO interlayer distance from 0.6 nm to 1.1 nm in the PCL/GO composite, which indicated the intercalation of the PCL chain into the GO layers, leading to a higher reinforcing effect than graphite on the mechanical properties of PCL.[146]

Nanocomposites based on PCL and thermally reduced graphene oxide (TRGO) were prepared via a solution mixing method at low TRGO loadings of 0.5 wt% and 2.0 wt% by Zhang and coworkers.[128] TEM observations revealed good dispersion of TRG throughout the PCL matrix and SEM measurements showed a strong interfacial adhesion between TRG and PCL matrix. The storage modulus of the PCL/TRGO nanocomposites had been greatly improved by ca. 200% and 300% at -80 oC with incorporating 0.5 and 2.0 wt% of TRGO respectively, as compared with neat PCL.128 A detailed review about the effect of nanofillers on the functional properties of biopolymer-based films had been published by Jamróz et al.[138]

## 1.4 Graphene and graphene related materials

Graphene, which was firstly discovered in 2004,[147] is a single atomic layer of $sp^2$ carbon atoms bonded together in hexagonal lattices,[79] as illustrated in Figure 1.5a. Being the stiffest and strongest known material with Young's modulus and ultimate strength of up to 1 TPa and 130 GPa,[148] respectively, graphene is one of the most promising nanomaterials, which has been making a huge impact in many fields of science and technology. The unique physicochemical properties has made it a great potential for providing new approaches and critical improvements in the field of electrochemistry. However, even different kinds of producing techniques had been developed,[81-83] the industrial-scale production of graphene still remains very challenging, which is restricting its applications in many fields. Graphene-

related materials (GRM), including single layer graphene, graphite nanoplatelets (GNP), graphene oxide (GO) and reduced graphene oxide (rGO), are multifunctional nanostructured building blocks with extraordinary properties, which are typically used by considering that their large-scale production for industrial applications are available.

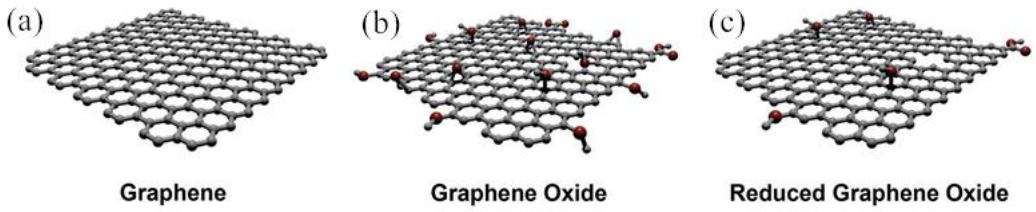


Figure 1.5 molecule structures of graphene (a), graphene oxide (b), reduced graphene oxide (c).

Graphite nanoplatelets which are also called graphite nanosheets (GNS) are another form of graphene consisting several stacked graphene sheets. The mostly used methods to produce GNP are the physical exfoliation and the thermal expansion of natural graphite flakes.[149, 150] GNP possesses very similar properties as graphene and it is a promising reinforcement for high-performance composites, however, the properties of GNP can be affected by many factors, such as the dimension, the number of graphene layers, as well as the preparation methods.[149] A number of GNP-based polymer nanocomposites had been successfully prepared for different application fields by using different preparation methods.[88, 93, 151-157]

Graphene oxide (GO) is an oxidized form of graphene that contains epoxide, carbonyl, and hydroxyl functional groups on the surface and edges, which allow the formation of hydrogen bonds, molecule structure of GO is shown in Figure 1.5b. GO consists of a single-layer of graphene oxide and is usually produced by the chemical treatment of graphite through oxidation, with subsequent dispersion and exfoliation in water or suitable organic solvents.[158, 159] The oxygen functional groups have been identified as mostly in the form of hydroxyl and epoxy groups on the basal plane, with smaller amounts of carboxy, carbonyl, phenol and lactone at the sheet edges.[160, 161] The oxygenated groups in GO can strongly affect its electronic, mechanical, and electrochemical properties due to the interactions of the groups between different GO flakes and the restrictions of the electron path.

In spite of the many advantages of GO, this nanomaterial is structurally defective, electrically insulating and mechanically poorer than graphene. To improve its properties, the chemical or thermal reduction of GO aimed at removing oxygen functional groups and regenerating the $sp^2$ network had been widely studied, providing rGO (molecule structure is shown in Figure 1.5c),[162-166] which can be considered as an intermediate structure between the ideal graphene sheet and the highly-oxidized GO, thus maintaining some and losing some other properties of both materials. Moreover, rGO can be obtained from both chemical and thermal reduction of GO, leading to a lower oxygen content than GO. The hydrogen bond between rGO and the polymer matrix, as well as between rGO sheets, is the main factor contributing to poor distribution of rGO in polymer matrix.[167]

Carbon nanotubes (CNTs) were firstly found by Iijima in 1991, and attracted worldwide attentions from researchers and industrialist due to their outstanding electrical, mechanical, and thermal properties.[168] A carbon nanotube can be defined as a cylinder composed of rolled-up graphene plane with diameters in nanometer scale. Although similar in chemical composition to graphene, CNTs are highly isotropic, and its special topology distinguishes nanotubes from other carbon structures and gives them unique properties. CNTs are tougher than steel, weightless when compared with aluminum, and far more electrically conductive than copper.[168] Besides being flexible, CNTs also have low density, high strength, and larger surface area.[169] There are basically two main kinds of CNTs: single walled carbon nanotubes (SWCNTs) and multi-walled carbon nanotubes (MWCNTs), structures of them are as illustrated in Figure 1.6. SWCNTs consists of a single graphene layer rolled up into a seamless cylinder with diameters of ca. 0.5-1.5 nm.[170] On the other hand, MWCNTs is defined by two or more concentric cylindrical shells of graphene sheets coaxially arranged around a central hollow core with van der Waals forces between adjacent layers.[169]

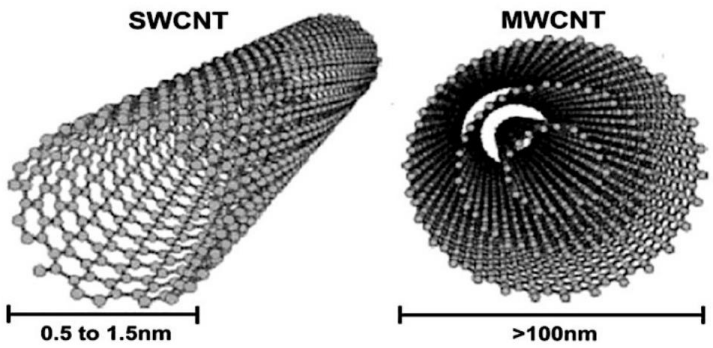


Figure 1.6 Molecule structure of SWCNT (left) and MWCNT (right).[171]

However, like other fillers, CNTs also have drawbacks that are limiting their applications to a certain extent. The major issue with CNTs is their dispersion ability in polymer matrices, caused by their entangled bundles during the growth, which are quite difficult to disperse. Researchers have tried different techniques to disperse CNTs uniformly into the polymer matrix. Indeed, the surface chemical modification with functional groups is one of the most used techniques to improve the dispersion of CNTs, which were combined with polymers using different mixing techniques such as solution mixing, melt blending, and in situ polymerization.[172-174]

## 1.5 Polyhedral oligomeric silsesquioxane

Polyhedral oligomeric silsesquioxane (POSS) has been described as a 3D “cage-shaped” molecule composed of a silicon–oxygen framework bonded to organic groups, which makes it compatible with a polymer matrix.[175] Unlike conventional nanofillers, POSS molecules formulated in the resin are induced by shear to “self-assemble” throughout the matrix into particle size of 25–200 nm. In the nanocomposites, POSS is reportedly that can provide modulus improvement and tensile strength improvement. In POSS, nucleating agents are reported to be useful for initiating the self-assembly of POSS nanoparticles and providing the property enhancements. POSS is unique in that it has an inorganic silicate core and organic exterior. This microstructure can provide mechanical stiffness and thermal stability as well as good fire retardant. POSS have also attracted a lot of attention due to their function that can

be used as ceramic precursors in nanocomposites. POSS has the capability to control the movement of polymer chains and simultaneously does not affect the process ability and mechanical reinforcement.

## 1.6 Layer-by-layer approach

Layer-by-layer (LbL) self-assembly[176] is a frequently-used method in nanomaterial fabrication, device fabrication. One of the important aspects of this technique is its universal application to almost all element assemblies that can be charged. Layer-by-layer self-assembly has several advantages including low process temperature, high molecular resolution of composition, easy for the thickness control, and a wide variety of appropriate building blocks. It has been widely used by researchers in different fields from the time it was firstly demonstrated. The alternate adsorption of oppositely charged macromolecules can be used to produce complex heterogeneous architectures.

# References

1. Bower, D. I., An Introduction to Polymer Physics. In *An Introduction to Polymer Physics*, Cambridge University Press: USA, 2002.

2. Logeshwaran, P.; Megharaj, M.; Chadalavada, S.; Bowman, M.; Naidu, R., Petroleum hydrocarbons (PH) in groundwater aquifers: An overview of environmental fate, toxicity, microbial degradation and risk-based remediation approaches. *Environmental Technology & Innovation* **2018,** *10*, 175-193.

3. Danso, D.; Chow, J.; Streit, W. R.; Drake, H. L., Plastics: Environmental and Biotechnological Perspectives on Microbial Degradation. *Applied and Environmental Microbiology* **2019,** *85* (19).

4. Yamaguchi, S.; Tanha, M.; Hult, A.; Okuda, T.; Ohara, H.; Kobayashi, S., Green polymer chemistry: lipase-catalyzed synthesis of bio-based reactive polyesters employing itaconic anhydride as a renewable monomer. *Polymer Journal* **2013,** *46* (1), 2-13.

5. Ragauskas, A. J.; Williams, C. K.; Davison, B. H.; Britovsek, G.; Cairney, J.; Eckert, C. A.; Frederick, W. J., Jr.; Hallett, J. P.; Leak, D. J.; Liotta, C. L.; Mielenz, J. R.; Murphy, R.; Templer, R.; Tschaplinski, T., The path forward for biofuels and biomaterials. *Science* **2006,** *311* (5760), 484-9.

6. Göpferich, A., Mechanisms of polymer degradation and erosion. *Biomaterials* **1996,** *17* (2), 103-114.

7. Besseling, E.; Quik, J. T. K.; Sun, M.; Koelmans, A. A., Fate of nano- and microplastic in freshwater systems: A modeling study. *Environ Pollut* **2017,** *220* (Pt A), 540-548.

8. Bouwmeester, H.; Hollman, P. C.; Peters, R. J., Potential Health Impact of Environmentally Released Micro- and Nanoplastics in the Human Food Production Chain: Experiences from Nanotoxicology. *Environ Sci Technol* **2015,** *49* (15), 8932-47.

9. Artham, T.; Sudhakar, M.; Venkatesan, R.; Madhavan Nair, C.; Murty, K. V. G. K.; Doble, M., Biofouling and stability of synthetic polymers in sea water. *International Biodeterioration & Biodegradation* **2009,** *63* (7), 884-890.

10. Siracusa, V., Microbial Degradation of Synthetic Biopolymers Waste. *Polymers (Basel)* **2019,** *11* (6).

11. Jacob, J.; Haponiuk, J. T.; Thomas, S.; Gopi, S., Biopolymer based nanomaterials in drug delivery systems: A review. *Materials Today Chemistry* **2018,** *9*, 43-55.

12. Wei, X.; Gong, C.; Gou, M.; Fu, S.; Guo, Q.; Shi, S.; Luo, F.; Guo, G.; Qiu, L.; Qian, Z., Biodegradable poly(epsilon-caprolactone)-poly(ethylene glycol) copolymers as drug delivery system. *Int J Pharm* **2009,** *381* (1), 1-18.

13. Jiang, W.-Z.; Cai, Y.; Li, H.-Y., Chitosan-based spray-dried mucoadhesive microspheres for sustained oromucosal drug delivery. *Powder Technology* **2017,** *312*, 124-132.

14. Pan, L.; Pei, X.; He, R.; Wan, Q.; Wang, J., Multiwall carbon nanotubes/polycaprolactone composites for bone tissue engineering application. *Colloids Surf B Biointerfaces* **2012,** *93*, 226-34.

15. Murray, E.; Thompson, B. C.; Sayyar, S.; Wallace, G. G., Enzymatic degradation of graphene/polycaprolactone materials for tissue engineering. *Polymer Degradation and Stability* **2015,** *111*, 71-77.

16. Kashirina, A.; Yao, Y.; Liu, Y.; Leng, J., Biopolymers as bone substitutes: a review. *Biomater Sci* **2019,** *7* (10), 3961-3983.

17. Porta, R.; Sabbah, M.; Di Pierro, P., Biopolymers as Food Packaging Materials. *Int J Mol Sci* **2020,** *21* (14).

18. Ludueña, L.; Vázquez, A.; Alvarez, V., Effect of lignocellulosic filler type and content on the behavior of polycaprolactone based eco-composites for packaging applications. *Carbohydrate Polymers* **2012,** *87* (1), 411-421.

19. Garavand, F.; Rouhi, M.; Razavi, S. H.; Cacciotti, I.; Mohammadi, R., Improving the integrity of natural biopolymer films used in food packaging by crosslinking approach: A review. *Int J Biol Macromol* **2017,** *104* (Pt A), 687-707.

20. Meinel, A. J.; Kubow, K. E.; Klotzsch, E.; Garcia-Fuentes, M.; Smith, M. L.; Vogel, V.; Merkle, H. P.; Meinel, L., Optimization strategies for electrospun silk fibroin tissue engineering scaffolds. *Biomaterials* **2009,** *30* (17), 3058-67.

21. Hoffman, A. S., Hydrogels for biomedical applications. *Advanced Drug Delivery Reviews* **2012,** *64*, 18-23.

22. Farzamfar, S.; Naseri-Nosar, M.; Samadian, H.; Mahakizadeh, S.; Tajerian, R.; Rahmati, M.; Vaez, A.; Salehi, M., Taurine-loaded poly (ε-caprolactone)/gelatin electrospun mat as a potential wound dressing material: In vitro and in vivo evaluation. *Journal of Bioactive and Compatible Polymers* **2017,** *33* (3), 282-294.

23. Akhavan-Kharazian, N.; Izadi-Vasafi, H., Preparation and characterization of chitosan/gelatin/nanocrystalline cellulose/calcium peroxide films for potential wound dressing applications. *Int J Biol Macromol* **2019,** *133*, 881-891.

24. Ye, S.; Jiang, L.; Su, C.; Zhu, Z.; Wen, Y.; Shao, W., Development of gelatin/bacterial cellulose composite sponges as potential natural wound dressings. *Int J Biol Macromol* **2019,** *133*, 148-155.

25. Vlierberghe., S. V.; Cnudde., V.; Dubruel., P.; Masschaele., B.; Cosijns., A.; Paepe., I. D.; Jacobs., P. J. S.; Hoorebeke., L. V.; Remon., J. P.; Schacht., E., Porous gelatin hydrogels: 1. Cryogenic formation and structure analysis. *Biomacromolecules* **2007,** *8* (2), 7.

26. Zhao, W.; Li, J.; Jin, K.; Liu, W.; Qiu, X.; Li, C., Fabrication of functional PLGA-based electrospun scaffolds and their applications in biomedical engineering. *Mater Sci Eng C Mater Biol Appl* **2016,** *59*, 1181-1194.

27. Siracusa, V.; Blanco, I.; Romani, S.; Tylewicz, U.; Rocculi, P.; Rosa, M. D., Poly(lactic acid)-modified films for food packaging application: Physical, mechanical, and barrier behavior. *Journal of Applied Polymer Science* **2012,** *125* (S2), E390-E401.

28. Jeon., Y.-J.; Kamil., J. Y. V. A.; Shahidi., F., Chitosan as an Edible Invisible Film for Quality Preservation of Herring and Atlantic Cod. *Journal of agricultural and food chemistry* **2002,** *50*, 12.

29. Möller., H.; Grelier., S.; Pardon., P.; Coma., V., Antimicrobial and Physicochemical Properties of Chitosan−HPMC-Based Films. *Journal of agricultural and food chemistry* **2004,** *52* (21), 6585-6591.

30. Chen., X. G.; Zheng., L.; Wang., Z.; Lee., C. Y.; Park., H. J., Molecular affinity and permeability of different molecular weight chitosan membranes. *Journal of Agricultural and Food Chemistry* **2002,** *50* (21),

5915-5918.

31. Zeng, D.; Wu, J.; Kennedy, J. F., Application of a chitosan flocculant to water treatment. *Carbohydrate Polymers* **2008,** *71* (1), 135-139.

32. Chaudhary, D.; Dong, Y.; Kar, K. K., Hydrophilic plasticized biopolymers: Morphological influence on physical properties. *Materials Letters* **2010,** *64* (7), 872-875.

33. Appendini., P.; Hotchkiss., J. H., Immobilization of Lysozyme on Food Contact Polymers as Potential Antimicrobial Films. *Packaging technology & science* **1997,** *10* (5), 271-279.

34. Fuglsang., C. C.; Johansen., C.; Christgau., S.; Adler-Nissen., J., Antimicrobial enzymes: applications and future potential in the food industry. *Trends in Food Science and Technology* **1995,** *6* (12), 390-396.

35. Schwach, G.; Coudane, J.; Engel, R.; Vert, M., Zn lactate as initiator of dl-lactide ring opening polymerization and comparison with Sn octoate. *Polymer Bulletin* **1996,** *37* (6), 771-776.

36. Save, M.; Soum, A., Controlled Ring-Opening Polymerization of Lactones and Lactide Initiated by Lanthanum Isopropoxide, 2. *Macromolecular Chemistry and Physics* **2002,** *203* (18), 2591-2603.

37. Dubois, P.; Jacobs, C.; Jerome, R.; Teyssie, P., Macromolecular engineering of polylactones and polylactides. 4. Mechanism and kinetics of lactide homopolymerization by aluminum isopropoxide. *Macromolecules* **1991,** *24* (9), 2266-2270.

38. Vink, E. T. H.; Davies, S., Life Cycle Inventory and Impact Assessment Data for 2014 Ingeo™ Polylactide Production. *Industrial Biotechnology* **2015,** *11* (3), 167-180.

39. Tams, J.; Joziasse, C. A. P.; Bos, R. R. M.; Rozema, F. R.; Grijpma, D. W.; Pennings, A. J., High-impact poly(l/d-lactide) for fracture fixation: in vitro degradation and animal pilot study. *Biomaterials* **1995,** *16* (18), 1409-1415.

40. P. Pawar, R.; U. Tekale, S.; U. Shisodia, S.; T. Totre, J.; J. Domb, A., Biomedical Applications of Poly(Lactic Acid). *Recent Patents on Regenerative Medicine* **2014,** *4* (1), 40-51.

41. Saini, P.; Arora, M.; Kumar, M., Poly(lactic acid) blends in biomedical applications. *Adv Drug Deliv Rev* **2016,** *107*, 47-59.

42. Mangaraj, S.; Yadav, A.; Bal, L. M.; Dash, S. K.; Mahanti, N. K., Application of Biodegradable Polymers in Food Packaging Industry: A Comprehensive Review. *Journal of Packaging Technology and Research* **2018,** *3* (1), 77-96.

43. Mahmoodi, A.; Ghodrati, S.; Khorasani, M., High-Strength, Low-Permeable, and Light-Protective Nanocomposite Films Based on a Hybrid Nanopigment and Biodegradable PLA for Food Packaging Applications. *ACS Omega* **2019,** *4* (12), 14947-14954.

44. Di Maio, L.; Scarfato, P.; Avallone, E.; Galdi, M. R.; Incarnato, L., Preparation and characterization of biodegradable active PLA film for food packaging. 2014; pp 338-341.

45. Ahmed, J.; Varshney, S. K., Polylactides—Chemistry, Properties and Green Packaging Technology: A Review. *International Journal of Food Properties* **2011,** *14* (1), 37-58.

46. Chen, Y.; Geever, L. M.; Killion, J. A.; Lyons, J. G.; Higginbotham, C. L.; Devine, D. M., Review of Multifarious Applications of Poly (Lactic Acid). *Polymer-Plastics Technology and Engineering* **2016,** *55* (10),

1057-1075.

47. Reddy, G.; Altaf, M.; Naveena, B. J.; Venkateshwar, M.; Kumar, E. V., Amylolytic bacterial lactic acid fermentation - a review. *Biotechnol Adv* **2008,** *26* (1), 22-34.

48. Nofar, M.; Sacligil, D.; Carreau, P. J.; Kamal, M. R.; Heuzey, M. C., Poly (lactic acid) blends: Processing, properties and applications. *Int J Biol Macromol* **2019,** *125*, 307-360.

49. Tsuji, H., Properties and morphologies of poly(?-lactide): 1. Annealing condition effects on properties and morphologies of poly(?-lactide). *Polymer* **1995,** *36* (14), 2709-2716.

50. Wootthikanokkhan, J.; Cheachun, T.; Sombatsompop, N.; Thumsorn, S.; Kaabbuathong, N.; Wongta, N.; Wong-On, J.; Na Ayutthaya, S. I.; Kositchaiyong, A., Crystallization and thermomechanical properties of PLA composites: Effects of additive types and heat treatment. *Journal of Applied Polymer Science* **2013,** *129* (1), 215-223.

51. Thakur, K. A. M.; Kean, R. T.; Zupfer, J. M.; Buehler, N. U.; Doscotch, M. A.; Munson, E. J., Solid State13C CP-MAS NMR Studies of the Crystallinity and Morphology of Poly(l-lactide). *Macromolecules* **1996,** *29* (27), 8844-8851.

52. Saeidlou, S.; Huneault, M. A.; Li, H.; Park, C. B., Poly(lactic acid) crystallization. *Progress in Polymer Science* **2012,** *37* (12), 1657-1677.

53. Kalb, B.; Pennings, A. J., General crystallization behaviour of poly(l-lactic acid). *Polymer* **1980,** *21* (6), 607-612.

54. Aliotta, L.; Cinelli, P.; Coltelli, M. B.; Righetti, M. C.; Gazzano, M.; Lazzeri, A., Effect of nucleating agents on crystallinity and properties of poly (lactic acid) (PLA). *European Polymer Journal* **2017,** *93*, 822-832.

55. Palade, L.-I.; Lehermeier, H. J.; Dorgan, J. R., Melt Rheology of Highl-Content Poly(lactic acid). *Macromolecules* **2001,** *34* (5), 1384-1390.

56. Tashiro, K.; Kouno, N.; Wang, H.; Tsuji, H., Crystal Structure of Poly(lactic acid) Stereocomplex: Random Packing Model of PDLA and PLLA Chains As Studied by X-ray Diffraction Analysis. *Macromolecules* **2017,** *50* (20), 8048-8065.

57. Chen, X.; Kalish, J.; Hsu, S. L., Structure evolution of α′-phase poly(lactic acid). *Journal of Polymer Science Part B: Polymer Physics* **2011,** *49* (20), 1446-1454.

58. Lim, L. T.; Auras, R.; Rubino, M., Processing technologies for poly(lactic acid). *Progress in Polymer Science* **2008,** *33* (8), 820-852.

59. Perego, G.; Cella, G. D.; Bastioli, C., Effect of molecular weight and crystallinity on poly(lactic acid) mechanical properties. *Journal of Applied Polymer Science* **1996,** *59* (1), 37-43.

60. Brüster, B.; Addiego, F.; Hassouna, F.; Ruch, D.; Raquez, J. M.; Dubois, P., Thermo-mechanical degradation of plasticized poly(lactide) after multiple reprocessing to simulate recycling: Multi-scale analysis and underlying mechanisms. *Polymer Degradation and Stability* **2016,** *131*, 132-144.

61. Lee, E. J.; Huh, B. K.; Kim, S. N.; Lee, J. Y.; Park, C. G.; Mikos, A. G.; Choy, Y. B., Application of Materials as Medical Devices with Localized Drug Delivery Capabilities for Enhanced Wound Repair. *Prog*

*Mater Sci* **2017,** *89*, 392-410.

62. de Jong, S. J.; Arias, E. R.; Rijkers, D. T. S.; van Nostrum, C. F.; Kettenes-van den Bosch, J. J.; Hennink, W. E., New insights into the hydrolytic degradation of poly(lactic acid): participation of the alcohol terminus. *Polymer* **2001,** *42* (7), 2795-2802.

63. Liu, S.; Qin, S.; He, M.; Zhou, D.; Qin, Q.; Wang, H., Current applications of poly(lactic acid) composites in tissue engineering and drug delivery. *Composites Part B: Engineering* **2020,** *199*.

64. Tyler, B.; Gullotti, D.; Mangraviti, A.; Utsuki, T.; Brem, H., Polylactic acid (PLA) controlled delivery carriers for biomedical applications. *Adv Drug Deliv Rev* **2016,** *107*, 163-175.

65. Muller, J.; Gonzalez-Martinez, C.; Chiralt, A., Combination of Poly(lactic) Acid and Starch for Biodegradable Food Packaging. *Materials (Basel)* **2017,** *10* (8).

66. Zhang, P.; Tian, R.; Lv, R.; Na, B.; Liu, Q., Water-permeable polylactide blend membranes for hydrophilicity-based separation. *Chemical Engineering Journal* **2015,** *269*, 180-185.

67. Xiong, Z.; Lin, H.; Zhong, Y.; Qin, Y.; Li, T.; Liu, F., Robust superhydrophilic polylactide (PLA) membranes with a TiO2 nano-particle inlaid surface for oil/water separation. *Journal of Materials Chemistry A* **2017,** *5* (14), 6538-6545.

68. Gu, J.; Xiao, P.; Chen, P.; Zhang, L.; Wang, H.; Dai, L.; Song, L.; Huang, Y.; Zhang, J.; Chen, T., Functionalization of Biodegradable PLA Nonwoven Fabric as Superoleophilic and Superhydrophobic Material for Efficient Oil Absorption and Oil/Water Separation. *ACS Appl Mater Interfaces* **2017,** *9* (7), 5968-5973.

69. Tao, Y.; Wang, H.; Li, Z.; Li, P.; Shi, S. Q., Development and Application of Wood Flour-Filled Polylactic Acid Composite Filament for 3D Printing. *Materials (Basel)* **2017,** *10* (4).

70. Su, R.; Liu, L.; Li, X.; Cui, M.; Ma, F., Study on synthesis and application of collagen-modified polylactic acid. *Polymer Composites* **2015,** *36* (1), 88-93.

71. Raquez, J.-M.; Habibi, Y.; Murariu, M.; Dubois, P., Polylactide (PLA)-based nanocomposites. *Progress in Polymer Science* **2013,** *38* (10-11), 1504-1542.

72. Brzeziński, M.; Biela, T., Polylactide nanocomposites with functionalized carbon nanotubes and their stereocomplexes: A focused review. *Materials Letters* **2014,** *121*, 244-250.

73. Sanusi, O. M.; Benelfellah, A.; Bikiaris, D. N.; Aït Hocine, N., Effect of rigid nanoparticles and preparation techniques on the performances of poly(lactic acid) nanocomposites: A review. *Polymers for Advanced Technologies* **2020**.

74. Guo, Y.; Yang, K.; Zuo, X.; Xue, Y.; Marmorat, C.; Liu, Y.; Chang, C.-C.; Rafailovich, M. H., Effects of clay platelets and natural nanotubes on mechanical properties and gas permeability of Poly (lactic acid) nanocomposites. *Polymer* **2016,** *83*, 246-259.

75. Espino-Pérez, E.; Bras, J.; Ducruet, V.; Guinault, A.; Dufresne, A.; Domenek, S., Influence of chemical surface modification of cellulose nanowhiskers on thermal, mechanical, and barrier properties of poly(lactide) based bionanocomposites. *European Polymer Journal* **2013,** *49* (10), 3144-3154.

76. Tenn, N.; Follain, N.; Fatyeyeva, K.; Poncin-Epaillard, F.; Labrugère, C.; Marais, S., Impact of

hydrophobic plasma treatments on the barrier properties of poly(lactic acid) films. *RSC Advances* **2014,** *4* (11).

77. Li, K.; Colonna, S.; Fina, A.; Monticelli, O., Polyhedral Oligomeric Silsesquioxane (POSS) Surface Grafting: A Novel Method to Enhance Polylactide Hydrolysis Resistance. *Nanomaterials (Basel)* **2019,** *9* (8).

78. Chaiwong, C.; Rachtanapun, P.; Wongchaiya, P.; Auras, R.; Boonyawan, D., Effect of plasma treatment on hydrophobicity and barrier property of polylactic acid. *Surface and Coatings Technology* **2010,** *204* (18-19), 2933-2939.

79. Geim, A. K.; Novoselov, K. S., The rise of graphene. *Nat Mater* **2007,** *6* (3), 183-91.

80. Allen, M. J.; Tung, V. C.; Kaner, R. B., Honeycomb carbon: a review of graphene. *Chem Rev* **2010,** *110* (1), 132-45.

81. Rollings, E.; Gweon, G. H.; Zhou, S. Y.; Mun, B. S.; McChesney, J. L.; Hussain, B. S.; Fedorov, A. V.; First, P. N.; de Heer, W. A.; Lanzara, A., Synthesis and characterization of atomically thin graphite films on a silicon carbide substrate. *Journal of Physics and Chemistry of Solids* **2006,** *67* (9-10), 2172-2177.

82. Li, X.; Cai, W.; An, J.; Kim, S.; Nah, J.; Yang, D.; Piner, R.; Velamakanni, A.; Jung, I.; Tutuc, E.; Banerjee, S. K.; Colombo, L.; Ruoff, R. S., Large-area synthesis of high-quality and uniform graphene films on copper foils. *Science* **2009,** *324* (5932), 1312-4.

83. Chae, S. J.; Güneş, F.; Kim, K. K.; Kim, E. S.; Han, G. H.; Kim, S. M.; Shin, H.-J.; Yoon, S.-M.; Choi, J.-Y.; Park, M. H.; Yang, C. W.; Pribat, D.; Lee, Y. H., Synthesis of Large-Area Graphene Layers on Poly-Nickel Substrate by Chemical Vapor Deposition: Wrinkle Formation. *Advanced Materials* **2009,** *21* (22), 2328-2333.

84. Ramanathan, T.; Abdala, A. A.; Stankovich, S.; Dikin, D. A.; Herrera-Alonso, M.; Piner, R. D.; Adamson, D. H.; Schniepp, H. C.; Chen, X.; Ruoff, R. S.; Nguyen, S. T.; Aksay, I. A.; Prud'Homme, R. K.; Brinson, L. C., Functionalized graphene sheets for polymer nanocomposites. *Nat Nanotechnol* **2008,** *3* (6), 327-31.

85. Saravanan, N.; Rajasekar, R.; Mahalakshmi, S.; Sathishkumar, T. P.; Sasikumar, K. S. K.; Sahoo, S., Graphene and modified graphene-based polymer nanocomposites – A review. *Journal of Reinforced Plastics and Composites* **2014,** *33* (12), 1158-1170.

86. Esbati, A. H.; Irani, S., Effect of functionalized process and CNTs aggregation on fracture mechanism and mechanical properties of polymer nanocomposite. *Mechanics of Materials* **2018,** *118*, 106-119.

87. Rana, S.; Cho, J. W.; Tan, L. P., Graphene-crosslinked polyurethane block copolymer nanocomposites with enhanced mechanical, electrical, and shape memory properties. *RSC Advances* **2013,** *3* (33).

88. Potts, J. R.; Dreyer, D. R.; Bielawski, C. W.; Ruoff, R. S., Graphene-based polymer nanocomposites. *Polymer* **2011,** *52* (1), 5-25.

89. Kumar, A.; Sharma, K.; Dixit, A. R., A review of the mechanical and thermal properties of graphene and its hybrid polymer nanocomposites for structural applications. *Journal of Materials Science* **2018,** *54* (8), 5992-6026.

90. Cho, J.; Lee, H.; Nam, K.-H.; Yeo, H.; Yang, C.-M.; Seong, D. G.; Lee, D.; Kim, S. Y., Enhanced electrical conductivity of polymer nanocomposite based on edge-selectively functionalized graphene

nanoplatelets. *Composites Science and Technology* **2020,** *189*.

91. Norazlina, H.; Kamal, Y., Graphene modifications in polylactic acid nanocomposites: a review. *Polymer Bulletin* **2015,** *72* (4), 931-961.

92. Li, S.-h.; Liu, J.-c.; Wang, D.-y.; Chen, Y.-w.; Wei, H.-z.; Qin, Z.-m.; Jia, H.-m., Research Progress on Preparation and Performance of Bio-Degradation PLA/Graphene Nanocomposites. *DEStech Transactions on Materials Science and Engineering* **2017,** (amst).

93. Xu, J.-Z.; Chen, T.; Yang, C.-L.; Li, Z.-M.; Mao, Y.-M.; Zeng, B.-Q.; Hsiao, B. S., Isothermal Crystallization of Poly(l-lactide) Induced by Graphene Nanosheets and Carbon Nanotubes: A Comparative Study. *Macromolecules* **2010,** *43* (11), 5000-5008.

94. Villmow, T.; Pötschke, P.; Pegel, S.; Häussler, L.; Kretzschmar, B., Influence of twin-screw extrusion conditions on the dispersion of multi-walled carbon nanotubes in a poly(lactic acid) matrix. *Polymer* **2008,** *49* (16), 3500-3509.

95. Wu, D.; Wu, L.; Zhang, M.; Zhao, Y., Viscoelasticity and thermal stability of polylactide composites with various functionalized carbon nanotubes. *Polymer Degradation and Stability* **2008,** *93* (8), 1577-1584.

96. Pellis, A.; Silvestrini, L.; Scaini, D.; Coburn, J. M.; Gardossi, L.; Kaplan, D. L.; Herrero Acero, E.; Guebitz, G. M., Enzyme-catalyzed functionalization of poly(L-lactic acid) for drug delivery applications. *Process Biochemistry* **2017,** *59*, 77-83.

97. Pellis, A.; Acero, E. H.; Weber, H.; Obersriebnig, M.; Breinbauer, R.; Srebotnik, E.; Guebitz, G. M., Biocatalyzed approach for the surface functionalization of poly(L-lactic acid) films using hydrolytic enzymes. *Biotechnol J* **2015,** *10* (11), 1739-49.

98. Guo, B.; Finne-Wistrand, A.; Albertsson, A.-C., Electroactive Hydrophilic Polylactide Surface by Covalent Modification with Tetraaniline. *Macromolecules* **2011,** *45* (2), 652-659.

99. Xu, F. J.; Yang, X. C.; Li, C. Y.; Yang, W. T., Functionalized Polylactide Film Surfaces via Surface-Initiated ATRP. *Macromolecules* **2011,** *44* (7), 2371-2377.

100. Gutierrez-Villarreal, M. H.; Ulloa-Hinojosa, M. G.; Gaona-Lozano, J. G., Surface functionalization of poly(lactic acid) film by UV-photografting ofN-vinylpyrrolidone. *Journal of Applied Polymer Science* **2008,** *110* (1), 163-169.

101. Wu, L.-L.; Wang, J.-j.; He, X.; Zhang, T.; Sun, H., Using Graphene Oxide to Enhance the Barrier Properties of Poly(lactic acid) Film. *Packaging Technology and Science* **2014,** *27* (9), 693-700.

102. Jiao, Y. H.; Li, Y.; Wang, S.; Zhang, K.; Jia, Y. G.; Fu, Y., Layer-by-layer assembly of poly(lactic acid) nanoparticles: a facile way to fabricate films for model drug delivery. *Langmuir* **2010,** *26* (11), 8270-3.

103. Halász, K.; Hosakun, Y.; Csóka, L., Reducing Water Vapor Permeability of Poly(lactic acid) Film and Bottle through Layer-by-Layer Deposition of Green-Processed Cellulose Nanocrystals and Chitosan. *International Journal of Polymer Science* **2015,** *2015*, 1-6.

104. Gong, Y.; Zhu, Y.; Liu, Y.; Ma, Z.; Gao, C.; Shen, J., Layer-by-layer assembly of chondroitin sulfate and collagen on aminolyzed poly(L-lactic acid) porous scaffolds to enhance their chondrogenesis. *Acta Biomater* **2007,** *3* (5), 677-85.

105. He, X.; Wu, L.-l.; Wang, J.-j.; Zhang, T.; Sun, H.; Shuai, N., Layer-by-layer assembly deposition of graphene oxide on poly(lactic acid) films to improve the barrier properties. *High Performance Polymers* **2015,** *27* (3), 318-325.

106. Orozco, V. H.; Kozlovskaya, V.; Kharlampieva, E.; López, B. L.; Tsukruk, V. V., Biodegradable self-reporting nanocomposite films of poly(lactic acid) nanoparticles engineered by layer-by-layer assembly. *Polymer* **2010,** *51* (18), 4127-4139.

107. Woodruff, M. A.; Hutmacher, D. W., The return of a forgotten polymer—Polycaprolactone in the 21st century. *Progress in Polymer Science* **2010,** *35* (10), 1217-1256.

108. Mohamed, R. M.; Yusoh, K., A Review on the Recent Research of Polycaprolactone (PCL). *Advanced Materials Research* **2015,** *1134*, 249-255.

109. Naz, F.; Mumtaz, F.; Chaemchuen, S.; Verpoort, F., Bulk Ring-Opening Polymerization of ε-Caprolactone by Zeolitic Imidazolate Framework. *Catalysis Letters* **2019,** *149* (8), 2132-2141.

110. Bailey, W. J.; Ni, Z.; Wu, S.-R., Synthesis of poly-ε-caprolactone via a free radical mechanism. Free radical ring-opening polymerization of 2-methylene-1,3-dioxepane. *Journal of Polymer Science: Polymer Chemistry Edition* **1982,** *20* (11), 3021-3030.

111. Goldberg, D., A review of the biodegradability and utility of poly(caprolactone). *Journal of Environmental Polymer Degradation* **1995,** *3* (2), 61-67.

112. Lam, C. X.; Savalani, M. M.; Teoh, S. H.; Hutmacher, D. W., Dynamics of in vitro polymer degradation of polycaprolactone-based scaffolds: accelerated versus simulated physiological conditions. *Biomed Mater* **2008,** *3* (3), 034108.

113. Vroman, I.; Tighzert, L., Biodegradable Polymers. *Materials* **2009,** *2* (2), 307-344.

114. Ghanbarzadeh, B.; Almasi, H., Biodegradable Polymers. In *Biodegradation - Life of Science*, 2013.

115. Lam, C. X.; Hutmacher, D. W.; Schantz, J. T.; Woodruff, M. A.; Teoh, S. H., Evaluation of polycaprolactone scaffold degradation for 6 months in vitro and in vivo. *J Biomed Mater Res A* **2009,** *90* (3), 906-19.

116. Sun, H.; Mei, L.; Song, C.; Cui, X.; Wang, P., The in vivo degradation, absorption and excretion of PCL-based implant. *Biomaterials* **2006,** *27* (9), 1735-40.

117. Castilla-Cortázar, I.; Más-Estellés, J.; Meseguer-Dueñas, J. M.; Escobar Ivirico, J. L.; Marí, B.; Vidaurre, A., Hydrolytic and enzymatic degradation of a poly(ε-caprolactone) network. *Polymer Degradation and Stability* **2012,** *97* (8), 1241-1248.

118. Van de Velde, K.; Kiekens, P., Biopolymers: overview of several properties and consequences on their applications. *Polymer Testing* **2002,** *21* (4), 433-442.

119. Zhuravlev, E.; Schmelzer, J. W. P.; Wunderlich, B.; Schick, C., Kinetics of nucleation and crystallization in poly(ε-caprolactone) (PCL). *Polymer* **2011,** *52* (9), 1983-1997.

120. Mehta, A.; Wunderlich, B., A study of molecular fractionation during the crystallization of polymers. *Colloid and Polymer Science* **1975,** *253* (3), 193-205.

121. Wunderlich, B.; Mehta, A., Macromolecular nucleation. *Journal of Polymer Science: Polymer Physics*

*Edition* **1974,** *12* (2), 255-263.

122. Xu, G.; Du, L.; Wang, H.; Xia, R.; Meng, X.; Zhu, Q., Nonisothermal crystallization kinetics and thermomechanical properties of multiwalled carbon nanotube-reinforced poly(ε-caprolactone) composites. *Polymer International* **2008,** *57* (9), 1052-1066.

123. Wang, G.-s.; Wei, Z.-y.; Sang, L.; Chen, G.-y.; Zhang, W.-x.; Dong, X.-f.; Qi, M., Morphology, crystallization and mechanical properties of poly(ε-caprolactone)/graphene oxide nanocomposites. *Chinese Journal of Polymer Science* **2013,** *31* (8), 1148-1160.

124. Wu, T.-M.; Chen, E.-C., Crystallization behavior of poly(ε-caprolactone)/multiwalled carbon nanotube composites. *Journal of Polymer Science Part B: Polymer Physics* **2006,** *44* (3), 598-606.

125. Wang, B.; Li, Y.; Weng, G.; Jiang, Z.; Chen, P.; Wang, Z.; Gu, Q., Reduced graphene oxide enhances the crystallization and orientation of poly(ε-caprolactone). *Composites Science and Technology* **2014,** *96*, 63-70.

126. Hua, L.; Kai, W. H.; Inoue, Y., Crystallization behavior of poly(ϵ-caprolactone)/graphite oxide composites. *Journal of Applied Polymer Science* **2007,** *106* (6), 4225-4232.

127. Ahmed, J.; Luciano, G.; Schizzi, I.; Arfat, Y. A.; Maggiore, S.; Arockia Thai, T. L., Non-isothermal crystallization behavior, rheological properties and morphology of poly(ε-caprolactone)/graphene oxide nanosheets composite films. *Thermochimica Acta* **2018,** *659*, 96-104.

128. Zhang, J.; Qiu, Z., Morphology, Crystallization Behavior, and Dynamic Mechanical Properties of Biodegradable Poly(ε-caprolactone)/Thermally Reduced Graphene Nanocomposites. *Industrial & Engineering Chemistry Research* **2011,** *50* (24), 13885-13891.

129. Mucha, M.; Tylman, M.; Mucha, J., Crystallization kinetics of polycaprolactone in nanocomposites. *Polimery* **2015,** *61* (11/12), 686-692.

130. Armentano, I.; Dottori, M.; Fortunati, E.; Mattioli, S.; Kenny, J. M., Biodegradable polymer matrix nanocomposites for tissue engineering: A review. *Polymer Degradation and Stability* **2010,** *95* (11), 2126-2146.

131. Cha, Y.; Pitt, C. G., The biodegradability of polyester blends. *Biomaterials* **1990,** *11* (2), 108-112.

132. Pitt, G.; Gratzl, M.; Kimmel, G.; Surles, J.; Sohindler, A., Aliphatic polyesters II. The degradation of poly (DL-lactide), poly (ε-caprolactone), and their copolymers in vivo. *Biomaterials* **1981,** *2* (4), 215-220.

133. Cha, Y.; Pitt, C. G., A one-week subdermal delivery system for l-methadone based on biodegradable microcapsules. *Journal of Controlled Release* **1988,** *7* (1), 69-78.

134. Jin, G.; Prabhakaran, M. P.; Kai, D.; Annamalai, S. K.; Arunachalam, K. D.; Ramakrishna, S., Tissue engineered plant extracts as nanofibrous wound dressing. *Biomaterials* **2013,** *34* (3), 724-34.

135. Medlicott, N. J.; Jones, D. S.; Tucker, I. G.; Holborow, D., Preliminary release studies of chlorhexidine (base and diacetate) from poly(ϵ-caprolactone) films prepared by solvent evaporation. *International Journal of Pharmaceutics* **1992,** *84* (1), 85-89.

136. Rhim, J.-W.; Park, H.-M.; Ha, C.-S., Bio-nanocomposites for food packaging applications. *Progress in Polymer Science* **2013,** *38* (10-11), 1629-1652.

137. Qiu, Z.; Wang, H.; Xu, C., Crystallization, mechanical properties, and controlled enzymatic degradation

of biodegradable poly(epsilon-caprolactone)/multi-walled carbon nanotubes nanocomposites. *J Nanosci Nanotechnol* **2011,** *11* (9), 7884-93.

138. Jamroz, E.; Kulawik, P.; Kopel, P., The Effect of Nanofillers on the Functional Properties of Biopolymer-based Films: A Review. *Polymers (Basel)* **2019,** *11* (4).

139. Zeng, H. L.; Gao, C.; Yan, D. Y., Poly(ε-caprolactone)-Functionalized Carbon Nanotubes and Their Biodegradation Properties. *Advanced Functional Materials* **2006,** *16* (6), 812-818.

140. Chrissafis, K.; Antoniadis, G.; Paraskevopoulos, K. M.; Vassiliou, A.; Bikiaris, D. N., Comparative study of the effect of different nanoparticles on the mechanical properties and thermal degradation mechanism of in situ prepared poly(ε-caprolactone) nanocomposites. *Composites Science and Technology* **2007,** *67* (10), 2165-2174.

141. Wang, Y.; Li, Z.; Wang, J.; Li, J.; Lin, Y., Graphene and graphene oxide: biofunctionalization and applications in biotechnology. *Trends Biotechnol* **2011,** *29* (5), 205-12.

142. Geim, A. K., Graphene: status and prospects. *Science* **2009,** *324* (5934), 1530-4.

143. Rao, R.; Pint, C. L.; Islam, A. E.; Weatherup, R. S.; Hofmann, S.; Meshot, E. R.; Wu, F.; Zhou, C.; Dee, N.; Amama, P. B.; Carpena-Nunez, J.; Shi, W.; Plata, D. L.; Penev, E. S.; Yakobson, B. I.; Balbuena, P. B.; Bichara, C.; Futaba, D. N.; Noda, S.; Shin, H.; Kim, K. S.; Simard, B.; Mirri, F.; Pasquali, M.; Fornasiero, F.; Kauppinen, E. I.; Arnold, M.; Cola, B. A.; Nikolaev, P.; Arepalli, S.; Cheng, H. M.; Zakharov, D. N.; Stach, E. A.; Zhang, J.; Wei, F.; Terrones, M.; Geohegan, D. B.; Maruyama, B.; Maruyama, S.; Li, Y.; Adams, W. W.; Hart, A. J., Carbon Nanotubes and Related Nanomaterials: Critical Advances and Challenges for Synthesis toward Mainstream Commercial Applications. *ACS Nano* **2018,** *12* (12), 11756-11784.

144. Wang, C.; Murugadoss, V.; Kong, J.; He, Z.; Mai, X.; Shao, Q.; Chen, Y.; Guo, L.; Liu, C.; Angaiah, S.; Guo, Z., Overview of carbon nanostructures and nanocomposites for electromagnetic wave shielding. *Carbon* **2018,** *140*, 696-733.

145. Wang, M.; Deng, X.-Y.; Du, A.-K.; Zhao, T.-H.; Zeng, J.-B., Poly(sodium 4-styrenesulfonate) modified graphene for reinforced biodegradable poly(ε-caprolactone) nanocomposites. *RSC Advances* **2015,** *5* (89), 73146-73154.

146. Kai, W.; Hirota, Y.; Hua, L.; Inoue, Y., Thermal and mechanical properties of a poly(ε-caprolactone)/graphite oxide composite. *Journal of Applied Polymer Science* **2008,** *107* (3), 1395-1400.

147. Novoselov, K. S.; Geim, A. K.; Morozov, S. V.; Jiang, D.; Zhang, Y.; Dubonos, S. V.; Grigorieva, I. V.; Firsov, A. A., Electric field effect in atomically thin carbon films. *Science* **2004,** *306* (5696), 666-9.

148. Lee, C.; Wei, X.; Kysar, J. W.; Hone, J., Measurement of the elastic properties and intrinsic strength of monolayer graphene. *Science* **2008,** *321* (5887), 385-8.

149. Geng, Y.; Wang, S. J.; Kim, J. K., Preparation of graphite nanoplatelets and graphene sheets. *J Colloid Interface Sci* **2009,** *336* (2), 592-8.

150. Viculis, L. M.; Mack, J. J.; Mayer, O. M.; Hahn, H. T.; Kaner, R. B., Intercalation and exfoliation

routes to graphite nanoplatelets. *Journal of Materials Chemistry* **2005,** *15* (9).

151. Hung, M. T.; Choi, O.; Ju, Y. S.; Hahn, H. T., Heat conduction in graphite-nanoplatelet-reinforced polymer nanocomposites. *Applied Physics Letters* **2006,** *89* (2).

152. Sun, X.; Ramesh, P.; Itkis, M. E.; Bekyarova, E.; Haddon, R. C., Dependence of the thermal conductivity of two-dimensional graphite nanoplatelet-based composites on the nanoparticle size distribution. *J Phys Condens Matter* **2010,** *22* (33), 334216.

153. Chee, W. K.; Lim, H. N.; Huang, N. M.; Harrison, I., Nanocomposites of graphene/polymers: a review. *RSC Advances* **2015,** *5* (83), 68014-68051.

154. Wei, T.; Luo, G.; Fan, Z.; Zheng, C.; Yan, J.; Yao, C.; Li, W.; Zhang, C., Preparation of graphene nanosheet/polymer composites using in situ reduction–extractive dispersion. *Carbon* **2009,** *47* (9), 2296-2299.

155. Das, B.; Eswar Prasad, K.; Ramamurty, U.; Rao, C. N., Nano-indentation studies on polymer matrix composites reinforced by few-layer graphene. *Nanotechnology* **2009,** *20* (12), 125705.

156. Sen, I.; Seki, Y.; Sarikanat, M.; Cetin, L.; Gurses, B. O.; Ozdemir, O.; Yilmaz, O. C.; Sever, K.; Akar, E.; Mermer, O., Electroactive behavior of graphene nanoplatelets loaded cellulose composite actuators. *Composites Part B: Engineering* **2015,** *69*, 369-377.

157. Nista, S. V. G.; Tsukamoto, J.; Moshkalev, S. A., Thin film conductive composites based on graphite nanoplatelets for heating applications. In *2019 34th Symposium on Microelectronics Technology and Devices (SBMicro)*, 2019; pp 1-4.

158. Ruoff, R., Graphene: calling all chemists. *Nat Nanotechnol* **2008,** *3* (1), 10-1.

159. Dimiev, A.; Kosynkin, D. V.; Alemany, L. B.; Chaguine, P.; Tour, J. M., Pristine graphite oxide. *J Am Chem Soc* **2012,** *134* (5), 2815-22.

160. Mermoux, M.; Chabre, Y.; Rousseau, A., FTIR and 13C NMR study of graphite oxide. *Carbon* **1991,** *29* (3), 469-474.

161. Lerf, A.; He, H.; Forster, M.; Klinowski, J., Structure of Graphite Oxide Revisited‖. *The Journal of Physical Chemistry B* **1998,** *102* (23), 4477-4482.

162. Pei, S.; Cheng, H.-M., The reduction of graphene oxide. *Carbon* **2012,** *50* (9), 3210-3228.

163. Trusovas, R.; Ratautas, K.; Račiukaitis, G.; Barkauskas, J.; Stankevičienė, I.; Niaura, G.; Mažeikienė, R., Reduction of graphite oxide to graphene with laser irradiation. *Carbon* **2013,** *52*, 574-582.

164. Mitra, M.; Chatterjee, K.; Kargupta, K.; Ganguly, S.; Banerjee, D., Reduction of graphene oxide through a green and metal-free approach using formic acid. *Diamond and Related Materials* **2013,** *37*, 74-79.

165. Kim, D.; Yang, S. J.; Kim, Y. S.; Jung, H.; Park, C. R., Simple and cost-effective reduction of graphite oxide by sulfuric acid. *Carbon* **2012,** *50* (9), 3229-3232.

166. Sharma, N.; Sharma, V.; Jain, Y.; Kumari, M.; Gupta, R.; Sharma, S. K.; Sachdev, K., Synthesis and Characterization of Graphene Oxide (GO) and Reduced Graphene Oxide (rGO) for Gas Sensing Application. *Macromolecular Symposia* **2017,** *376* (1).

167. Barrett, J. S. F.; Abdala, A. A.; Srienc, F., Poly(hydroxyalkanoate) Elastomers and Their Graphene

Nanocomposites. *Macromolecules* **2014,** *47* (12), 3926-3941.

168. Iijima, S., Helical microtubules of graphitic carbon. *Nature* **1991,** *354* (6348), 56-58.

169. Ibrahim, K. S., Carbon nanotubes-properties and applications: a review. *Carbon letters* **2013,** *14* (3), 131-144.

170. Kuzmany, H.; Plank, W.; Hulman, M.; Kramberger, C.; Grüneis, A.; Pichler, T.; Peterlik, H.; Kataura, H.; Achiba, Y., Determination of SWCNT diameters from the Raman response of the radial breathing mode. *The European Physical Journal B* **2001,** *22* (3), 307-320.

171. Martins-Junior, P. A.; Alcantara, C. E.; Resende, R. R.; Ferreira, A. J., Carbon nanotubes: directions and perspectives in oral regenerative medicine. *J Dent Res* **2013,** *92* (7), 575-83.

172. Krishnaiah, P.; Ratnam, C. T.; Manickam, S., Development of silane grafted halloysite nanotube reinforced polylactide nanocomposites for the enhancement of mechanical, thermal and dynamic-mechanical properties. *Applied Clay Science* **2017,** *135*, 583-595.

173. Xie, X.; Mai, Y.; Zhou, X., Dispersion and alignment of carbon nanotubes in polymer matrix: A review. *Materials Science and Engineering: R: Reports* **2005,** *49* (4), 89-112.

174. Breuer, O.; Sundararaj, U., Big returns from small fibers: A review of polymer/carbon nanotube composites. *Polymer Composites* **2004,** *25* (6), 630-645.

175. Zhou, H.; Ye, Q.; Xu, J., Polyhedral oligomeric silsesquioxane-based hybrid materials and their applications. *Materials Chemistry Frontiers* **2017,** *1* (2), 212-230.

176. Richardson, J. J.; Cui, J.; Bjornmalm, M.; Braunger, J. A.; Ejima, H.; Caruso, F., Innovation in Layer-by-Layer Assembly. *Chem Rev* **2016,** *116* (23), 14828-14867.

# 2 POSS surface grafting to enhance the hydrolysis resistance of polylactide

## 2.1 Introduction

Polylactide (PLA), a biodegradable polyester, is one of the most interesting and sustainable substitutes of polymers from fossil resources.[1] Nevertheless, one of the major issues that reduces its exploitation in durable applications is its low hydrolytic stability compared with similar materials.[2] Indeed, PLA degrades by hydrolysis of the backbone ester groups, which reaction was demonstrated to be auto-catalyzed by the polymer carboxylic acid end groups.[3] In particular, the degradation rate can be influenced by many features, such as the polymer chemical structure, molecular mass, molecular mass distribution, morphology, water diffusion rate into the matrix and water amount in the polymer.[3] The polymer decomposition is affected mainly by the polymer reactivity with water and availability of the ester groups to water and catalysts and it is accelerated by temperature.[3-5] In order to improve such features, several methods were developed based on the modification of the polymer structure,[1] on the blending with other polymers,[3] or with suitable fillers/nanofillers.[6-8] Although the above approaches were found to affect the polymer degradation, several drawbacks have to be taken into account for their use, including the change of the polymer features such as the transparency and the dispersibility of the additives. In this light, the development of easy approaches, using mild conditions, capable of enhancing the hydrolysis resistance of the polymer without affecting the bulk properties is a crucial issue for extending PLA exploitation.

On this basis, a valuable method should consider the change of the polymer surface without affecting its bulk. It is worth underling that the surface of PLA film was mainly modified by using plasma[9, 10] and gas phase treatment.[11] In general, these methods were applied to enhance the PLA surface hydrophilicity, which modification turned out to increase the polymer hydrolytic degradation.[8-10]

In our innovative approach, with the aim at limiting the hydrolytic degradation of PLA, an

amino-functionalized polyhedral silsesquioxane (POSS) was used to graft to the surface of the polymer through an aminolysis reaction,[12] thus modifying the surface properties. Indeed, POSS are soluble in common organic solvents and they are generally combined with polymers in order to obtain organic/inorganic systems with enhanced properties with respect to the matrix.[13, 14] Generally, in order to produce polymer/POSS systems, melt or solvent blending were applied, by using a solvent capable of solubilizing both the silsesquioxane and the polymer in the case of the latter method.[15] In our approach, the polymer film is simply exposed to a solution of POSS to obtain a heterogenous reaction on the polymer surface. The reaction mechanism between POSS-$NH_2$ and PLLA was shown in Figure 2.1. Both the neat and treated films were characterized by using Fourier Transform Infrared Spectroscopy (FTIR), X-ray Photoelectron Spectroscopy (XPS), Field Emission Scanning Electron Microscopy (FE-SEM), Differential Scanning Calorimetry (DSC), Thermo-Gravimetric Analysis (TGA) and contact angle measurements, while the hydrolytic degradation was followed by monitoring the film morphology over time.

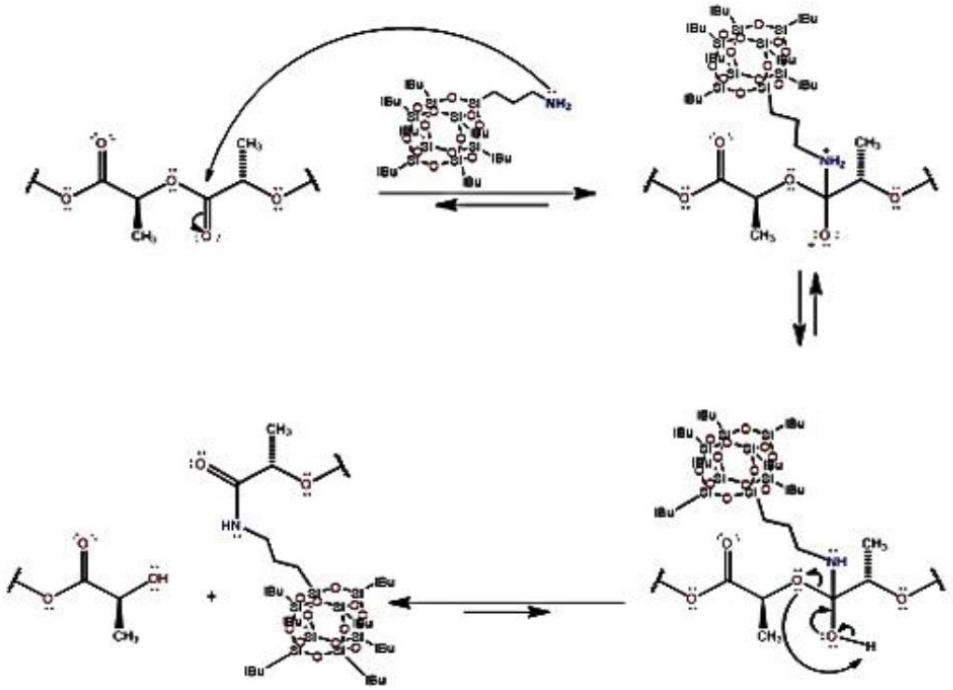

Figure 2.1 Mechanism of the reaction between POSS-$NH_2$ and PLLA.

## 2.2 Experimental

### 2.2.1 Materials

Poly(l-lactide) (PLLA) was purchased from Nature Works (BV, Naarden, The Netherlands), grade 2002D, Mn = 100,000 g/mol, with a residual monomer content less than 0.3% by mass, while aminopropyl heptaisobutyl-POSS (structure was shown in Figure 2.2, referred as POSS-$NH_2$ from now on) was obtained from Hybrid Plastics (Hattiesburg, MS, USA). Hexane and dichloromethane (Sigma-Aldrich, Milano, Italy) were used without further purification.

### 2.2.2 The preparation of POSS grafted PLLA films

PLLA was dissolved in dichloromethane (concentration of 2 g/dL), cast on a glass Petri dish and it was allowed to air-dry. Then, with the aim at completely removing the solvent, the resulting films were dried in vacuum for 4 h at 40 ºC and 4 h at 80 ºC. Finally, the transparent films, which were formed on the dish with thickness of about 100 μm, were peeled off. The films were cut into squares of size 2 × 2 $cm^2$ and were dipped in 20 mL of a solution of POSS-$NH_2$ in hexane (2% w/w) by applying different time (4 and 8 h) and temperatures (40 ºC and 60 ºC). The above solvent was chosen on the basis of its capability of dissolving the silsesquioxane but not the polymer. The treated film was then washed with 20 mL of fresh hexane for one hour at the same temperature applied for the reaction under magnetic stirring and with another 20 mL of fresh hexane overnight at room temperature. At the end, the film was allowed to dry in air and underwent the same thermal treatment as that used for the neat PLLA film, namely 4 h at 40 ºC and 4 h at 80 ºC. The samples were defined by indicating in the code the treatment time and temperature (as an example: PLLA_POSS_4_40 indicates a film treated with POSS-$NH_2$ for 4 h at 40 ºC).

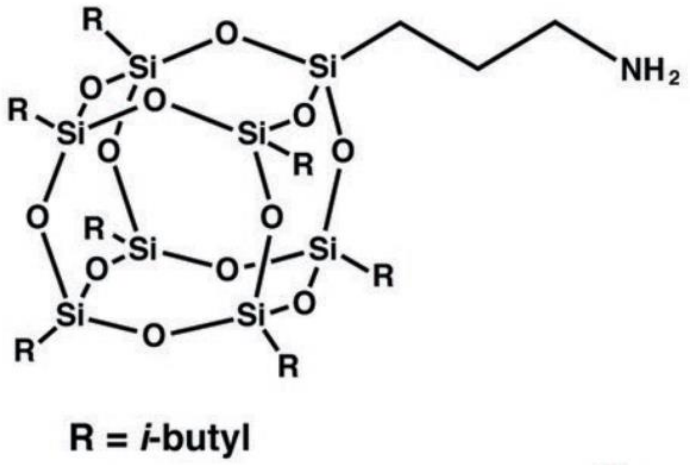


Figure 2.2 The structure of aminopropyl heptaisobutyl POSS (POSS-NH2).

### 2.2.3 Characterization

A field emission scanning electron microscope (Supra 40 VP from Zeiss, Jena, Germany), holding a backscattered electron detector, was used to examine the developed material morphologies. The films were submerged in liquid nitrogen (30 min) and then they were fractured cryogenically. A sputter coater (Polaron E5100 by Quorum Technologies Ltd, Laughton, UK) was used to thinly sputter-coat the films with carbon.

A Mettler-Toledo (Greifensee, Switzerland) TGA 1 thermo-gravimetric analyzer was applied, under a flow of nitrogen of 80 mL/min, from 25 to 800 ºC, with a heating rate of 20 ºC/min, to study the thermal decomposition of the neat PLLA and of the treated films. Volatilization onset temperatures ($T_{onset}$) were taken at 3% weight loss and temperatures for maximum volatilization rate ($T_{max}$) were taken from at the maximum of derivative weight plot. Both $T_{onset}$ and $T_{max}$ are typically reproducible to ± 3 ºC.

IR spectra were recorded by means of an IFS66 spectrometer by Bruker (Milano, Italy) considering a spectral range of 400-4000 $cm^{-1}$.

Differential scanning calorimetric analysis was performed between 25 and 250 ºC, with the same heating and cooling rate of 10 ºC/min, under a continuous nitrogen purge by using a DSC1 STAR$^e$ calorimetric apparatus from Mettler (Greifensee, Switzerland). Glass transition temperatures ($T_g$) were taken at midpoint of the transition on second heating plots, while cold

crystallization temperatures ($T_{cc}$) and melting temperatures were taken ($T_m$) were taken as peak values on the second heating plot. $T_g$, $T_{cc}$ and $T_m$ are typically reproducible to ± 1°.

Contact angle experiments were carried out at room temperature by means of an attention contact angle meter and by exploiting pure water as probe liquid. In order to evaluate the film resistance to hydrolysis, small pieces of PLLA films (area of 1 × 1 $cm^2$), which were previously dried overnight, were dipped into 10 mL of 0.1 M phosphate buffer solution (pH = 7.4) at 50 °C. The morphology of the degraded films was evaluated by FE-SEM analysis.

XPS measurements were accomplished by using a VersaProbe5000 by Physical Electronics (Chanhassen, MN, USA) equipped with a monochromatic Al source and a hemispherical analyzer. Both survey scans and high-resolution spectra were recorded by using a spot size of 100 μm. In order to eliminate the adsorbed molecules, the films were kept under vacuum for 15 h prior to the tests. A Shirley background function was exploited to adjust the spectra background. The curve fitting was accomplished by using a Gaussian (80%)–Lorentzian (20%) peak shape by minimizing the total square-error fit.

## 2.3 Results and Discussion

The characteristics of the films treated with POSS-NH2 were compared with those of the neat PLLA films by investigating the influence of reaction temperature and contact time on the final features of the materials. At first, the occurrence of the reaction was studied by means of infrared spectroscopy. Figure 2.5 compares the FTIR spectrum of the neat PLLA film with that of a film treated with POSS-$NH_2$ at 60 °C for 8 h (PLLA_8_60). For the former sample, typical bands for PLA[2] were detected. In the treated film, together with the typical bands of PLLA spectrum, a new band at ca. 1600 $cm^{-1}$ and a shoulder at ca. 1650 $cm^{-1}$ (enlarged spectra were shown in Figure 2.4) appear, which can be ascribed to amide group formation.[12] Moreover, in the spectrum of the treated film, a slight deformation of the band at ca. 1080 $cm^{-1}$ is visible, this change might be related to the presence of the silsesquioxane on the surface (Figure 2.4B). Indeed, a strong signal is present in this region in the spectrum of

POSS,[14] which belongs to the stretching of Si-O. Despite no strict correlation between the intensity of the above signals with contact time and the temperature was found, in the case of the samples exposed to the silsesquioxane for a shorter reaction time, namely PLLA_POSS_4_40 and PLLA_POSS_4_60, the band at 1600 $cm^{-1}$ is barely visible.

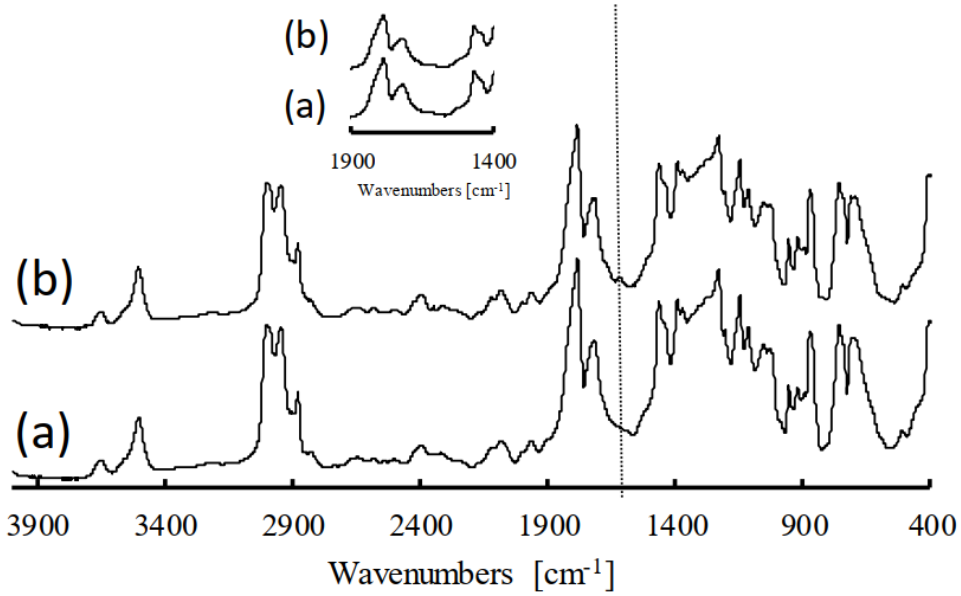


Figure 2.3 FTIR spectra of (a) neat PLLA and (b) PLLA_8_60 film.

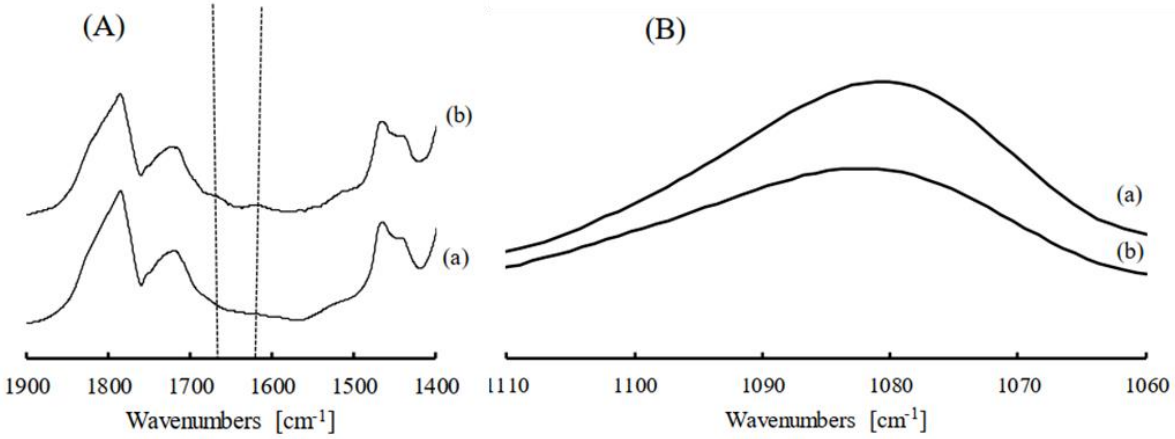


Figure 2.4 (A) FTIR spectra of: (a) PLLA neat film, (b) PLLA_POSS_8_60 in the range 1900-1400 $cm^{-1}$, (B) FTIR spectra of: (a) PLLA neat film, (b) PLLA_POSS_8_60 in the range 1110-1060 $cm^{-1}$.

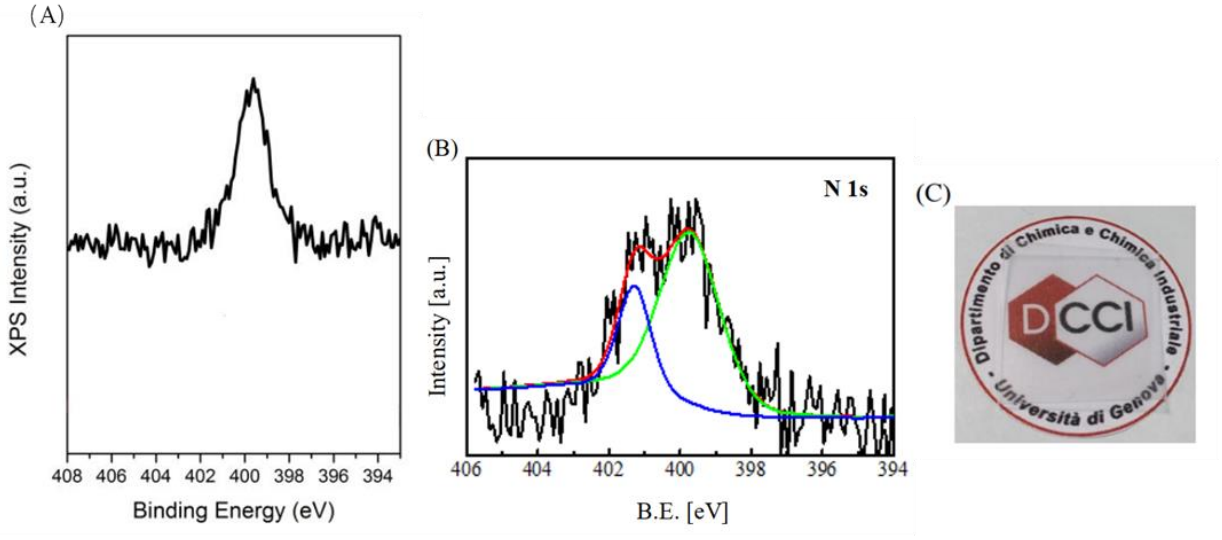


Figure 2.5 (A) XPS spectrum of POSS-$NH_2$ in the energy region typical for N 1s photoelectrons, (B) XPS spectrum of PLLA_8_60 materials film and (C) photo of PLLA_8_60 film.

XPS measurements were performed to further corroborate these findings. The survey scans indicated the presence of Si in the treated samples, with a concentration around 5% in the films PLLA_POSS_8_40 and PLLA_POSS_8_60. Moreover, considering the chemical environment of N atoms, while POSS-$NH_2$ (Figure 2.5A), as previously reported,[16] was found to hold a single N 1s peak centered at (399.7 ± 0.2) eV, which is ascribable to the presence of –$NH_2$ functionalities, the XPS spectrum of PLLA_POSS_8_60 showed two N species: one centered at (399.8 ± 0.2) eV, and the second centered at (401.6 ± 0.2) eV (Figure 2.5B). All other treated films showed a similar behavior. This finding demonstrates the modification of N chemical environment, which can be associated to the reaction of POSS-$NH_2$. The surface and the cross-sections of the treated films were analyzed by FE-SEM measurements coupled with Energy-Dispersive X-ray Spectroscopy (EDS) analysis, considering in particular Si dispersion, related to POSS distribution. Figure 2.6 shows a cross-section micrograph of the film, along with the elemental analysis. Indeed, while EDS measurements evidenced the presence of Si on the surface, whose concentration was found to be the same in the various analyzed points. The above element was not detectable in the cross section, further evidenced the deposition of POSS on the surface, which, as proved by FTIR and XPS measurements,

was found to be covalently linked to the surface (reaction scheme reported in Figure 2.1). It is worth underlining that despite the silsesquioxane deposition, the film appears to be transparent (Figure 2.5C), which property results to be essential for the practical applications of the material.

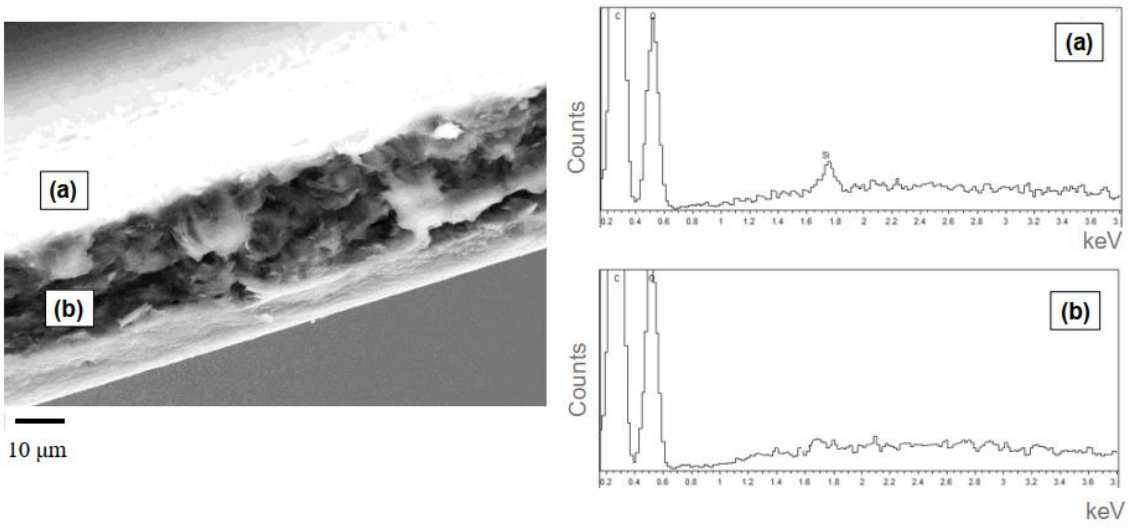


Figure 2.6 (left) FE-SEM of PLLA_POSS_8_60 film cross-section and (right) EDS analyses of the surface (point a) and cross-section (point b).

The thermal properties of the films were analyzed by DSC and TGA measurements. While DSC results evidenced a scarce influence of POSS deposition on PLLA crystallization. As shown in Table 2-1, the glass transition temperature, cold crystallization temperature and melting temperature of the reacted films did not have any difference compared to that of the untreated PLLA film, which is within our expectation due to the low POSS-$NH_2$ that only exists on the surface. TGA measurements demonstrated a slight improvement on thermal stability of the treated films, as shown in Table 2-2. Compared to the untreated PLLA film, both the onset degradation temperature ($T_{onset}$) and the temperature corresponding to the maximum weight loss rate ($T_{max}$) turned out to increase by increasing the reaction temperature and contact time that applied in the treatment of the films with POSS-$NH_2$. The maximum difference of $T_{max}$ between neat PLLA and treated films was found to be around 10 ºC for the sample PLLA_POSS_8_60. It is worth to underline that the influence of POSS on the

degradation temperature of nanocomposites was widely studied and its specific effect was related to the formation of a silica layer on the surface of the polymer, behaving as a barrier and limiting the material decomposition.[17]

Table 2-1 DSC results from second heating.

| Sample code | $T_g$ (°C) | $T_{cc}$ (°C) | $T_m$ (°C) | $\Delta H_{cc}$ (J/g) | $\Delta H_m$ (J/g) |
|---|---|---|---|---|---|
| PLLA | 60 | 130 | 153 | 5 | 6 |
| PLLA_POSS_4_40 | 61 | 133 | 154 | 5 | 6 |
| PLLA_POSS_8_40 | 60 | 131 | 154 | 4 | 6 |
| PLLA_POSS_4_60 | 60 | 130 | 153 | 5 | 6 |
| PLLA_POSS_8_60 | 60 | 130 | 153 | 5 | 6 |

$T_g$: glass transition temperature, $T_{cc}$: cold crystallization temperature, $T_m$: melting temperature, $\Delta H_{cc}$: enthalpy of the cold crystallization, $\Delta H_m$: melting enthalpy.

Table 2-2 TGA and contact angle results of the treated and untreated films.

| Sample code | $T_{onset}$ (°C) | $T_{max}$ (°C) | Contact angle (°) |
|---|---|---|---|
| PLLA | 329 | 367 | 71 ± 2 |
| PLLA_POSS_4_40 | 331 | 369 | 87 ± 1 |
| PLLA_POSS_8_40 | 334 | 371 | 91 ± 2 |
| PLLA_POSS_4_60 | 341 | 374 | 91 ± 2 |
| PLLA_POSS_8_60 | 348 | 378 | 101 ± 1 |

In order to analyze the effect of the treatment on the surface wettability of the film, contact angle measurements were carried out. As previously mentioned, among various factors affecting the decomposition of PLA (which mostly occurs through hydrolysis of the backbone ester groups), the polymer reactivity with water and the accessibility of its ester groups to water were found to strongly determine the polymer degradation rate.[4] On this basis, considering that a modification of the surface wettability can directly lead to a change of the polymer hydrolytic decomposition, it is possible to infer that contact angle measurements can give significant information on the material behavior. Figure 2.7 showed the contact angle measurements of the samples as a function of the reaction conditions, namely the reaction temperature and time, and the results were also summarized in Table 2-2. The untreated PLLA film was found to be characterized by a contact angle of 71° ± 2°, which is similar to that reported in the literature for neat PLA.[18] It is clear that the treatment with the silsesquioxane

had leaded to an increase of the contact angle, which was found to be incrementally affected by the applied conditions, as this value increased by increasing the reaction time and temperature. In particular, the contact angle of the film treated for 8 h at 60 °C, namely PLLA_POSS_8_60, reached ca. 100°, which value proves the formation of a hydrophobic surface or might be related to an increase of the surface roughness. The influence of silsesquioxanes on surface properties was previously demonstrated for other POSS/polymer systems. Misra et al.[19] found an increase of surface hydrophobicity for PP/octaisobutyl-POSS nanocomposites with respect to the neat polymer matrix. While in a previous work of ours, the increment of contact angle was obtained for nanostructured films based on poly(styrene-co-maleic anhydride) and POSS.[16] These latter results were explained by considering the effect of the hydrophobic groups, linked to the silsesquioxane structure and the enhancement of surface roughness of the nanocomposite films. Also in our case, the increase of contact angle can be attributed to the hydrophobicity of POSS molecules, which, as previously demonstrated, turned out to be grafted to the polymer surface.

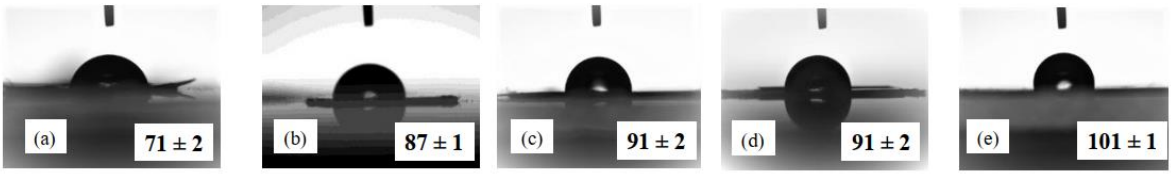


Figure 2.7 Water droplet placed on: (a) neat PLLA film, (b) PLLA_POSS_4_40 film, (c) PLLA_POSS_8_40 film, (d) PLLA_POSS_4_60 film and (e) PLLA_POSS_8_60 film.

The decomposition behavior of the PLA-based films was investigated by analyzing the macroscopic and microscopic morphology of films. Both neat and treated samples were put in contact with water at 50 °C. The evaluation of the degradation process by measuring the weight loss of the samples turned out to be difficult, as mainly for the neat PLLA films, a relevant loss of integrity appears already after 20 days and was totally broken into small pieces after 4 weeks in water at 50 °C, as shown in Figure 2.8. Contrarily, the films treated with POSS-$NH_2$, which were also kept in the same condition as the neat PLLA film (contact with buffer for 4 weeks at 50 °C), have maintained their dimensional integrity, showing a much

higher stability with respect to the neat PLLA film.

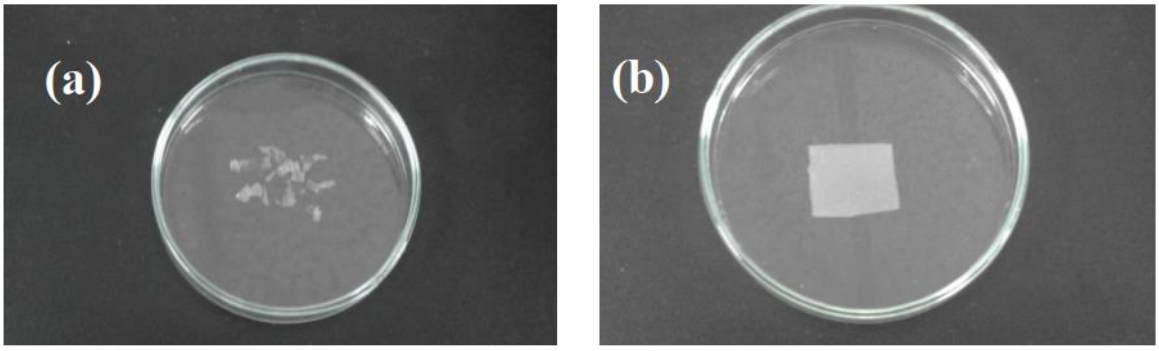


Figure 2.8 Photos of (a) PLLA film and (b) PLLA_POSS_8_60 film after being in contact with the buffer for 4 weeks at 50 °C.

The morphology of the degraded films was analyzed by means of FE-SEM measurements. Figure 2.9 shows the micrographs of the surfaces of the samples PLLA and PLLA_POSS_8_60, which were put in contact with the buffer at 50 °C for two and four weeks. While the surface of the neat films appeared to be homogeneous and uniform, significant changes were visible in the films which underwent a degradation process. The neat PLLA films showed the morphology typical of banded spherulites, which gave evidence of the presence of PLA crystallites,[20] while increasing the contact time the surface roughness and cracks seemed to increase (Figure 2.9c). This phenomenon is explained by considering that the hydrolysis of the film, which involves the amorphous fraction of the polymer and produces short chains, easily solubilized in water, making the crystalline structure become visible. In the case of the POSS-treated samples, although the degradation led to an increase of the surface roughness, the spherulite morphology was not visible. This finding demonstrates that the degradation mechanism of the films is significantly affected by the presence of the silsesquioxane. It is possible to infer that the POSS surface grafting limits the degradation of the polymer amorphous fraction, thus leading to an enhancement of the materials resistance.

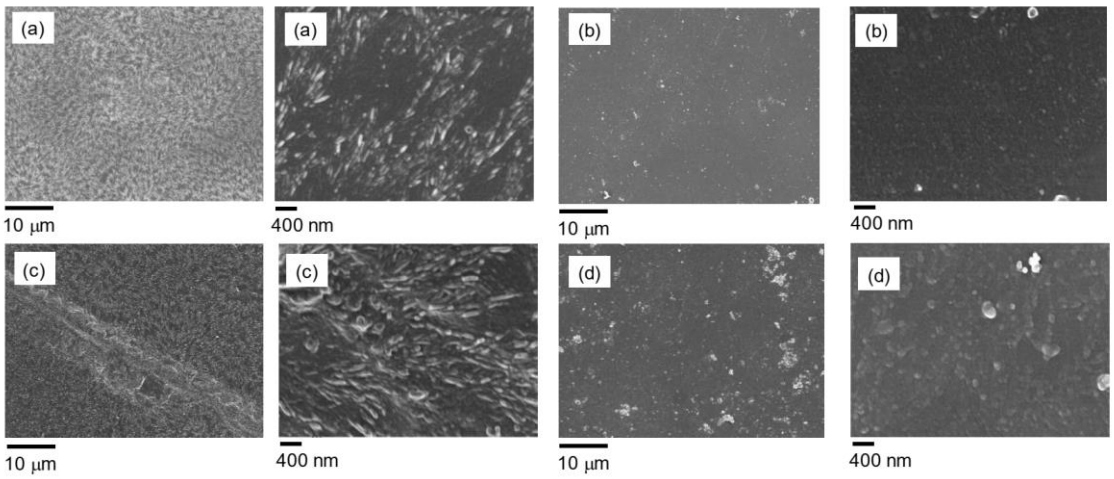


Figure 2.9 FE-SEM micrographs of: (a) neat PLLA film treated with the phosphate buffer solution at 50 °C for two weeks (left image at lower magnification, right image at higher magnification), (b) PLLA_POSS_8_60 film treated with the phosphate buffer solution at 50 °C for two weeks (left image at lower magnification, right image at higher magnification), (c) neat PLLA film treated with the phosphate buffer solution at 50 °C for four weeks (left image at lower magnification, right image at higher magnification), (d) PLLA_POSS_8_60 film treated with the phosphate buffer solution at 50 °C for four weeks (left image at lower magnification, right image at higher magnification).

## 2.4 Conclusions

This work demonstrated the effectiveness of the surface grafting of an amino-functionalized polyhedral oligomeric silsesquioxanes on improving the resistance to the hydrolytic degradation of poly(l-lactide) films. The developed method, which is simple and easily scalable, is based the aminolysis reaction between the amino group of the silsesquioxane and the polymer functionalities. The characterization measurements gave evidence of the POSS grafting occurrence as well as the increment of the surface hydrophilicity, which limited the hydrolytic degradation of the films.

# Reference

1. Garlotta, D., A Literature Review of Poly(Lactic Acid). *Journal of Polymers and the Environment* **2001,** *9* (2), 63-84.

2. Auras, R. A. L., L.T.; Selke, S.E.; Tsuji, H., Poly(lactic acid): Synthesis, Structures, Properties, Processing, and Applications; Part IV: Degradation and Environmental Issues. John Wiley & Sons: Hoboken: USA, 2010.

3. Elsawy, M. A.; Kim, K.-H.; Park, J.-W.; Deep, A., Hydrolytic degradation of polylactic acid (PLA) and its composites. *Renewable and Sustainable Energy Reviews* **2017,** *79*, 1346-1352.

4. de Jong, S. J.; Arias, E. R.; Rijkers, D. T. S.; van Nostrum, C. F.; Kettenes-van den Bosch, J. J.; Hennink, W. E., New insights into the hydrolytic degradation of poly(lactic acid): participation of the alcohol terminus. *Polymer* **2001,** *42* (7), 2795-2802.

5. Tsuji, H.; Ikada, Y., Properties and morphology of poly( l -lactide) 4. Effects of structural parameters on long-term hydrolysis of poly( l -lactide) in phosphate-buffered solution. *Polymer Degradation and Stability* **2000,** *67* (1), 179-189.

6. Iñiguez-Franco, F.; Auras, R.; Rubino, M.; Dolan, K.; Soto-Valdez, H.; Selke, S., Effect of nanoparticles on the hydrolytic degradation of PLA-nanocomposites by water-ethanol solutions. *Polymer Degradation and Stability* **2017,** *146*, 287-297.

7. Benali, S.; Aouadi, S.; Dechief, A.-L.; Murariu, M.; Dubois, P., Key factors for tuning hydrolytic degradation of polylactide/zinc oxide nanocomposites. *Nanocomposites* **2015,** *1* (1), 51-61.

8. Paul, M. A.; Delcourt, C.; Alexandre, M.; Degée, P.; Monteverde, F.; Dubois, P., Polylactide/montmorillonite nanocomposites: study of the hydrolytic degradation. *Polymer Degradation and Stability* **2005,** *87* (3), 535-542.

9. Jordá-Vilaplana, A.; Fombuena, V.; García-García, D.; Samper, M. D.; Sánchez-Nácher, L., Surface modification of polylactic acid (PLA) by air atmospheric plasma treatment. *European Polymer Journal* **2014,** *58*, 23-33.

10. Stoleru, E.; Dumitriu, R. P.; Munteanu, B. S.; Zaharescu, T.; Tănase, E. E.; Mitelut, A.; Ailiesei, G.-L.; Vasile, C., Novel procedure to enhance PLA surface properties by chitosan irreversible immobilization. *Applied Surface Science* **2016,** *367*, 407-417.

11. Moraczewski, K.; Rytlewski, P.; Malinowski, R.; Żenkiewicz, M., Comparison of some effects of modification of a polylactide surface layer by chemical, plasma, and laser methods. *Applied Surface Science* **2015,** *346*, 11-17.

12. Zhu, Y.; Mao, Z.; Gao, C., Aminolysis-based surface modification of polyesters for biomedical applications. *RSC Adv.* **2013,** *3* (8), 2509-2519.

13. Monticelli, O.; Putti, M.; Gardella, L.; Cavallo, D.; Basso, A.; Prato, M.; Nitti, S., New Stereocomplex PLA-Based Fibers: Effect of POSS on Polymer Functionalization and Properties. *Macromolecules* **2014,** *47* (14), 4718-4727.

14. Zhou, H.; Ye, Q.; Xu, J., Polyhedral oligomeric silsesquioxane-based hybrid materials and their

applications. *Materials Chemistry Frontiers* **2017,** *1* (2), 212-230.

15. Forouharshad, M.; Putti, M.; Basso, A.; Prato, M.; Monticelli, O., Biobased System Composed of Electrospun sc-PLA/POSS/Cyclodextrin Fibers To Remove Water Pollutants. *ACS Sustainable Chemistry & Engineering* **2015,** *3* (11), 2917-2924.

16. Monticelli, O.; Fina, A.; Cozza, E. S.; Prato, M.; Bruzzo, V., POSS vapor phase grafting: a novel method to modify polymer films. *Journal of Materials Chemistry* **2011,** *21* (44).

17. Zhang, W.; Camino, G.; Yang, R., Polymer/polyhedral oligomeric silsesquioxane (POSS) nanocomposites: An overview of fire retardance. *Progress in Polymer Science* **2017,** *67*, 77-125.

18. Monticelli, O.; Bocchini, S.; Gardella, L.; Cavallo, D.; Cebe, P.; Germelli, G., Impact of synthetic talc on PLLA electrospun fibers. *European Polymer Journal* **2013,** *49* (9), 2572-2583.

19. Misra, R.; Fu, B. X.; Morgan, S. E., Surface energetics, dispersion, and nanotribomechanical behavior of POSS/PP hybrid nanocomposites. *Journal of Polymer Science Part B: Polymer Physics* **2007,** *45* (17), 2441-2455.

20. Sun, G.; Weng, L.-T.; Schultz, J. M.; Chan, C.-M., Formation of banded and non-banded poly(l-lactic acid) spherulites during crystallization of films of poly(l-lactic acid)/poly(ethylene oxide) blends. *Polymer* **2014,** *55* (7), 1829-1836.

# 3 Graphite oxide nanocoating as a sustainable route to extend the applicability of biopolymer-based film

## 3.1 Introduction

The challenge for the large-scale exploitation of polymers from renewable resources, as alternative to fossil based polymers, is mainly related to their production costs and properties.[1] On this basis, the methods applied for improving their characteristics or disclosing new properties have to take into account the economic impact while maintaining the "bio" nature of the material.[1] One of the most promising and widely applied biopolymers is polylactic acid (PLA), which is mainly used as packaging material.[2, 3] However, the exploitation of PLA is limited in applications requiring high gas barrier or antistatic properties. In order to improve PLA barrier properties different strategies, based mainly on the bulk inclusion of organic or inorganic additives, have been developed aiming at creating tortuous paths capable of slowing down diffusing gas molecules.[2, 3] On the other hand, antistatic properties are traditionally obtained by the bulk inclusion of organic antistatic agents, which form electrostatic discharge channels upon migration onto the surface and by absorbing moisture.[4, 5] A relevant drawback of this method is that long-term antistatic effects cannot be maintained due to additive loss from the polymer surface.[6] In order to solve this issue, carbon materials,[7] metals[8] and more recently graphite/graphene[9, 10] were employed as conductive additives. Indeed, these fillers may be added to the polymer matrix by different methods to confer electrical conductivity properties as long as their concentration is high enough to produce conduction pathways.[11] Unfortunately, the formation of efficient tortuous paths or conducting percolated networks is strictly related to the filler optimal dispersion within the polymer matrix, which is typically challenging. To improve particles dispersion, a chemical modification may be exploited to improve compatibility with the polymer.[12] However, this implies laborious and not always environmental friendly processes. In addition, the additives added to the pristine polymer to enhance gas barrier and/or surface electrical conductivity usually reduce the transparency of

the resulting composite/nanocomposite films. It is thus apparent that the development of biopolymer films suitable to be used in the gas barrier/antistatic packaging fields should take into account several issues. In this context, the use of an approach capable of producing films characterized by high transparency, low gas permeability and good antistatic properties while maintaining the sustainable features of the polymer would allow for a step forward in the exploitation of biopolymers. From this point of view, the use of the Layer-by-Layer (LbL) assembly as surface nano-structuring tool represents an ideal solution. Indeed, the LbL technique offers several advantages such as: coating design freedom, green features and the possibility to use conducting carbon-based material as layer components.[13] As far as PLA is concerned, the LbL was mainly applied in the biomedical field.[14, 15] Carbon based materials can be easily incorporated into LbL coatings targeting gas barrier or electrical properties.[16-18] For example, graphite oxide (GO) has been recently employed in combination with positively charged polyelectrolytes.[16] Indeed, GO is negatively charged in aqueous solution because of its functional groups such as carboxylic acid and phenolic hydroxyl groups.[17] Chemical reduction and annealing post treatments can be employed in order to recovery the electrical properties of the LbL assembled multilayered GO films.[18] It was found that, in reduced GO LbL films, both the sheet resistance and the optical transmittance can be effectively controlled by changing the number of bi-layers. Thus, in the present work, focusing on the development of poly(L-lactide) (PLLA) films applicable in the field of antistatic packing, we applied the LbL process as an environmental friendly method capable of maintaining the bulk properties of the biopolymer while modifying its surface. To the best of the authors' knowledge, this manuscript represents the first attempt employing the LbL in order to produce antistatic PLA. To this aim, positively charged chitosan (CH) or branched polyethylenimine (BPEI) have been coupled with graphite oxide (GO) in a LbL fashion.

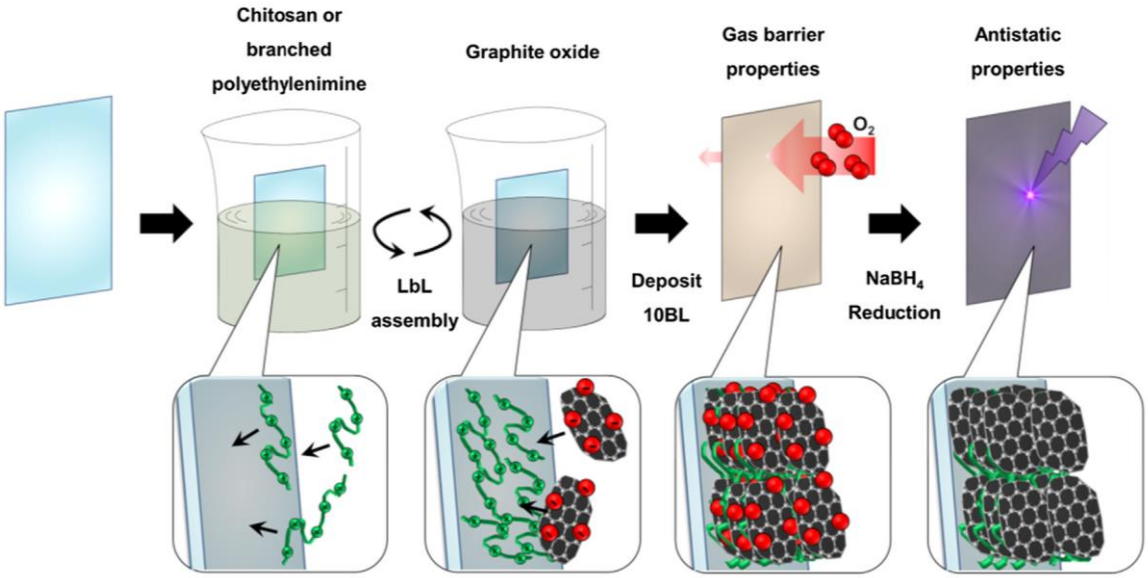


Figure 3.1 Scheme of the Layer-by-layer deposition procedure.

In the assembly, BPEI and CH have been selected as positive counterparts due to their peculiar features when employed in LbL assemblies. BPEI is well known for its good adhesion properties and stable coating growth.[19] On the other hand, CH represents a green polysaccharide which efficiency in the build-up of efficient gas barrier coatings has been already demonstrated.[20] A comparison between the two systems would allow for the selection of the optimal solution based on coating growth and performances. In order to maintain the procedure as sustainable as possible the deposition process was performed in water and the subsequent GO reduction was accomplished by water-soluble reducing agent. The characteristics of the modified films, in terms of morphology, wettability, permeability and surface electrical conductivity, were studied as function of the number of deposited bilayers and the type of positive polyelectrolyte.

## 3.2 Materials and methods

### 3.2.1 Materials

Poly (L-lactide) (PLLA) is a commercial product purchased from Nature Works Co. Ltd. U.S.A. (2002D, Mn = 100.000 g/mol) with a residual monomer content less than 0.3% by mass. Dichloromethane, sodium borohydride ($NaBH_4$), branched poly(ethyleneimine) (BPEI,

Mw ~ 25.000 g/mol) and chitosan (CH, Mw ~ 190.000–310.000 g/mol) were purchased from Sigma-Aldrich. Graphite oxide (GO), as 1 wt.% suspension in water, was purchased from AVANZARE Innovacion Tecnologica (Navarrete-La Rioja, Spain). Solutions and suspensions employed were prepared using ultrapure water having a resistance of 18.2 MΩ, supplied by a Q20 Millipore system (Milano, Italy). Single side polished (1 0 0) silicon wafer was used to study the growth of the layers. BPEI solution had a solid content of 1 wt.% and chitosan 0.5 wt.%; the pH was kept unmodified for BPEI while it was adjusted to 4 with 0.25 wt.% of acetic acid for chitosan.

### 3.2.2 PLLA film preparation and LbL deposition on films

Films were obtained by solubilizing PLLA pellets at a final concentration of 0.5 wt.% in dichloromethane. The obtained PLLA solution (10 mL) was then casted in a Petri dish (10 cm diameter) and dried in air to remove the solvent. Then, the solidified films were further dried in a vacuum oven for 4 h at 40 °C and 4 h at 80 °C. Finally, the films were cut into squares of size 3.5 × 3.5 $cm^2$ to be used for the LbL deposition. As shown in Figure 3.1, PLLA films were alternately immersed into negatively and positively charged suspensions. The first immersion period for the BPEI activation layer was set at 20 min, in order to promote the homogeneous growth of the subsequent BPEI/GO bi-layer (BL). The subsequent layers were obtained with 4 min of dipping. After each immersion step, the film was washed with deionized water for 1 min to remove the excess of ionic species and dried by a flow of compressed air. The process was repeated until films characterized by a different number of BL (5, 10 and 15) were prepared. The same procedure was applied for the LbL deposition based on CH. The samples are coded by the type and the number of BL (as an example: PLLA_BPEI_GO_15 indicates 15 BL of BPEI and GO onto PLLA).

$NaBH_4$ solution in water with a concentration of 0.1 mol/L was used for the reduction of GO-based films (GOr in the code of the films). The films were dip in 20 mL of the above solution for two hours at room temperature, then they were extensively washed and finally dried in

vacuum overnight at 40 °C.

Si wafers employed to monitor the coating growth were alternately dipped into solutions of positively charged polyelectrolytes (BPEI or CH) and negatively charged (GO) in order to deposit a coating consisting of 10 BL repetitive unit, following the totally same procedures as used for PLLA films. Infrared spectroscopy measurement was performed after each BL deposition to monitor the growth of the signals belonging to GO.

## 3.3 Characterization

Fourier Transform Infrared (FT-IR) spectroscopy was used to monitor the growth of the LbL assembly using a Perkin Elmer Frontier FT-IR/FIR spectrophotometer (16 scans and 4 $cm^{-1}$ resolution). IR spectra were acquired after each deposition step.

A Zeiss Supra 40 VP field emission scanning electron microscope (FE-SEM) equipped with a backscattered electron detector was used to examine the composite morphologies. The samples were sputter-coated with a thin carbon layer using a Polaron E5100 sputter coater.

Contact angle measurements were carried out by a Basler as A780 contact angle analyzer, using the sessile drop method, and the Oneattension software at a minimum of 2 different locations for each film.

Oxygen and water vapor permeability measurements were performed using an Extraperm apparatus (Extra Solutions, Italy). The test were performed at 23 °C in dry (0% R.H.) and humid (50% R.H) conditions for oxygen permeability while water vapor permeability was assessed at 23 °C and 50% R.H. Due to the small size of the prepared films, the samples were tested using an aluminum mask to reduce the exposed area to 2.0 $cm^2$.

Conductivity tests, which were performed accordingly with the ASTM D257 method, were carried by applying a picoammeter (Keithley) and by using films of 1 × 1 cm (with a thickness of ca. 100 μm). The instrument was zeroed before the 300 V voltage application. Two rectangles of silver glue (3 × 8 mm), spaced 3 mm apart, were deposited on the films in order to form the electrical contact. The surface resistivity ($\rho_s$) was calculated by applying the

following equation:

$\rho_s = R_s P/G$: where $R_s$ is the surface resistance, P is the perimeter of electrodes and G is the gap between electrodes.

## 3.4 Results and discussion

In this work, the surface modification of poly(L-lactide) (PLLA) films was performed by applying the Layer by Layer (LbL) technique and by using two types of positively charged polyelectrolytes, chitosan (CH) and branched polyethylenimine (BPEI). Indeed, these molecules, holding amino groups and being positively charged, are potentially capable of interacting with the surface of PLLA as well as of promoting the GO deposition. The concentrations of CH and BPEI were chosen on the basis of the conditions reported in the literature and on their solubility.[21, 22]

The coating growth was monitored by IR spectroscopy. The spectra of neat CH, neat BPEI and GO are reported in Figure 3.2. The IR spectrum of CH (Figure 3.2a) shows peaks at approximately 3380 and 3296 $cm^{-1}$ associated to O-H and N-H stretching, while signals at 2922, 2868, 1406 and 1320 $cm^{-1}$ were assigned to C-H bond.[21] The sharp peak at 1578 $cm^{-1}$ and the shoulder at 1636 $cm^{-1}$ can be attributed to asymmetric and symmetric stretching vibration mode of the protonated amine $NH3^+$. The latter signal is also ascribed to O-H stretching vibration in residual water. The peaks at 1070 and 1140 $cm^{-1}$ were assigned to pyranose rings and amino groups. BPEI shows a similar spectrum (Figure 3.2b) with bands at 3320 (N-H stretching), 2947, 2832, 1466 and 1299 $cm^{-1}$ (C-H bond), 1555 $cm^{-1}$ (N-H bending), 1405 and 1031 $cm^{-1}$ (C-N stretching).[22] Neat GO (Figure 3.2c) shows a broad band at 3346 $cm^{-1}$ which can be assigned to the stretching mode of O-H group. The main signals are related to COOH functional groups and are found at 1616 and 1410 $cm^{-1}$ for the deprotonated form COO- (asymmetric and symmetric stretching, respectively) and 1704 $cm^{-1}$ for C=O in the undissociated form. The peaks at 1194 and 1038 $cm^{-1}$ may be attributed to C-OH and C-O, respectively.[23]

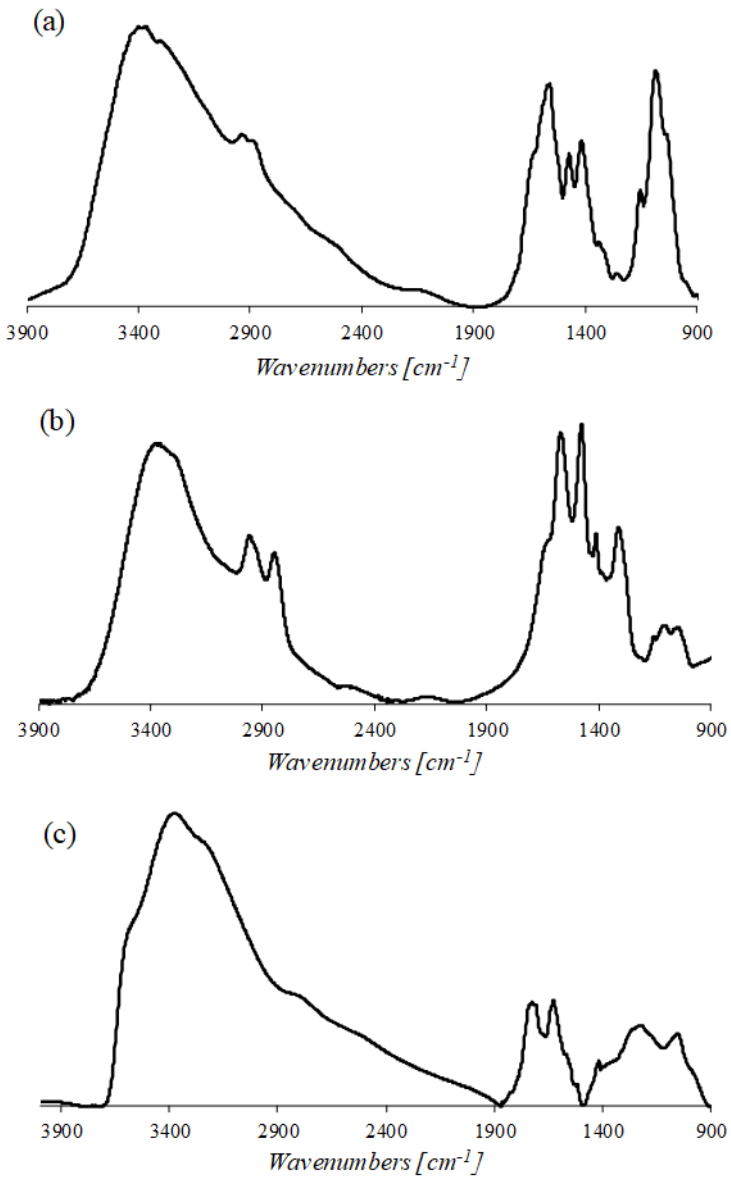


Figure 3.2 FT-IR spectra of: (a) CH, (b) BPEI and (c) GO.

The LbL assemblies of the CH/GO and BPEI/GO systems on model silicon substrate are reported as 3D plot in Figure 3.3, along with the evolution in absorbance for selected functional groups as a function of deposited BL number (Figure 3.4) and the SEM images of the cross sections of 10 BL coatings (Figure 3.5). As far as CH/GO is concerned, the characteristic signals of both components can be found at 1115, 1185, 1288, 1495 and 1701 $cm^{-1}$. In particular, the signals at 1631 and 1731 $cm^{-1}$ (related to GO) turned out to grow proportionally to the number of deposited BL (Figure 3.4a), thus confirming the occurrence

of a LbL assembly, in agreement with what previously reported in the literature.[24] In the case of the films based on BPEI (Figure 3.3b), the observed signals appear more intense with respect to CH/GO. In particular, the characteristic peaks associated to dissociated carboxylic groups on GO are well visible at 1631 and 1388 $cm^{-1}$ (asymmetric and symmetric stretching, respectively). These signals appear more intense with respect to those found in neat GO and CH/GO assembly. This is explained by considering that the ionization degree of GO carboxyl groups is pH dependent. Indeed, while for neat GO and CH/GO IR spectra are collected after adsorption from acidic pH, during BPEI adsorption the adsorbed GO is exposed to basic pH values (pH = 9–10) that promote the dissociation of carboxyl groups.[19, 25]

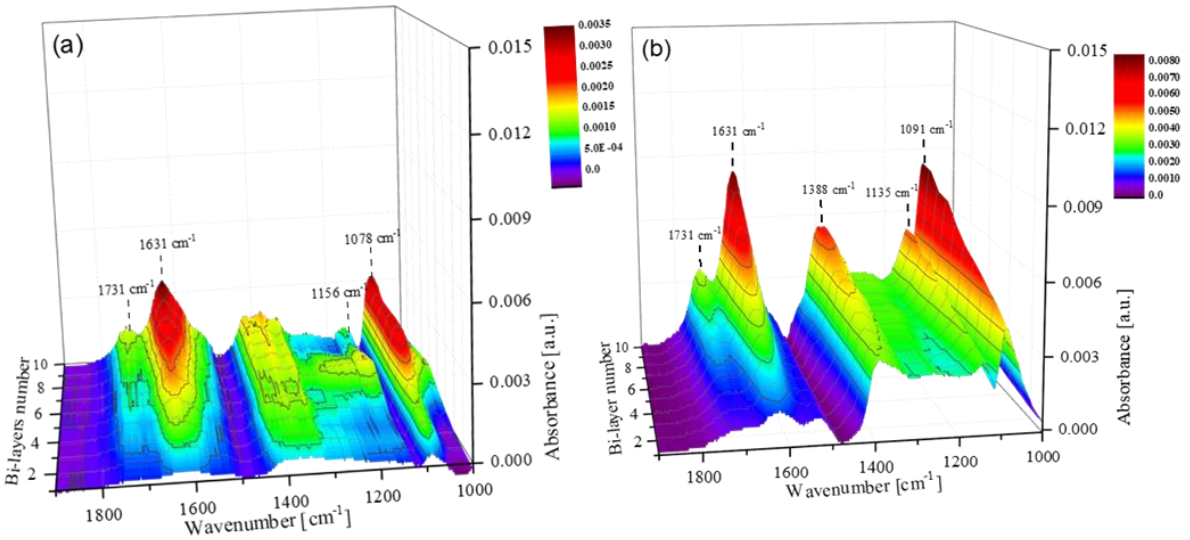


Figure 3.3 Coating growth as a function of each deposited BL by infrared spectroscopy of restricted IR region between 1000 and 2000 $cm^{-1}$ of: (a) CH/GO and (b) BPEI/GO on model silicon surface.

In the final LbL assembly, this phenomenon results in a strong increase of the signals associated to COO- and a decrease of the COOH peak. In addition, the signals related to COO- show a shift with respect to neat GO; this is ascribed to the interaction of the functional group with the BPEI protonated amines and further highlights the occurrence of a LbL deposition through electrostatic interactions. As observed for the CH-based system, the peaks characteristic of GO linearly increased as function of BL number (Figure 3.4b).

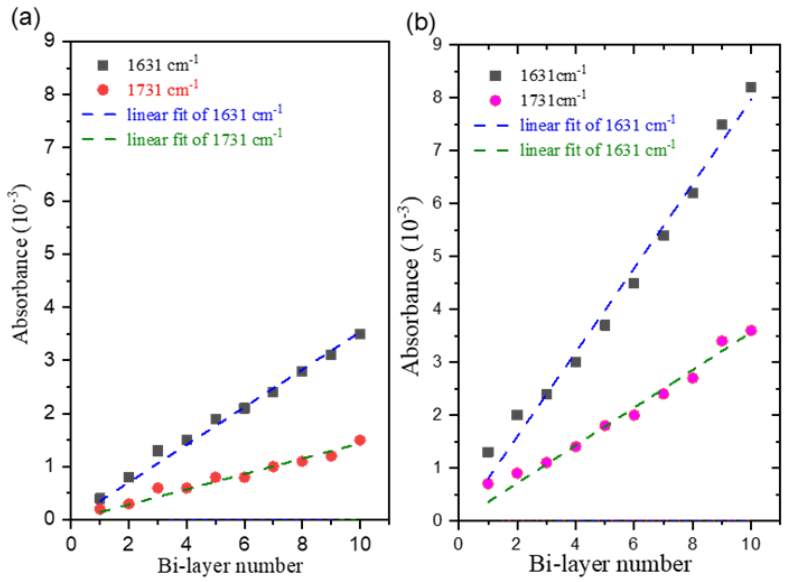


Figure 3.4 Evolution of the IR signals at 1631 and 1731 $cm^{-1}$ as function of bi-layer number of: (a) CH/GO and (b) BPEI/GO.

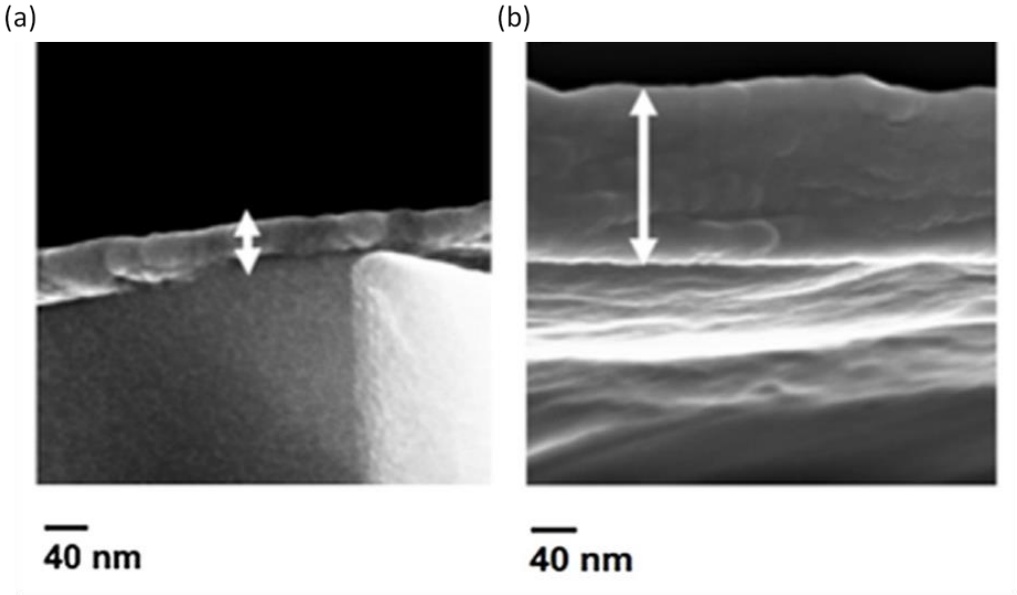


Figure 3.5 SEM micrographs of the cross section of the 10 BL coating deposited on silicon wafer of: (a) of CH/GO and (b) BPEI/GO.

The remarkable difference in intensity at 10 BL between the two systems suggests that BPEI/GO grows thicker than CH/GO. This is further confirmed by FE-SEM observations performed on the cross-section of 10 BL assemblies (Figure 3.5) where thicknesses of 40 and 200 nm were evaluated for CH- and BPEI-based systems, respectively. This can be ascribed to the different nature of the employed polycations. Indeed, as previously commented, BPEI

is well known for its good adhesion and coating growth promoting properties; in addition, the change of local pH during the assembly also plays a crucial role as also demonstrated for other BPEI LbL assemblies.[19]

During BPEI adsorption the increased dissociation of GO carboxyl groups in the previously adsorbed layer results in an increased negative charge to be compensated. Similarly, the acidic pH of GO suspension improves the protonation degree of BPEI and results in more GO adsorbed. Such phenomena do not occur in the CH-based assembly due to the acidic pH of the chitosan solution and limit the amount of adsorbed CH and GO at each deposition step thus resulting in a thinner coating with respect to BPEI as also demonstrated by SEM observations in Figure 3.5. The influence of the treatment on the film wettability was studied by static contact angle measurements on neat PLLA and films treated by a different number of deposition BL (Figure 3.6). The values obtained are summarized in Table 3-1.

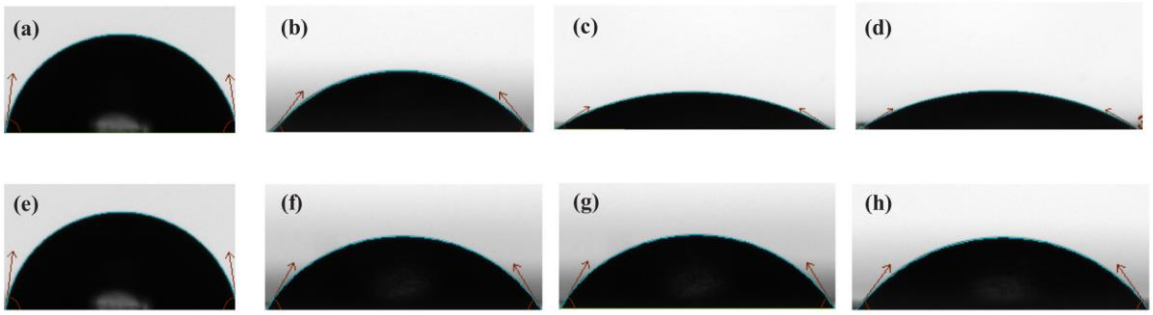


Figure 3.6 Water contact angle images of: (a) PLLA, (b) PLLA_BPEI_GO_5, (c) PLLA_BPEI_GO_10, (d) PLLA_BPEI_GO_15, (e) PLLA, (f) PLLA_CH_GO_5, (g) PLLA_CH_GO_10 and (h) PLLA_CH_GO_15.

Table 3-1 Contact angle of the neat PLLA film and of the LbL treated films.

| Sample code | Contact angle (°) | Sample code | Contact angle (°) |
|---|---|---|---|
| PLLA | 80.6 ± 0.2 | PLLA | 80.6 ± 0.2 |
| PLLA_BPEI_GO_5 | 50.5 ± 0.3 | PLLA_CH_GO_5 | 59.6 ± 0.3 |
| PLLA_BPEI_GO_10 | 31.7 ± 0.5 | PLLA_CH_GO_10 | 59.6 ± 0.1 |
| PLLA_BPEI_GOr_10 | 68.3 ± 0.5 | PLLA_CH_GOr_10 | 77.0 ± 0.3 |
| PLLA_BPEI_GO_15 | 30.2 ± 0.5 | PLLA_CH_GO_15 | 54.8 ± 0.1 |

The neat PLLA film (Figure 3.6a and 3.6e) was found to hold a contact angle of ca. 80°, in agreement with the data reported in the literature.[26] The deposition of a single layer of BPEI or CH did not produce a significant modification of the material wettability and the measured contact angles (85° for CH based film and 78° for BPEI based film) were in agreement with previous reports for the two neat polymers.[27, 28] On the contrary, the deposition of an assembly containing GO resulted in a reduction of the contact angle, which value turned out to decrease by increasing the number of the deposition BL. This was more relevant for BPEI-based assemblies. Indeed, in the case of CH, the maximum contact angle after15 BL was 54.8° while for PLLA_BPEI_GO_15 reached 30.2°.

Wettability data for systems containing GO, either on the surface or in the bulk, are reported in the literature.[28-32] In the case of bulk addition of GO within a polymer, the wettability turned out to depend on the matrix characteristics, the GO concentration and its functionalization.[28] The presence of GO typically resulted in hydrophilic surfaces, with water contact angles smaller than or equal to 45°.[30-33] Nevertheless, different aspects have to be taken into account. Indeed, when GO is deposited on a surface, as in the case of our systems, the substrate effect as well as the homogeneity of the deposition might influence the surface wettability. Moreover, as previously mentioned, the characteristics of graphene oxide, in terms of its functionalization degree, was found to affect the contact angle values. On the basis of these aspects, it is possible to hypothesize that by increasing the number of the deposition layers, the homogeneity of the deposited coatings increases. Indeed, as reported in Table 3-1, the variation of the contact angles turned out to decrease by increasing the number of deposition BL and reached a plateau after 10 BL. The different values between CH- and BPEI-based systems can be ascribed to the different contributions of the employed polycations and the different percentage of ionized groups/ionic bonds in the final assembly as evaluated by IR spectroscopy. This choice was mainly related to the need to keep the developed approach as simple as possible in order to make it more easily applicable. In this light, it is desirable to use as few depositions as possible.

On this basis, considering the slight difference between 10 and 15 BL, only 10 BL coatings were further investigated. Moreover, also the different wettability obtained by using the two types of polycations might be explained by taking into account the morphology of the deposition, which should depend on the specific interactions of the molecules with the polymer surface and with GO. In order to assess the film morphology, both optical microscopy and FE-SEM measurements were carried out. The photos of the neat and the 10 BL treated films, are reported in Figure 3.7. The above images evidenced for the formation of a homogeneous coating at micron scale, highlighting the presence of GO nanoplatelets of variable dimensions.

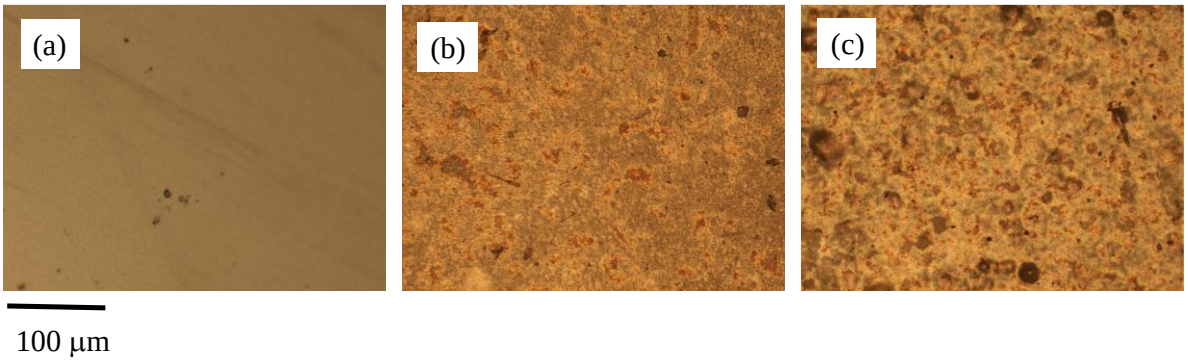


Figure 3.7 Optical images of: (a) neat PLLA film, (b) PLLA_CH_GO_10 and PLLA_BPEI_GO_10.

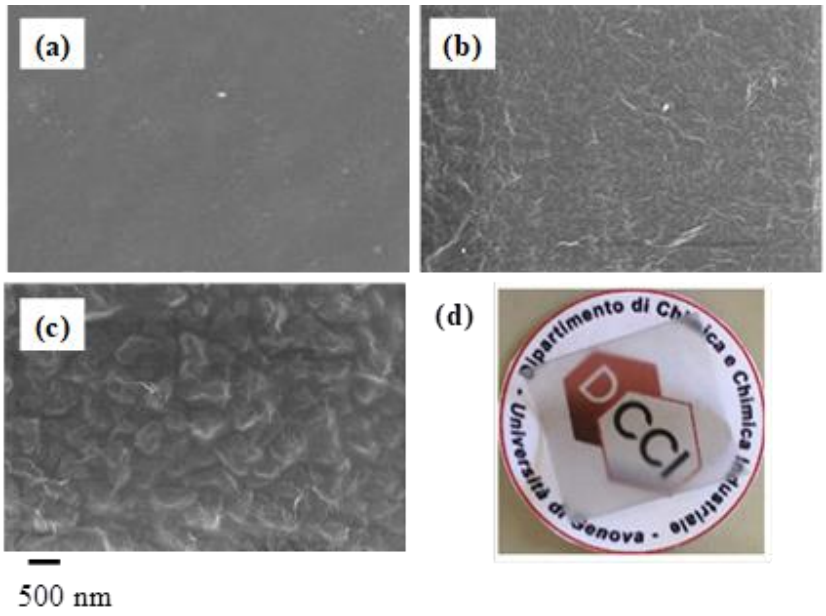


Figure 3.8 SEM micrographs of: (a) PLLA, (b) PLLA_BPEI_GO_10 and (c) PLLA_CH_GO_10. (d) Photograph of PLLA_BPEI_GO_10 film after reduction.

FE-SEM micrographs of 10 BL samples (Figure 3.8) evidenced a wrinkled morphology typical of GO-based coatings while showing further differences in the two film surface morphologies. Indeed, while the film based on BPEI (Figure 3.8b) was characterized by a rather flat and a homogenous GO layer, the one prepared by using chitosan (Figure 3.8c), displayed a much higher roughness. As previously mentioned, one key feature for the films applicability is related to their transparency. Digital images of the films after the reduction treatment highlight the characteristic black color typical of graphite while also showing a good transparency of the LbL treated film (Figure 3.8d). This demonstrates that, conversely to bulk modification, this LbL treatment allows to maintain a fairly good transparency of the coated film.

With the aim at obtaining films characterized by surface electrical conductivity, the GO deposited on the surface of the PLLA films was reduced by sodium borohydride ($NaBH_4$).[18] As reported in the literature, contact angle measurements can give evidence of the reducing occurrence by showing a decreased wettability.[18] For example, in the case of GO nanopaper, the contact angle increased from 45.1° to 67.3° after aluminum reduction at 100-200 °C.[28] Similarly, Some et al.[34] described a reduction treatment under light exposure based on sodium benzophenone or sodium benzophenone in the presence of hydrazine, which increased the contact angle of GO films from 48.3° to 98.9°. As far as samples prepared in this work are concerned, values reported in Table 3-1 and images in Figure 3.9 clearly show an increase in contact angle for 10 BL films after reduction. This was more apparent for BPEI/GO system that displayed an overall increase of 38.1° with respect to the 17.7° increase measured for CH/GO. By comparing these values with those reported in the literature, it is possible to infer that the applied reduction treatment, although based on mild conditions, leaded to a relevant increase of the surface hydrophobicity thus indicating a significant degree of reduction. The reduction of GO was also evaluated by means of IR spectroscopy (Figure 3.10). Only the BPEI/GO sample was evaluated as in the case of CH the presence of the oxygen contained in the polymer chemical structure might affect the results of the measurements. By comparing

the spectra before and after reduction, it is possible to observe a decrement of the absorption bands at 1700 $cm^{-1}$ and at 1100 $cm^{-1}$, which can be related to the oxygen-based groups. This further confirms the occurrence of the reduction reaction.

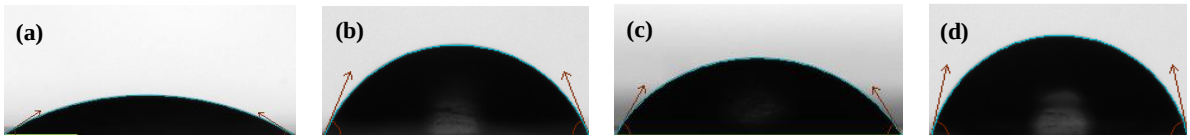


Figure 3.9: Water contact angle images of: (a) PLLA_BPEI_GO_10, (b) PLLA_BPEI_GOr_10, (c) PLLA_CH_GO_10 and (d) PLLA_CH_GOr_10.

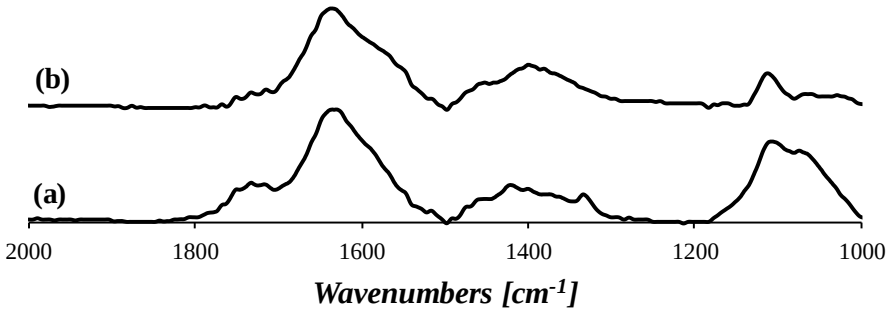


Figure 3.10 FT-IR spectra of: (a) 10 BL of BPEI/GO deposited on silicon wafer before reduction and (b) 10 BL of BPEI/GO deposited on silicon wafer after reduction.

The barrier and permeability performances of PLA films have been widely studied because of the relevant impact of these features on the material applications.[35, 36] Oxygen barrier properties in dry and humid conditions as well as water vapor permeability have been evaluated for neat PLLA and 10 BL treated films (Figure 3.11 and Table 3-2).

A common approach to improve PLA gas barrier properties is represented by the bulk inclusion of layered silicates that normally results in a 50% reduction in oxygen permeability but also shows negative impact on the optical properties.[35, 36] A more efficient approach is based on the LbL deposition of clay, which was found to decrease the oxygen permeability by 96%.[37] In this work, the films treated with BPEI/GO showed a 70% reduction of the oxygen permeability both at low and at high relative humidity (RH). Such results can be ascribed to the well-known LbL brick and mortar structures where nanoplatelets are oriented parallel to the film surface and perpendicular to the gas flux. This creates a tortuous path towards the molecules of the permeating gas thus resulting in improved barrier performances.

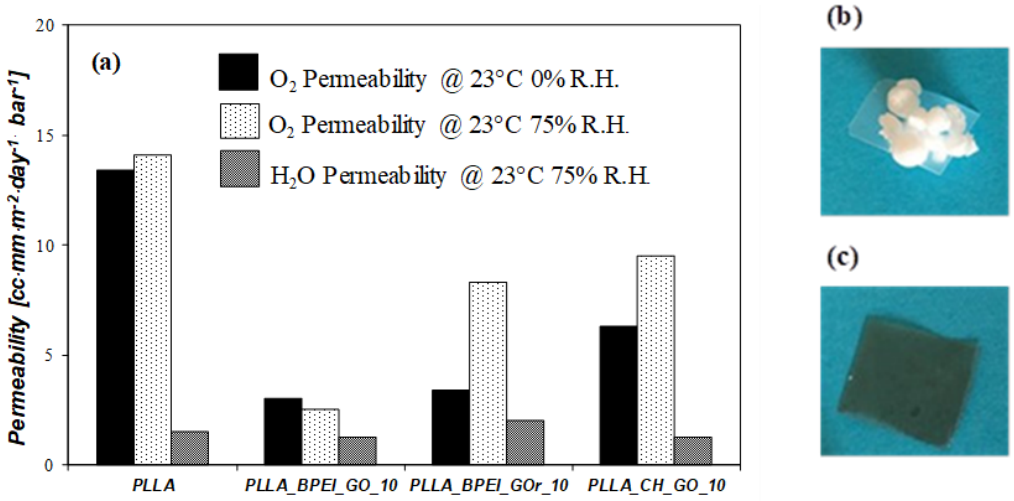


Figure 3.11 (a) $O_2$ and $H_2O$ permeability of: PLLA, PLLA_BPEI_GO_10, PLLA_BPEI_GOr_10 and PLLA_CH_GO_10, photos of: (b) PLLA and (c) PLLA_BPEI_GOr_10 films after being rubbed with a woolen cloth and putted in contact with polystyrene particles.

Table 3-2 Oxygen and water permeability of the neat PLLA and of the LbL treated films.

| | $O_2$ Permeability [cc•mm•m$^{-2}$•day$^{-1}$•bar$^{-1}$] @ 23°C 0% RH | $O_2$ Permeability [cc•mm•m$^{-2}$•day$^{-1}$•bar$^{-1}$] @ 23°C 75% RH | $H_2O$ Permeability [g•mm•m$^{-2}$•day$^{-1}$•bar$^{-1}$] @ 23°C 75% R.H. |
|---|---|---|---|
| PLLA | 13.4 ± 4.0 | 14.1 ± 3.6 | 1.5 ± 0.4 |
| PLLA_BPEI_GO_10 | 3.0 ± 0.3 | 2.5 ± 1.0 | 1.3 ± 0.2 |
| PLLA_BPEI_GOr_10 | 3.4 ± 0.3 | 8.3 ± 2.4 | 2.0 ± 0.1 |
| PLLA_CH_GO_10 | 6.3 ± 1.1 | 9.5 ± 0.6 | 1.3 ± 0.4 |

The performed reduction treatment leads to an increase of the permeability, which increment resulted to be slight at low RH and relevant only at high RH. On the other hand, CH/GO films showed a more limited decrease of the permeability. This finding is in agreement with the previous characterization that provided evidence of the formation of a thinner and rougher deposition layer for the chitosan-based films. The obtained results have been compared with previous works dealing with PLA films modified for improved barrier properties. To this aim, LbL surface modification and bulk nanocomposites approaches have been considered.[20, 37-41] A detailed permeability values in dry and humid conditions from various literatures are summarized and reported in Table 3-3. As far as LbL assemblies are concerned, it is possible

to observe that relevant reductions in permeability were achieved only after depositing either 30–70 BL or 10 quad-layers (QL).

Table 3-3 Oxygen permeability values of PLA films from various literatures.

| | $O_2$ Permeability @ 23°C 0% RH [cc•mm•m$^{-2}$•day$^{-1}$•bar$^{-1}$] | $O_2$ Permeability @ 23°C 50% RH [cc•mm•m$^{-2}$•day$^{-1}$•bar$^{-1}$] |
|---|---|---|
| CHI/HMMT-LbL[37] | N.A | 0.635 |
| CHI/MMT-LbL[22] | 1.2 (10BL) | N.A |
| BPEI/NFC-LbL[38] | N.A | 5.5 (20BL), 1.02 (50BL) |
| BPEI/CMC-LbL[38] | N.A | 5.8 (20BL), 1.26 (50BL) |
| BPEI/NF-LBL[9] | 11.4 | 10.5 |
| BPEI/NF/BPEI/MMT-LbL[9] | 2.1 (6QL), 0.25 (10QL) | 3.2 (6QL), 0.5 (10QL) |
| PLA/NFNS composite[10] | 4.72 | N.A. |
| PLA/EFNS composite[10] | 2.03 | N.A. |
| PLA/AFMMT composite[10] | 8.81 | N.A. |
| PLA/ EFMMT composite[10] | 8.63 | N.A. |
| PLA/OMM composite[41] | N.A. | 10.7 (5%wt), 9.4 (10%wt) |

N.A. Not Available, HMMT: homogenized montmorillonite, NFC: nano-fibrillated cellulose, CMC: carboxymethyl cellulose, QL: quad-layer, NF: nafion, NFNS: amino functionalized nano-silica, EFNS: epoxy functionalized nano-silica, AFMMT: amino functionalized MMT, EFMMT: epoxy functionalized MMT, OMM: organic-modified mica.

The results obtained in this work with 10 BL of BPEI/GO are in the same range of a 10 BL coating comprising chitosan and montmorillonite[20] and superior to previously developed systems based on BPEI coupled with either cellulose nanofibrils or carboxymethyl cellulose.[38] On the other hand, permeability values similar to 10 BL of BPEI/GO can be achieved by bulk nanocomposites prepared by in situ polymerization of L-lactide in the presence of functionalized nanoparticles followed by solvent casting from chloroform.[40] However, this latter approach appears less practical and more complicated than the surface nano-structuration proposed in this manuscript. The effect of the surface treatment on the antistatic properties of the films was evaluated by measuring the surface resistivity of the optimal

formulation based on BPEI and by employing a practical method. Considering the Figure 3.10b and 3.10c resulted from the procedures exhibited in Figure 3.12, it is apparent that the neat PLLA film, after being charged, was capable of attracting the polystyrene particles, while the coated PLLA did not retain those.

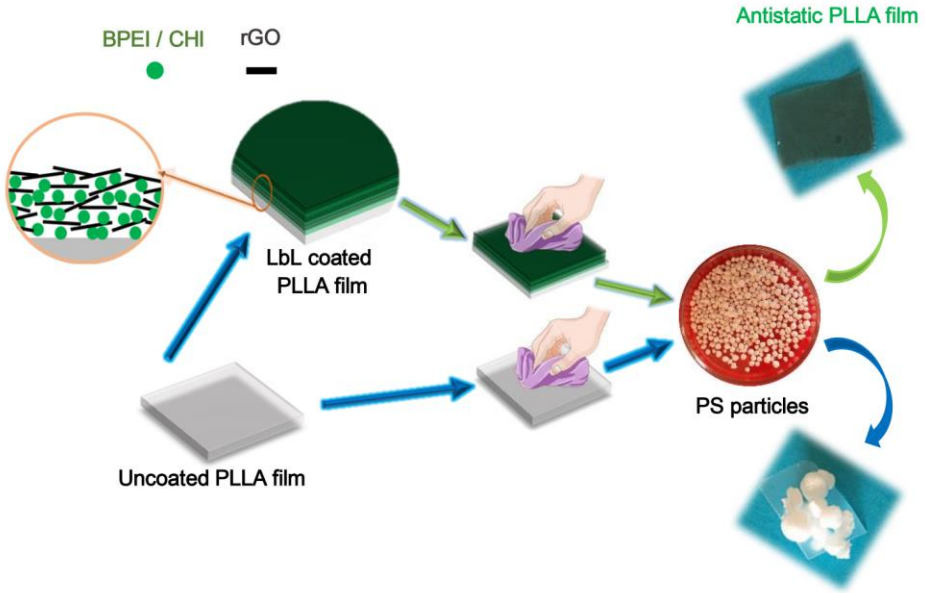


Figure 3.12 Comparison of antistatic properties of the neat PLLA and reduced LBL coated PLLA films.

Although the above method is very simple, it gives a preliminary indication of the antistatic features of the treated films, it has been widely used for industrial applications. A quantification of the effect of the coating was evaluated by accomplished surface resistivity ($\rho_s$) measurements by using a picoammeter. Indeed, a decrease of the film surface resistivity from $6.3 \times 10^{12}$ Ohms/square for PLLA film to $7.3 \times 10^{11}$ Ohms/square for PLLA_BPEI_GOr_10 was found. Although the above decrement is not as high as those reported in the literature for other systems,[9] it has been demonstrated to be enough to result in an antistatic surface. From an overall point of view, the achieved barrier and antistatic properties make the developed BPEI/GO assembly a promising and attractive alternative to the classical antistatic packaging systems for PLLA.

## 3.5 Conclusions

In this work, modified PLLA films with good oxygen barrier, transparency and antistatic

properties were developed. This set of properties makes the prepared materials applicable in the antistatic packaging field. Indeed, the proposed approach involves the Layer-by-Layer (LbL) deposition of functional coatings comprising either deposition of chitosan (CH) or branched polyethylenimine (BPEI) in combination with graphite oxide (GO). The characterization results evidenced the more effectiveness of BPEI with respect to CH as positive counterpart in the LbL assemblies. Coating growth was investigated by IR spectroscopy coupled with microscopy observations showing that the BPEI/GO system is capable of growing thicker, while producing more homogeneous coatings than CH/GO. This was further confirmed by static contact angle measurements. Film coated by 10 BL BPEI/GO showed a 70% reduction in oxygen permeability in both dry and humid conditions. The same coating was subjected to a reduction post treatment capable to confer antistatic properties to the coated film. The conditions applied in the LbL deposition, with a limited number of bilayers, and the subsequent reduction of GO, carried out in water and at room temperature, result in a sustainable and easily scalable method for the modification of polymer surface properties. This is of particular interest in the case of biopolymers, such as PLA, allowing extending their applicability range towards novel and attractive application, by the engineering of surface properties and retaining the bulk properties.

# Reference

1. Ebnesajjad, S., *Handbook of biopolymers and biodegradable plastics properties, processing, and applications*. Elsevier Inc: UK, 2013.

2. Lim, L. T.; Auras, R.; Rubino, M., Processing technologies for poly(lactic acid). *Progress in Polymer Science* **2008,** *33* (8), 820-852.

3. Nagarajan, V.; Mohanty, A. K.; Misra, M., Perspective on Polylactic Acid (PLA) based Sustainable Materials for Durable Applications: Focus on Toughness and Heat Resistance. *ACS Sustainable Chemistry & Engineering* **2016,** *4* (6), 2899-2916.

4. Zheng, A.; Xu, X.; Xiao, H.; Li, N.; Guan, Y.; Li, S., Antistatic modification of polypropylene by incorporating Tween/modified Tween. *Applied Surface Science* **2012,** *258* (22), 8861-8866.

5. Tsurumaki, A.; Tajima, S.; Iwata, T.; Scrosati, B.; Ohno, H., Evaluation of ionic liquids as novel antistatic agents for polymethacrylates. *Electrochimica Acta* **2017,** *248*, 556-561.

6. Costa, J. C.; Oliveira, M.; Machado, A. V.; Lanceros-Méndez, S.; Botelho, G., Effect of antistatic additives on mechanical and electrical properties of polyethylene foams. *Journal of Applied Polymer Science* **2009,** *112* (3), 1595-1600.

7. Zhang, M.; Zhang, C.; Du, Z.; Li, H.; Zou, W., Preparation of antistatic polystyrene superfine powder with polystyrene modified carbon nanotubes as antistatic agent. *Composites Science and Technology* **2017,** *138*, 1-7.

8. Jiang, H.; Moon, K.-s.; Li, Y.; Wong, C. P., Surface Functionalized Silver Nanoparticles for Ultrahigh Conductive Polymer Composites. *Chemistry of Materials* **2006,** *18* (13), 2969-2973.

9. Wang, Q.; Wang, Y.; Meng, Q.; Wang, T.; Guo, W.; Wu, G.; You, L., Preparation of high antistatic HDPE/polyaniline encapsulated graphene nanoplatelet composites by solution blending. *RSC Advances* **2017,** *7* (5), 2796-2803.

10. Wang, H.; Xie, G.; Fang, M.; Ying, Z.; Tong, Y.; Zeng, Y., Electrical and mechanical properties of antistatic PVC films containing multi-layer graphene. *Composites Part B: Engineering* **2015,** *79*, 444-450.

11. Sengupta, R.; Bhattacharya, M.; Bandyopadhyay, S.; Bhowmick, A. K., A review on the mechanical and electrical properties of graphite and modified graphite reinforced polymer composites. *Progress in Polymer Science* **2011,** *36* (5), 638-670.

12. Pöllänen, M.; Pirinen, S.; Suvanto, M.; Pakkanen, T. T., Influence of carbon nanotube–polymeric compatibilizer masterbatches on morphological, thermal, mechanical, and tribological properties of polyethylene. *Composites Science and Technology* **2011,** *71* (10), 1353-1360.

13. Richardson, J. J.; Cui, J.; Bjornmalm, M.; Braunger, J. A.; Ejima, H.; Caruso, F., Innovation in Layer-by-Layer Assembly. *Chem Rev* **2016,** *116* (23), 14828-14867.

14. El Fagui, A.; Wintgens, V.; Gaillet, C.; Dubot, P.; Amiel, C., Layer-by-Layer Coated PLA Nanoparticles with Oppositely Charged β-Cyclodextrin Polymer for Controlled Delivery of Lipophilic Molecules. *Macromolecular Chemistry and Physics* **2014,** *215* (6), 555-565.

15. Hashide, R.; Yoshida, K.; Hasebe, Y.; Takahashi, S.; Sato, K.; Anzai, J., Insulin-containing layer-by-layer films deposited on poly(lactic acid) microbeads for pH-controlled release of insulin. *Colloids Surf B Biointerfaces* **2012,** *89*, 242-7.

16. Lee, T.; Min, S. H.; Gu, M.; Jung, Y. K.; Lee, W.; Lee, J. U.; Seong, D. G.; Kim, B.-S., Layer-by-Layer Assembly for Graphene-Based Multilayer Nanocomposites: Synthesis and Applications. *Chemistry of Materials* **2015,** *27* (11), 3785-3796.

17. Chen, J. T.; Fu, Y. J.; An, Q. F.; Lo, S. C.; Huang, S. H.; Hung, W. S.; Hu, C. C.; Lee, K. R.; Lai, J. Y., Tuning nanostructure of graphene oxide/polyelectrolyte LbL assemblies by controlling pH of GO suspension to fabricate transparent and super gas barrier films. *Nanoscale* **2013,** *5* (19), 9081-8.

18. Guex, L. G.; Sacchi, B.; Peuvot, K. F.; Andersson, R. L.; Pourrahimi, A. M.; Strom, V.; Farris, S.; Olsson, R. T., Experimental review: chemical reduction of graphene oxide (GO) to reduced graphene oxide (rGO) by aqueous chemistry. *Nanoscale* **2017,** *9* (27), 9562-9571.

19. Battegazzore, D.; Alongi, J.; Frache, A.; Wågberg, L.; Carosio, F., Layer by Layer-functionalized rice husk particles: A novel and sustainable solution for particleboard production. *Materials Today Communications* **2017,** *13*, 92-101.

20. Laufer, G.; Kirkland, C.; Cain, A. A.; Grunlan, J. C., Clay-chitosan nanobrick walls: completely renewable gas barrier and flame-retardant nanocoatings. *ACS Appl Mater Interfaces* **2012,** *4* (3), 1643-9.

21. Battegazzore, D.; Frache, A.; Carosio, F., Sustainable and High Performing Biocomposites with Chitosan/Sepiolite Layer-by-Layer Nanoengineered Interphases. *ACS Sustainable Chemistry & Engineering* **2018,** *6* (8), 9601-9605.

22. Li, Y.; Wang, X.; Sun, J., Layer-by-layer assembly for rapid fabrication of thick polymeric films. *Chem Soc Rev* **2012,** *41* (18), 5998-6009.

23. Rodríguez-García, S.; Santiago, R.; López-Díaz, D.; Merchán, M. D.; Velázquez, M. M.; Fierro, J. L. G.; Palomar, J., Role of the Structure of Graphene Oxide Sheets on the CO2 Adsorption Properties of Nanocomposites Based on Graphene Oxide and Polyaniline or Fe3O4-Nanoparticles. *ACS Sustainable Chemistry & Engineering* **2019**.

24. Maddalena, L.; Carosio, F.; Gomez, J.; Saracco, G.; Fina, A., Layer-by-layer assembly of efficient flame retardant coatings based on high aspect ratio graphene oxide and chitosan capable of preventing ignition of PU foam. *Polymer Degradation and Stability* **2018,** *152*, 1-9.

25. Kharlampieva, E.; Sukhishvili, S. A., Ionization and pH Stability of Multilayers Formed by Self-Assembly of Weak Polyelectrolytes. *Langmuir* **2003,** *19* (4), 1235-1243.

26. Gardella, L.; Colonna, S.; Fina, A.; Monticelli, O., A Novel Electrostimulated Drug Delivery System Based on PLLA Composites Exploiting the Multiple Functions of Graphite Nanoplatelets. *ACS Applied Materials & Interfaces* **2016,** *8* (37), 24909-24917.

27. Luo, Y.; Pan, X.; Ling, Y.; Wang, X.; Sun, R., Facile fabrication of chitosan active film with xylan via direct immersion. *Cellulose* **2014,** *21* (3), 1873-1883.

28. Sengupta, P.; Prasad, B. L. V., Surface Modification of Polymers for Tissue Engineering Applications:

Arginine Acts as a Sticky Protein Equivalent for Viable Cell Accommodation. *ACS Omega* **2018,** *3* (4), 4242-4251.

29. Chee, W. K.; Lim, H. N.; Huang, N. M.; Harrison, I., Nanocomposites of graphene/polymers: a review. *RSC Advances* **2015,** *5* (83), 68014-68051.

30. Wan, D.; Yang, C.; Lin, T.; Tang, Y.; Zhou, M.; Zhong, Y.; Huang, F.; Lin, J., Low-temperature aluminum reduction of graphene oxide, electrical properties, surface wettability, and energy storage applications. *ACS Nano* **2012,** *6* (10), 9068-78.

31. Yi, W.; Wu, H.; Wang, H.; Du, Q., Interconnectivity of Macroporous Hydrogels Prepared via Graphene Oxide-Stabilized Pickering High Internal Phase Emulsions. *Langmuir* **2016,** *32* (4), 982-90.

32. Zheng, Z.; Zheng, X.; Wang, H.; Du, Q., Macroporous graphene oxide-polymer composite prepared through pickering high internal phase emulsions. *ACS Appl Mater Interfaces* **2013,** *5* (16), 7974-82.

33. Hernandez, S. C.; Bennett, C. J.; Junkermeier, C. E.; Tsoi, S. D.; Bezares, F. J.; Stine, R.; Robinson, J. T.; Lock, E. H.; Boris, D. R.; Pate, B. D.; Caldwell, J. D.; Reinecke, T. L.; Sheehan, P. E.; Walton, S. G., Chemical gradients on graphene to drive droplet motion. *ACS Nano* **2013,** *7* (6), 4746-55.

34. Some, S.; Kim, S.; Samanta, K.; Kim, Y.; Yoon, Y.; Park, Y.; Lee, S. M.; Lee, K.; Lee, H., Fast synthesis of high-quality reduced graphene oxide at room temperature under light exposure. *Nanoscale* **2014,** *6* (19), 11322-7.

35. Najafi, N.; Heuzey, M. C.; Carreau, P. J., Polylactide (PLA)-clay nanocomposites prepared by melt compounding in the presence of a chain extender. *Composites Science and Technology* **2012,** *72* (5), 608-615.

36. Guo, Y.; Yang, K.; Zuo, X.; Xue, Y.; Marmorat, C.; Liu, Y.; Chang, C.-C.; Rafailovich, M. H., Effects of clay platelets and natural nanotubes on mechanical properties and gas permeability of Poly (lactic acid) nanocomposites. *Polymer* **2016,** *83*, 246-259.

37. Svagan, A. J.; Akesson, A.; Cardenas, M.; Bulut, S.; Knudsen, J. C.; Risbo, J.; Plackett, D., Transparent films based on PLA and montmorillonite with tunable oxygen barrier properties. *Biomacromolecules* **2012,** *13* (2), 397-405.

38. Aulin, C.; Karabulut, E.; Tran, A.; Wagberg, L.; Lindstrom, T., Transparent nanocellulosic multilayer thin films on polylactic acid with tunable gas barrier properties. *ACS Appl Mater Interfaces* **2013,** *5* (15), 7352-9.

39. Carosio, F.; Colonna, S.; Fina, A.; Rydzek, G.; Hemmerlé, J.; Jierry, L.; Schaaf, P.; Boulmedais, F., Efficient Gas and Water Vapor Barrier Properties of Thin Poly(lactic acid) Packaging Films: Functionalization with Moisture Resistant Nafion and Clay Multilayers. *Chemistry of Materials* **2014,** *26* (19), 5459-5466.

40. Ortenzi, M. A.; Basilissi, L.; Farina, H.; Di Silvestro, G.; Piergiovanni, L.; Mascheroni, E., Evaluation of crystallinity and gas barrier properties of films obtained from PLA nanocomposites synthesized via “in situ” polymerization of l-lactide with silane-modified nanosilica and montmorillonite. *European Polymer Journal* **2015,** *66*, 478-491.

41. Sanchez-Garcia, M. D.; Lagaron, J. M., Novel clay-based nanobiocomposites of biopolyesters with synergistic barrier to UV light, gas, and vapour. *Journal of Applied Polymer Science* **2010,** *118* (1), 188-199.

# 4 Polycaprolactone/graphite nanoplates composite nanopapers

## 4.1 Introduction

Nanopapers, which are thin sheets or films composed of self-assembled individual nanoparticles, generally obtained by filtration of a suspension in a solvent, have gained increasing interest for their unique properties, such as mechanical properties, gas barrier and flame retardancy.[1-6] Indeed, the above features are mainly related to the highly concentrated nanoparticles, which are tightly packed in the thin film, because of their strong self-interactions[7, 8] or mediated through a binding polymer, in the so-called brick and mortar structures.[9-14] Among the different lamellar nanoparticles which can be exploited in the preparation of nanopapers, graphene-related nanomaterials, such as graphite nanoplatelets (GNP) and multilayer graphene represent ideal systems for producing high-performance nanopapers, they being characterized by ultrahigh strength, excellent electrical and thermal conductivity.[15-19] Concerning the preparation of GNP nanopapers, two issues have to be considered, which are the exfoliation and dispersion of individual graphene nanosheets in a medium and the strong bonding among graphene nanosheets in the resulting nanopapers. In order to overcome the dispersion problem, covalently functionalization of graphene was usually exploited.[17, 20-24] Huang et al.[17] prepared graphene nanopapers by flow-directed assembly starting from benzenesulfonic acid functionalized graphene nanosheets, which approach facilitated the dispersion of graphene nanosheets in water and allowed the preparation of nanopapers. Mechanical and electrical properties of the above nanopapers turned out to depend on the annealing temperature as well as on the degree of functionality. Similarly, Korkut et al.[25] produced graphene network by tape casting surfactant-stabilized aqueous suspensions of functionalized graphene sheets. In this case, the removal of the polymer matrix and the surfactant allowed obtaining a self-supporting and electrically conducting graphene-based tapes. An alternative strategy to promote the graphene dispersion consists in the application of graphene oxide (GO),[26, 27] which, containing hydroxyl and epoxy

groups on the basal planes and carboxyl groups on the hedges, results to be easily dispersible in water.[26, 28-30] By applying this approach, Chen et al.[16] prepared graphene papers starting from GO dispersions reduced with hydrazine. Indeed, the above reduction step, which is essential to restore the conductivity properties of the material, represents a limitation of the method as the complete reduction of GO can be hardly achieved and the graphite structure can be partially damaged.[31-35]

The major drawbacks of the graphite-based nanopapers, particularly of those made of GNP, is their limited toughness and deformability, which is mainly related to the scarce bonding among nanosheets. Indeed, as reported in the literature, typically the elongation at break is less than 1.0 %, thus limiting the nanopapers practical applications.[16, 17, 25, 36] As such, the incorporation of limited amount of polymers into the GNP nanopapers, in a brick and mortar organization, may enhance their toughness and deformability. However, the presence of non-conductive polymer between GNP is clearly expected to decrease thermal and electrical conductivity of the nanostructure. In this light, the development of one-step method to prepare GNP-based nanopapers with high mechanical properties and thermal conductivity still remains challenging for industrial applications. To promote the thermal conductivity, highly crystalline polymers should be applied,[37-44] while to enhance the final ductility of the nanopaper, sufficient polymer mobility should be granted. With this in mind, polycaprolactone (PCL) was selected, based on its high crystallinity and capability of strong nucleation on carbon nanostructures[45] coupled with a low glass transition temperature. Furthermore, the PCL is a biodegradable and biocompatible polymer, in principle allowing application of the GNP/polymer system also in the biomedical field.[46-48] In this work, GNP/PCL nanopapers were prepared with a polymer content ranging from 5 wt.% to 20 wt.% by applying a solution blending approach, followed by filtration, drying and pressing treatments. The nanopapers have been characterized for their crystallinity, morphology mechanical and thermal conductivity properties, highlighting a set of performance suitable for application in flexible heat exchangers, including flexible electronics[49] as well as wearable

and implantable devices.[50, 51]

## 4.2 Experimental part

### 4.2.1 Materials

Polycaprolactone (PCL) is a commercial product purchased from Perstorp UK limited (Capa6500, $M_n$ = 50000, $T_m$ = 56 °C, $T_c$ = 29 °C). Graphite nanoplatelets (GNP) used in this work is supplied by AVANZARE (Navarrete, La Rioja, Spain) prepared via rapid thermal expansion of over oxidized-intercalated graphite, as previously reported[52] and used as supplied without any further treatments. Dimethylformamide (DMF) (99.8%,) purchased from Sigma-Aldrich was used as solvent.

### 4.2.2 Preparation methods

Nanopapers were prepared by filtration following the procedure, presented in Figure 4.1 and described hereunder.

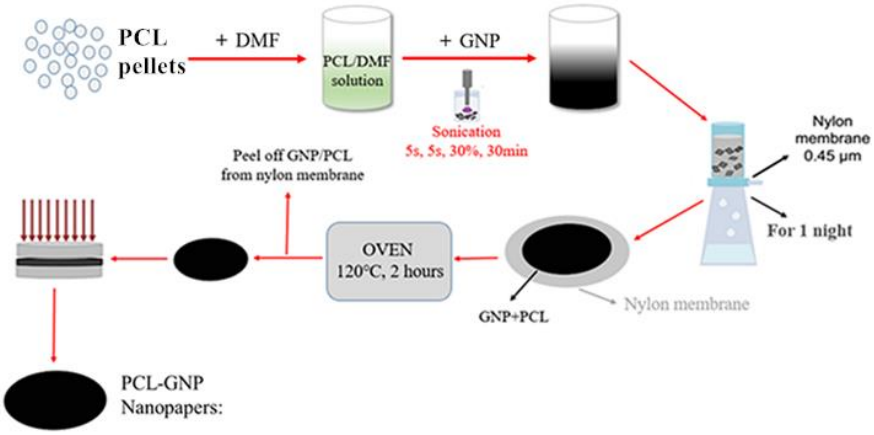


Figure 4.1 Preparation procedure of the nanopapers.

Different amount of PCL pellets (25 mg, 50 mg, 250 mg and 500 mg) were dissolved into 150 ml DMF at 60 °C for 1 hour in order to obtain solutions with different polymer concentrations. GNP powder (50 mg) was added into the prepared PCL solutions. Homogeneous suspensions (no obvious big GNP particles can be seen when transferred to the filter) were obtained by applying a sonication treatment in pulsed mode (5 s on and 5 s off) for 30 min with power set

at 30% of the full output power (750 W), accomplished with an ultra-sonication probe (Sonics Vibracell VCX-750, Sonics &Materials Inc.) with a 13 mm diameter Ti-alloy tip. The suspension was transferred into a filtration system equipped with a polyamide supported membrane (0.45μm nominal pore size, diameter 47 mm, Whatman) and left for filtration overnight. After filtration, the cake containing GNP and adsorbed PCL, over the nylon membrane, was dried in two steps, firstly at 70 ºC for 2 hours to remove most of the solvent and later at 120 ºC for 1 hour to complete solvent removal. Drying in two steps was adopted to avoid cracking of the film, observed when drying in one step at 120 ºC, due to the high solvent evaporation rate. Finally, nanopapers were obtained by applying a 6 tons load for 30 minutes on the PCL-GNP cakes after being peeled off from nylon membrane at room temperature (RT). Larger nanopapers were also prepared using 90 mm membrane filters and using 200 mg GNP suspended in 600 ml DMF, while maintaining the same preparation procedure. Hot pressing (80ºC and then cooled down to 30ºC by water cooling of compression plates) was applied to specimens, to further consolidate the nanopaper structure. Samples codes was defined by indicating the initial ratio of PCL and GNP in the suspensions before filtering, the dimension of the prepared nanopapers and the pressing method, as shown in Table 4-1.

Table 4-1 Nanopapers list, with codes and preparation conditions.

| Sample code | Ratio PCL : GNP in suspension | Diameter [mm] | Pressing method |
|---|---|---|---|
| PCL10-GNP1-SC | 10 : 1 | 47 | RT |
| PCL10-GNP1-LH | 10 : 1 | 90 | 80ºC |
| PCL5-GNP1-SC | 5 : 1 | 47 | RT |
| PCL5-GNP1-LH | 5 : 1 | 90 | 80ºC |
| PCL1-GNP1-SC | 1 : 1 | 47 | RT |
| PCL1-GNP1-LH | 1 : 1 | 90 | 80ºC |
| PCL1-GNP2-SC | 1 : 2 | 47 | RT |

### 4.2.3 Characterization

Thermal gravimetrical analysis (TGA) was performed with a Mettler-Toledo TGA 1 thermo-gravimetric analyzer. Samples with weight of 5-8 mg were heated from 35 ºC to 900 ºC under a nitrogen flow of 80 ml/min and then were kept at 900 ºC for 20 minutes under oxygen at the same flow rate.

A Zeiss Supra 40 VP field emission scanning electron microscope (FE-SEM) equipped with a backscattered electron detector was used to examine the morphologies of the nanopapers.

Differential scanning calorimetric (DSC) analysis was performed under a continuous nitrogen purge on a Mettler calorimetric apparatus, model DSC1 STARe/E System. The samples, having a mass between 2.5 and 6 mg, were firstly heated from -10 ºC to 200 °C, then cooled down to -100 ºC and finally heated to 200 °C again. A scanning rate of 10 °C/min was used on both heating and cooling.

The crystallinities ($X_c$) of PCL into different nanopapers were calculated by considering their real contents $\Phi_{PCL}$, following the equation as below:

$$X_c(\%) = \frac{\Delta H_m}{\Delta H_m^0 \times \emptyset_{PCL}} \times 100\% \quad (1)$$

where $\Delta H_m$ is the measured heat of fusion, $\emptyset_{PCL}$ is the PCL content in the nanopapers and $\Delta H_m^0$ is melting enthalpy of the 100% PCL crystalline (139.5 J/g).

Successive self-nucleation and annealing tests were performed on 2.5 ± 0.3 mg to compensate for the heating rate increase. The following experimental protocol was adopted: (a) heating up to 175 °C (3 min isotherm at 175 °C) to erase thermal history and crystalline memory; (b) Cooling from the melt (i.e., 175 °C) to 0 °C at 20 °C/min to create a standard crystalline state; (c) Fractionation 1: Heating the sample until a $T_{s1}$~$T_m$, end of the studied transition, e.g., 127 °C. Held this temperature for 5 minutes and then cooling to 0 °C at 50 °C/min. Then, heat the sample until the $T_{s2}$, which will be equal to $T_{s1}$-2.5 °C. At least fourth $T_s$ is studying to cover the highest melting peak. (d). Fractionation 2: After Fractionation 1, the sample was cooled until 0 °C at 20 °C/min (then the other steps were performed at 50 °C/min). In this case, the fractionation window was changed from 2.5 to 5 °C. Generally, the first $T_s$ in

Fractionation 2 was 92 °C. Then, a range of around 50 °C (92 to 42 °C) was covered to fractionate the transitions calculated at approximately 85 and 76 °C. (e). Final Heating: Heat the sample from 0 °C to 175 °C at 20 ºC/min.

The thermal diffusivity (α) of the prepared nanopapers was measured at 25°C using the xenon light flash analysis (LFA) (Netzsch LFA 467 Hyperflash). The samples were cut in disks with a diameter of 23 mm and the measurements were carried out in a special in-plane sample holder, in which the sample is heated in the central region and the temperature rise was measured on the outer ring of the sample. Measurements were carried out five times for each sample to get an average thermal diffusivity.

Wide Angle X-ray Scattering (WAXS) measurements were performed on a Xeuss 2.0 SAXS/WAXS system (Xenocs SA, France). X-ray radiation (wavelength = 1.5418 Å) was produced by means of the Cu Kα radiation generator (GeniX3D Cu ULD) at 50 kV and 0.6 mA. Scattered signals were collected by a semiconductor detector (Pilatus 300 K, DECTRIS, Swiss) with a resolution of 487 × 619 pixels (pixel size 172 × 172 μm$^2$).

Thermal conductivity was calculated from the measured diffusivity values, multiplied by the density and specific heat capacity of the different materials:

$$K = \rho \times \alpha \times C_p \quad (2)$$

*K, thermal conductivity; ρ, density of the nanopapers; $C_p$, specific heat capacity of different materials.*

The specific heat capacities of nanopapers ($C_{pn}$) were calculated by the weighted average of $C_p$ values of PCL and graphite (0.71 Jg$^{-1}$K$^{-1}$at RT)[53] for each sample:

$$C_{pn} = C_{pP} \times \Theta_{PCL} + C_{pG} \times (1- \Theta_{PCL}) \quad (3)$$

*$C_{pP}$, specific heat capacity of PCL, which is around 2.0 Jg$^{-1}$K$^{-1}$at RT;[54] $\Theta_{PCL}$, weight percentage of PCL in the nanopapers; $C_{pG}$, specific heat capacity of graphite.*

Thermomechanical properties of nanopapers at different temperatures were investigated by using a Q800 Dynamic Mechanical Analyzer (DMA). The samples were cut into rectangular specimens with dimension of 5×20 mm$^2$. The specimen was performed a temperature scan, from room temperature to 150 ºC at a heating rate of 2 ºC/min, strain of 0.05% and frequency of 1 Hz. Deformation under constant load was carried out at 120 °C under 5 MPa, for 8 hours,

followed by deformation recovery at zero load and the same temperature for 8 hours.

## 4.3 Result and discussion

Composite nanopapers easily obtained by filtration of GNP/PCL suspension demonstrated high flexibility. Indeed, freestanding nanopapers can easily be bent and even folded and then again restored to planar, without breaking, which is impossible for the neat GNP nanopaper, exhibiting remarkable brittleness. As a representative example, pictures for PCL10-GNP1-SC nanopaper are reported in Figure 4.2.

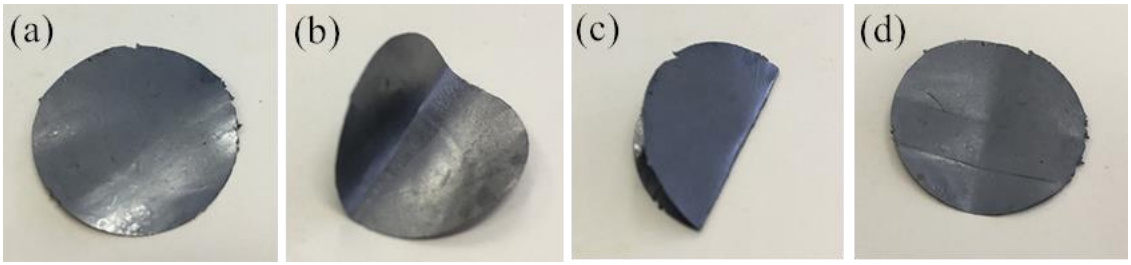


Figure 4.2 Photographs of freestanding nanopaper PCL10-GNP1-SC: (a) initial nanopaper; (b) nanopaper bent 90°; (c) folded nanopaper; (d) recovery after being bended and folded.

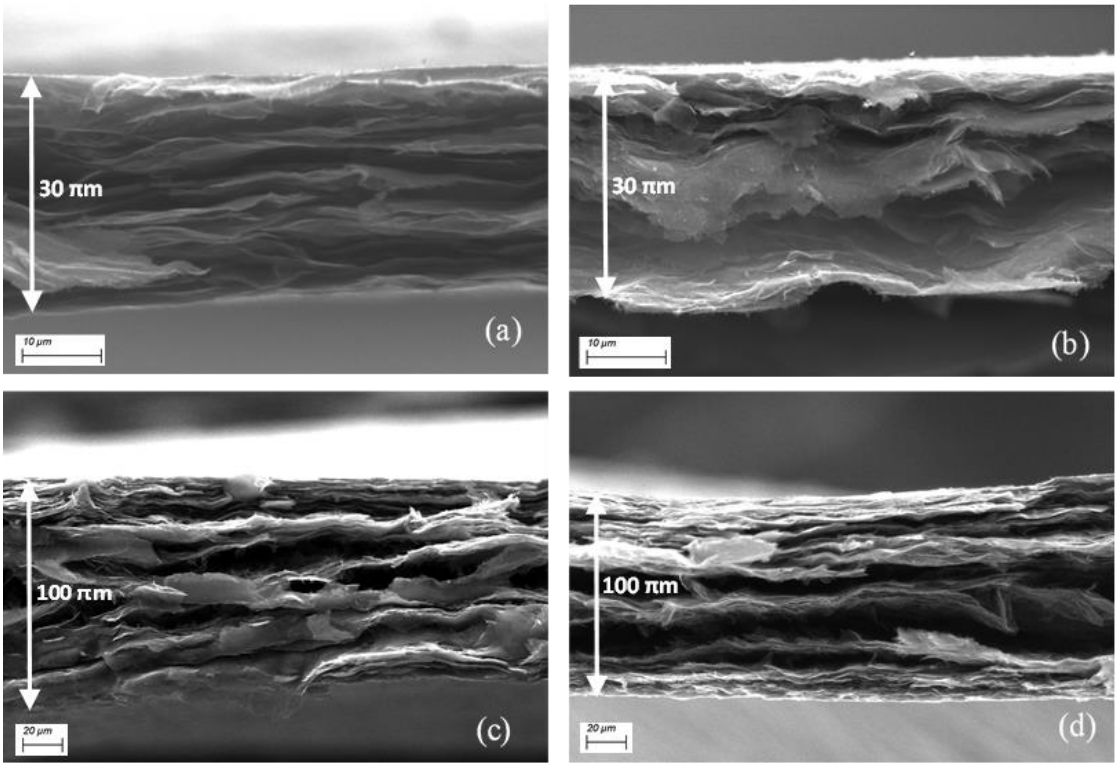


Figure 4.3 SEM micrograph for cross-section of different nanopapers, (a) PCL1-GNP1-LH, (b) PCL10-GNP1-LH, (c) PCL1-GNP1-SC, (d) PCL10-GNP1-SC.

The morphology of nanopapers in cross-section were investigated by SEM (Figure 4.3), showing thin deposition of PCL onto the highly oriented GNP flakes. Comparing nanopapers compressed at room temperature vs the corresponding prepared by hot pressing, significant differences can be found in both thickness and porosity. Indeed, room temperature compressed nanopapers (Figure 4.3c and d) exhibit a higher thickness, typically in the range of 100 μm and delaminated structure. On the other hand, hot pressed counterparts (Figure 4.3a and b) are clearly thinner (approx. 30 μm) and more compact, especially for higher PCL/GNP ratio, evidencing the hot pressing stage to consolidate the structure once PCL is above its melting temperature.

The amount of PCL retained by GNP flakes during filtration was investigated by thermogravimetry measurements. Indeed, as PCL has a much lower decomposition temperature ($T_{max}$ at ca. 400 °C) than GNP, it is possible to calculate the polymer content inside the nanopapers from the residual weight at 600°C, as summarized in Table 4-2.

Table 4-2 PCL content inside nanopapers, obtained from TGA residual weight.

| Sample | Weight percentage of PCL (wt.%) |
|---|---|
| PCL10-GNP1-SC | 17 ± 3 |
| PCL10-GNP1-LH | 20 ± 3 |
| PCL5-GNP1-SC | 10 ± 1 |
| PCL5-GNP1-LH | 15 ± 3 |
| PCL1-GNP1-SC | 6.3 ± 0.5 |
| PCL1-GNP1-LH | 7.6 ± 1 |
| PCL1-GNP2-SC | 6 ± 0.6 |

The polymer fraction in the nanopapers is clearly much lower than the polymer concentration in the suspension, relative to GNP, demonstrating that only a limited fraction of PCL can be adsorbed onto the GNP flakes and retained in the nanopapers. However, the PCL concentration within the nanopapers is increased by increasing the initial concentration of

PCL in the suspensions, relative to GNP. Indeed, ca. 6 wt.% PCL was obtained in PCL1-GNP2-SC whereas concentrations up to about 20 wt.% were obtained for PCL10-GNP1-LH nanopapers. The PCL content in nanopapers is affected by the initial concentration of the polymers, but it appears to be mainly dependent on the interaction between PCL molecule chains and GNP surface. When the concentration of PCL in the initial suspensions is low, such as PCL1-GNP1 and PCL1-GNP2, the low viscosity of the PCL solution leads to a relatively fast filtration process. When the concentration of PCL solution is gradually increased, the viscosity is increased and this may contribute to retain a higher PCL fraction.

To investigate the organization of PCL chains between GNP, the PCL crystallinity within the nanopapers was addressed, as chain confinement is known to potentially affect crystallinity.[55, 56] Beside the fundamental study, crystallinity is also related to the envisaged application of these nanaopapers in heat exchangers. Indeed, crystallinity is one of the most important factors controlling thermal conductivity of polymer materials.[38, 40, 42, 43] Crystalline polymers exhibit higher thermal conductivity than amorphous polymers due to the ordered crystal structure, while the random chain conformation in amorphous polymers reduces the phonon mean free path and causes phonon scattering, thus decreasing the heat transfer efficiency.[39, 43] The crystallization and melting behaviors of the prepared nanopapers and the neat PCL were characterized by using DSC and results are reported in Figure 4.4 and Table 4-3. On cooling plots (Figure 4.4a) crystallization of pristine PCL can be clearly observed as a sharp peak with max temperature at ca. 28 °C, which is consistent with the well-known crystallization of PCL. On the other hand, the crystallization temperature ($T_c$) for PCL in the presence of GNP raised to ca. 47 ºC, i.e. about 20 ºC higher than that of the neat PCL, suggesting a significant nucleation activity of GNP flakes on PCL. This crystallization peak is clearly visible for PCL10-GNP1-LH and PCL10-GNP1-SC, while significantly lower and broader signals were obtained for PCL5-GNP1-SC, PCL1-GNP-SC and PCL1-GNP2-SC, which can be partially explained in terms of lower polymer contents within the latter nanopapers.

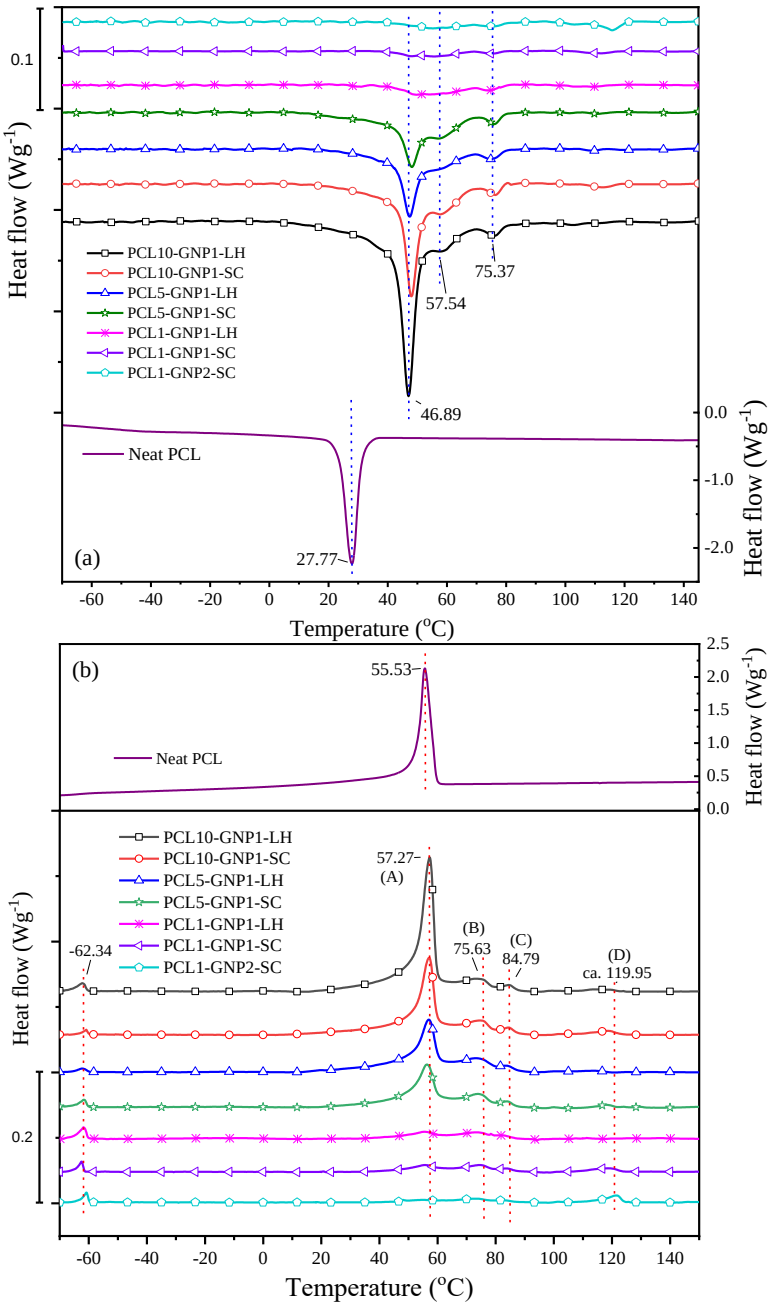


Figure 4.4 DSC curves for the cooling (a) and second heating (b) stage.

The increased $T_c$ for PCL within the nanopapers can be interpreted based on previous literature reports describing strong nucleation activity of graphene-related materials in nanocomposites.[57-60] For PCL, Ahmed et al.[61] reported the effect of GO on the non-isothermal crystallization behavior of PCL, demonstrating an increase in $T_c$ of PCL/GO nanocomposite to ca. 35 ºC, compared to ca. 26 ºC for the neat PCL, with 1.0 wt.% GO loading. Similar

results were reported for PCL/rGO nanocomposite by Wang et al.,[59] with an increase of ca. 10 ºC on $T_c$ for the nanocomposite compared to neat PCL. Zhang and coworkers[62] produced nanocomposite based on PCL and thermally reduced graphene oxide (TRGO) and reported $T_c$ of nanocomposite to increase to around 36 ºC with TRGO loading of 2 wt.% from 25 ºC of neat PCL. Zeng et al.[63] studied the crystallization behavior of PCL/Poly(sodium 4-styrenesulfonate) functionalized GNP (FGNP) composites. Under cooling rate of 10 ºC/min, they found that, $T_c$ increase of ca. 8°C and 11°C with addition of 0.05 wt.% and 1 wt.% of FGNP, respectively. A detailed study on non-isothermal crystallization behavior of PCL and PCL nanocomposites with different nanofillers (including GO and graphite powder) and different loadings was done by Kai el at.,[64] the increase in $T_c$ for all the prepared composite being within 10 ºC.

Crystallization temperature shift obtained in this work are significantly higher than previously reported for PCL containing graphene related materials, which can be explained by the limited fraction of PCL into the nanopapers, leading to a high interfacial area between GNP and the polymer chains, maximizing nucleation density. Beside $T_c$ shift, it is important to note that extra crystallization peaks at ca. 58, 76 ºC and a broad signal above 100 ºC were found for all the nanopapers, which did not exist in the case of neat PCL. Relative intensities for these signals, compared to the main crystallization peak, seems to increase when decreasing the total PCL content, thus suggesting such signals to become more important when having little PCL, strongly confined onto GNP flakes.

From the results of second heating, a main endothermic signal in the range between 55 and 58 °C, corresponding to the well-known melting of PCL is clearly observable for both pristine polymer and nanopapers, except for PCL1-GNP2-SC (Figure 4.4b). Furthermore, additional signals are found in thermograms for the nanopapers. Indeed a first distinctive features for the nanopapers is found at ca. -62 ºC, which is assigned to the glass transition of PCL.[65] This signal is not visible in pristine PCL, and may therefore suggest a significant fraction of PCL in nanopapers to remain amorphous during the cooling stage. It is worth noting that the main

melting signal for PCL in nanopapers is slightly delayed to higher temperature, compared to pristine PCL, which might be related to the adsorption effect of PCL crystal on the GNP surface. In addition, extra melting peaks at ca. 75, 84 and a broad signal around 120 °C were observed for the composite nanopapers, which were not found for neat PCL, and corresponding to the above described signals for the cooling stage, suggesting the existence of different PCL chain organization. To the best of the authors' knowledge, such high PCL chain organization were never reported for the crystallization of PCL and might be related to a peculiar organization of PCL chains on the surface of GNP.

In principle, melting peaks at higher temperatures may be related to higher stability PCL crystals, possibly characterized by higher lamellar thickness or different crystalline forms. However, the thermodynamic melting temperature of PCL was reported to be around 70 °C,[66] so that crystals with melting point above that temperature may not correspond to the same crystalline phase.

It is worth mentioning that the effect of temperature during nanopapers pressing appears to have some effect on the crystallization behavior of the PCL in nanopapers at relative high temperatures. Indeed, by the comparison of PCL10-GNP1-LH vs PCL10-GNP1-SC, as well as PCL1-GNP1-LH vs PCL1-GNP1-SC, smaller enthalpies were found for the PCL high temperature melting peaks, suggesting annealing at 80°C may affect the organization structure of the higher stability PCL fraction, as shown in Table 4-3.

To quantify the relative amounts of the different crystalline population, the enthalpies of the peaks from second heating stage were calculated, taking into account of the actual PCL contents in nanopapers, and reported in Table 4-3. The melting enthalpy of the most intense peak (at ca. 57 °C) was found to increase with increase content of PCL in the nanopapers, which is found to be reverse for peaks at relative high temperatures (peak B, C, D) (Figure 4.5). Trends for melting signals A, B and C suggest a strong role of GNP in organizing PCL crystals upon cooling. When a limited amount of PCL present in between GNP, the interaction between PCL chains and GNPs could promote the nucleation process, resulting in higher $T_c$

of PCL. Furthermore, GNPs could also restrict cooperative movements of PCL chains causing a reduction in the total crystallinity of PCL inside the nanopapers. Indeed, the total crystallinity of all the peaks for PCL in nanopapers is always lower than in pristine PCL and is found to decrease with decreasing PCL contents.

Table 4-3 Calculated enthalpy and the total crystallinity of the peaks from second heating stage.

| **Samples** | **ΔH (J/g) of the peaks from second heating stage** | | | | | |
|---|---|---|---|---|---|---|
| | A | B | C | D | Total | $X_c$ |
| Neat PCL | 66.3 | - | - | - | 66.3 | 47.5% |
| PCL10-GNP1-LH | 33.0 | 2.3 | 0.5 | - | 35.8 | 25.6% |
| PCL10-GNP1-SC | 27.2 | 2.8 | 0.9 | 0.8 | 31.7 | 22.7% |
| PCL5-GNP1-LH | 22.7 | 3.4 | 0.8 | - | 26.9 | 19.3% |
| PCL5-GNP1-SC | 24.0 | 3.6 | 1.0 | 1.2 | 29.8 | 21.4% |
| PCL1-GNP1-LH | 5.3 | 1.5 | 1.4 | 0.4 | 8.6 | 6.2% |
| PCL1-GNP1-SC | 4.5 | 2.7 | 1.9 | 4.1 | 13.2 | 9.5% |
| PCL1-GNP2-SC | 2.0 | 3.0 | 1.8 | 4.8 | 11.6 | 8.3% |

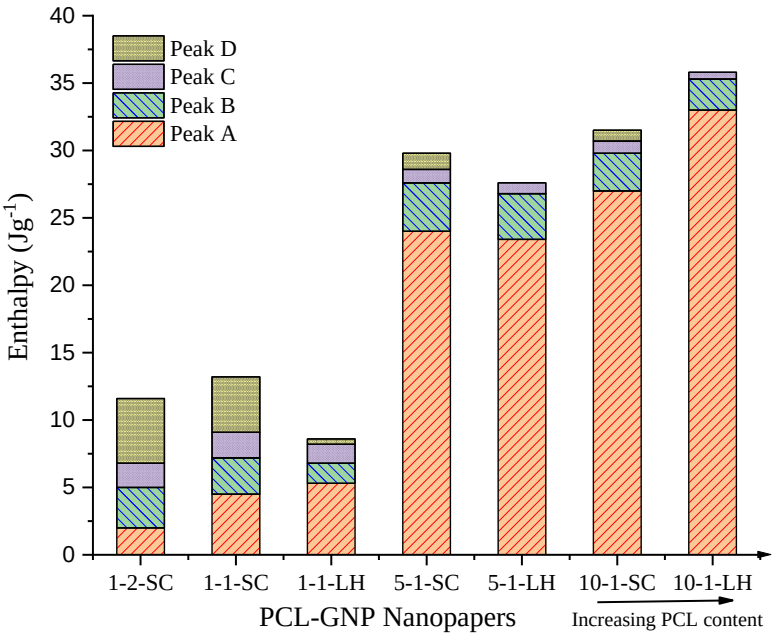


Figure 4.5 Integral enthalpy values of the peaks from 2nd heating vs PCL content.

To further investigate the crystalline organization of PCL within the nanopapers, X-ray

diffraction was carried out on the cold-pressed nanopapers. As expected, the high content of GNP determines a strong signal at 2θ = 26.5° (Figure 4.6), corresponding to an interlayer spacing of 0.34 nm with an index of (002).[58] It is relevant to underline that, from the XRD result on PCL5-GNP1-SC with a 10 times larger accumulation time (Figure 4.6b), only the characteristics peaks of PCL were found at 2θ = 21.4°, 22.0° and 23.7°, corresponding to (110), (111) and (200) planes of the orthorhombic crystal form,[67] which provides evidence for the existence of only one PCL crystalline form.

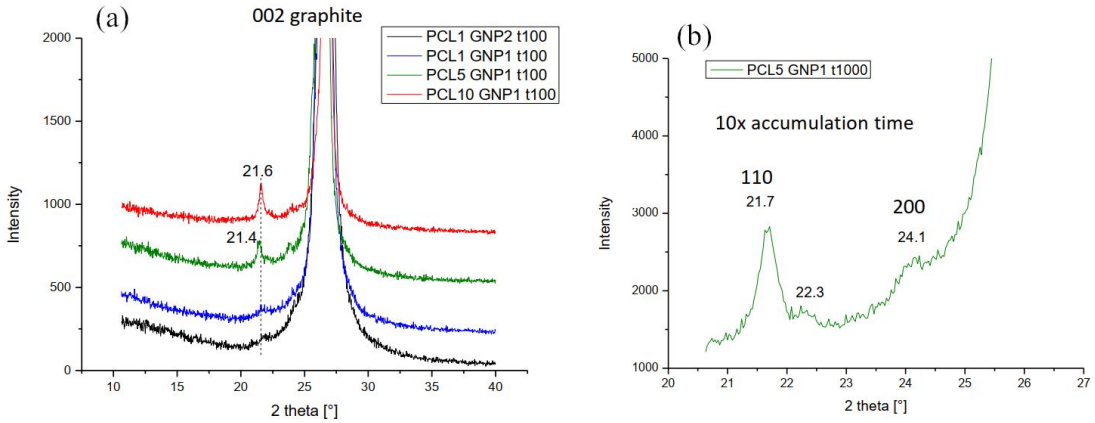


Figure 4.6 XRD patterns of the cold-pressed nanopapers.

To further study the origin of the signals that are found at relatively high temperatures, the successive self-nucleation and annealing (SSA) treatments were applied to all the nanopapers, focusing on the transitions of the potential crystal structures at the higher temperatures (e.g., 76, 85, and 120 °C). The general protocol is shown in Figure 4.7 and described in the characterization part.

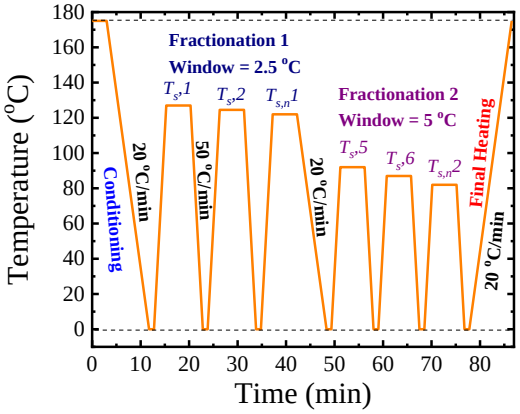


Figure 4.7 SSA protocol employed to all the samples.

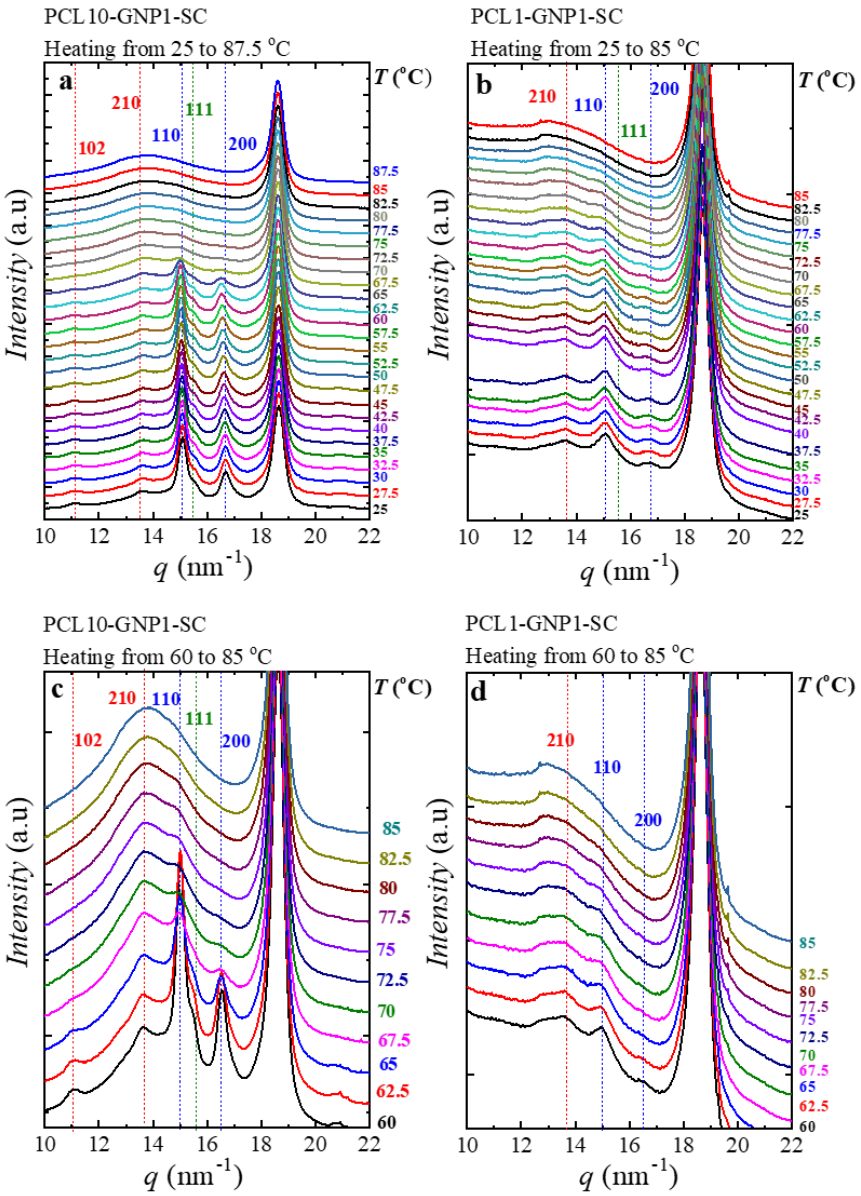


Figure 4.8 WAXS patterns taken during the final heating of SSA on the selected nanopapers; (a), (b): at range of 25 to 87.5 °C, and (c), (d): from 60 to 85 °C. The vertical dashed lines indicate the position of the PCL main planes.

WAXS patterns were taken on the previously fractionated nanopapers, PCL1-GNP1-SC and PCL10-GNP1-SC (without the final heating) in a hot stage. The SSA final heating of the above samples was performed in the hot stage of the BSRF, in which WAXS patterns can be taken simultaneously. The selected heating rate was 5 °C/min, exposure time of 25 seconds was used, and a period time of 5 seconds. Thus, a pattern was taken every 30 seconds (every 2.5 °C). The WAXS patterns at selected temperatures are shown in Figure 4.8.

Figure 4.8a shows the main peaks of the PCL, corresponding to the reflections of the (110) and (200) planes. The reflections of the (102) and (210) planes were also detected, although they are weaker compared to the main plane reflections. These signals are not typically reported in the literatures. Regarding the GNP, the intense peak at q~ 19 $nm^{-1}$ corresponds to GNP in both PCL10-GNP1 (Figure 4.8a) and PCL1-GNP1 (Figure 4.8b).

Figure 4.8b also shows the main peaks of the PCL, which are much weaker compared to Figure 4.8a due to its low PCL content in the nanopaper. In this case, interestingly, the peaks of the (200) and (210) planes have comparable intensities as the characteristic peaks of PCL. In Figure 4.8c and d, we selected the patterns from 60 to 85 °C, which corresponds to the fractionated PCL. In both cases, it is observed that the main peak of the PCL becomes less intense at 67.5 °C. It is interesting to note that the peak of the (210) plane has a similar intensity as that of the (110). In Figure 4.8c, before obtaining an amorphous halo, it is still observed two weak signals between 77.5 and 80 °C. It is worth noting that these temperatures are comparable or even higher to the equilibrium melting point of the PCL. Figure 4.8d shows similar behavior as Figure 4.8c. At 85 °C, it is clearly observed that the PCL is completely molten; hence the endothermic peak at around 85 °C does not correspond to the melting process of the PCL.

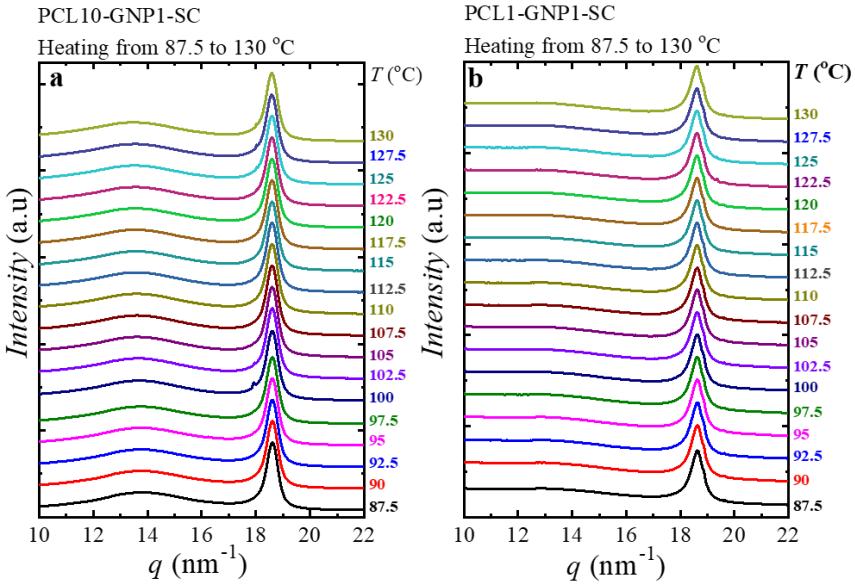


Figure 4.9 WAXS patterns taken during the final heating of SSA from 87.5 to 130 °C.

Figure 4.9 shows that in the range from 87.5 to 130 °C, the PCL is completely molten; hence the transitions signals detected by DSC experiments do not correspond to the thermal transition of the PCL.

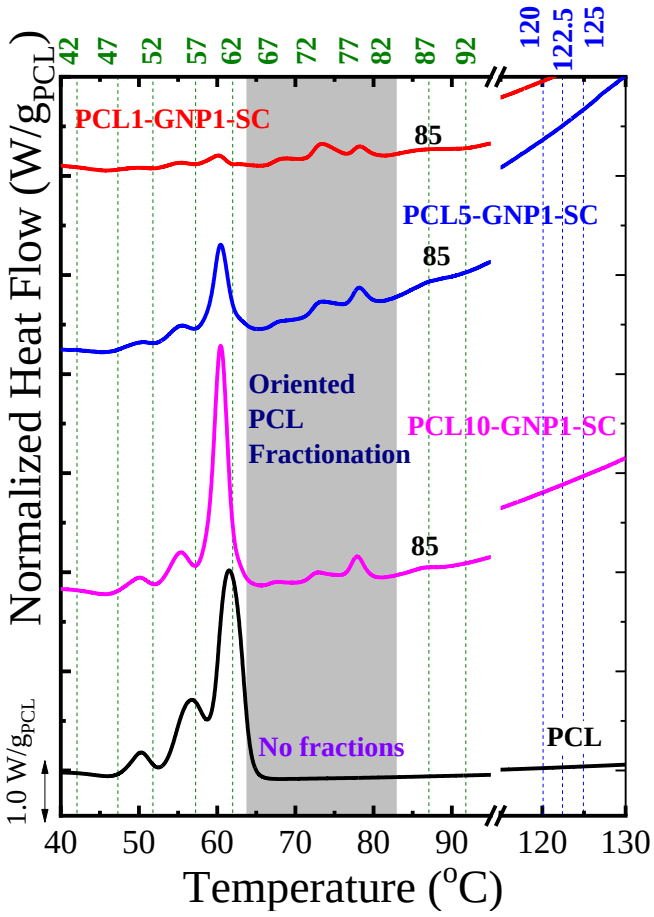


Figure 4.10 SSA Final Heating for the selected nanopapers. The blue dashed lines indicates the fractionation at high temperatures, with a fractionation windows of 2.5 °C; whereas the green dashed lines indicated the fractionation performed at lower temperatures, with a fractionation windows of 5 °C.

For comparison purposes, the SSA experiments were repeated to have the same SSA profile in all the cold-pressed samples, including the neat PCL. Figure 4.10 compares the SSA final heating of the neat PCL, PCL1-GNP1-SC, PCL5-GNP1-SC, and PCL10-GNP1-SC.

As shown in the figure above, only the peak at ca. 75 °C (non-isothermal test) can be fractionated, whereas the peaks at ca. 85 and 125 °C remain unfractionated, despite the applied protocol. Let us consider that the $T_s$ = 42 to 57 °C fractionated the "unoriented" PCL, and $T_s$ = 62 to 82 °C fractionated the "oriented" PCL (the shadow zone). If we calculated the

partial areas of the mentioned regions, we can found that as the ratio PCL/GNP decrease, the "oriented" PCL area increase. For the PCL1/GNP1, the sum of the partial area corresponding to the unoriented PCL is 38.2%, whereas for the oriented PCL is 61.8%. For the PCL5-GNP1, the unoriented PCL is 63.2%, and the oriented PCL is 36.8%, and for the PCL10-GNP1, the unoriented PCL is 72.2%, and the oriented PCL is 27.8%. These results, together with the ones of the other samples, are summarized in Table 4-4, indicating that with a higher GNP surface, more PCL chains can be absorbed and oriented, which is in line with the WAXS results.

Table 4-4 Ratio of oriented and unoriented PCL in partial area for the cold-pressed nanopapers.

| Sample | Partial Area, unoriented PCL (%) | Partial Area, oriented PCL (%) |
|---|---|---|
| PCL1-GNP2-SC | 24.0 | 76.0 |
| PCL1-GNP1-SC | 38.2 | 61.8 |
| PCL5-GNP1-SC | 63.2 | 36.8 |
| PCL10-GNP1-SC | 72.2 | 27.8 |
| PCL20-GNP1-SC | 92.2 | 7.8 |

From the results of WAXS and SSA, we already knew that the peak at ca. 120 ºC is not related to any crystalline or oriented structures of PCL, the absorption effect of PCL chains on GNP surface was assumed and thus the recycled rinse treatments in toluene were performed on this basis. The nanopapers, PCL10-GNP1-SC and PCL1-GNP1-SC, were selected to be washed for 12 hours, and the washed nanopapers were dried in vacuum at 30 ºC for 1 day to remove the solvent completely, after which DSC measurements were performed following the same procedures as before, results were shown in Figure 4.11.

It is very clear that, after the washing treatments, the signals under 100 ºC from the 2$^{th}$ heating of DSC measurements disappeared completely for both nanopapers and only the peak at around 125 ºC survived. Moreover, the DSC cooling showed the similar behavior as heating, demonstrating that this behavior is reversible, further supporting for our assumption that this peak at such high temperature might be related to the adsorption behavior of PCL chains on the GNP surface.

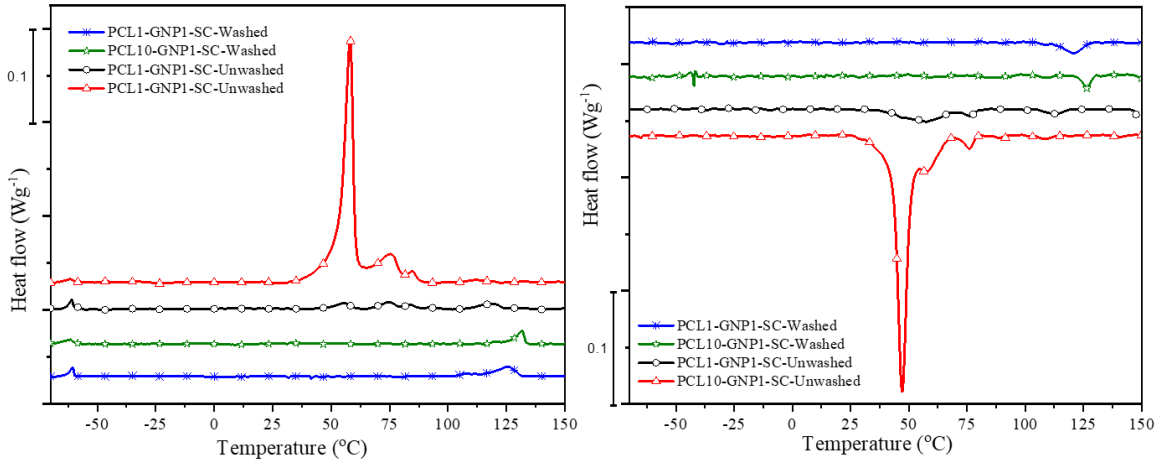


Figure 4.11 DSC measurements on selected nanopapers before and after being washed.

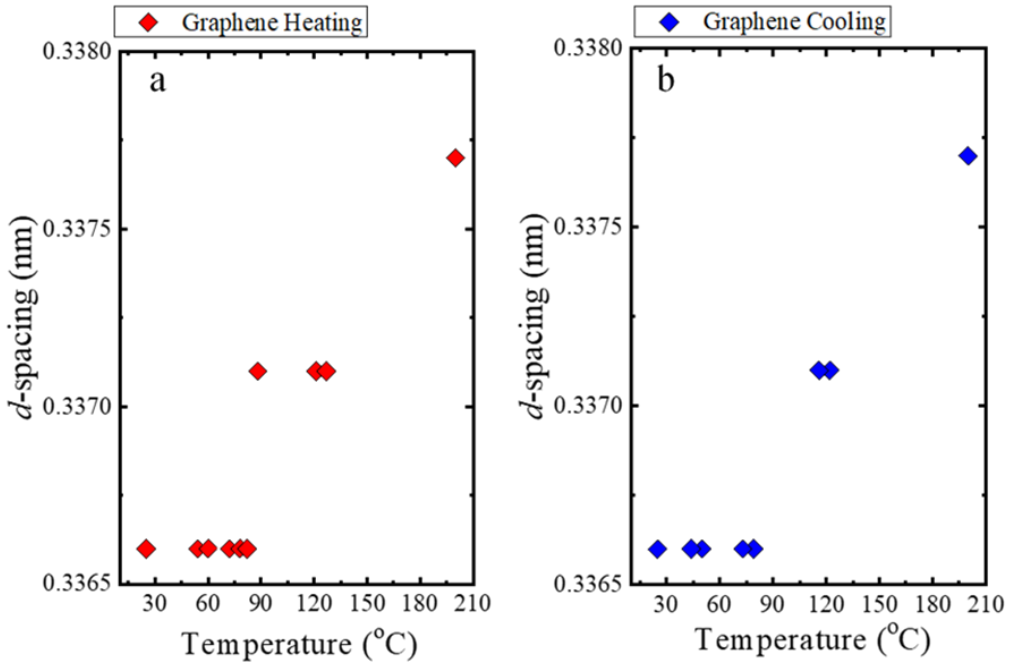


Figure 4.12 The d-spacing as a function of temperature calculated from shift of the q values upon heating.

In the case of the graphene, we have detected some shift of the q values upon heating (from 25 to 200 ºC) and upon cooling from the melt (from 200 C to 25 ºC). We have calculated the d-spacings and plotted as a function of the temperature, as shown in Figure 4.12. Jumps in *d*-spacing at around 88 ºC during the heating, and 121 ºC during the cooling, as well as a final jump from 127 to 200 ºC (heating) and 200 to 124 ºC (cooling) occurred, in both cases such jumps coincides with the endotherms or exothermic peaks detected by DSC. These jumps

might be related to the thermal expansion of the graphene, however further studies are needed in order to determine their origin.

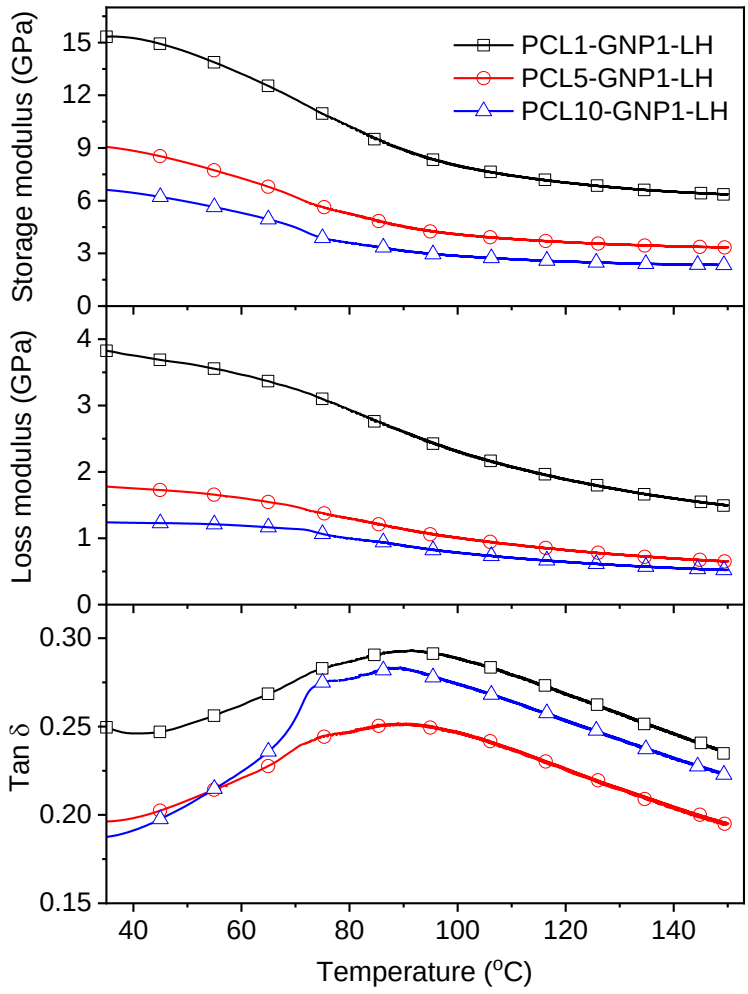


Figure 4.13 Temperature sweep DMTA measurement on selected nanopapers.

To investigate the thermomechanical properties of the nanopapers, temperature sweep measurements were performed on hot pressed nanopapers, namely PCL10-GNP1-LH, PCL5-GNP1-LH and PCL1-GNP1-LH by DMTA, results are shown in Figure 4.13. These nanopapers demonstrated a significant stiffness at room temperature, with a storage modulus ranging between approx. 7 and 15 GPa, higher stiffness corresponding to lower PCL content, as expected. Interestingly, storage and loss moduli decay vs temperature is relatively limited and remarkable stiffness are retained for temperature far above the melting of PCL. Indeed, the storage modulus at 150 ºC is about 2.3 and 6.4 GPa of PCL10-GNP1-LH and PCL1-

GNP1-LH, respectively, suggesting a very strong adhesion of GNP plates to PCL, even after the polymer melting. The α transition, taken as the maximum of tanδ, is observable at about 90 °C in all nanopapers, suggesting a remarkable confinement of PCL macromolecules in galleries between GNP flakes.

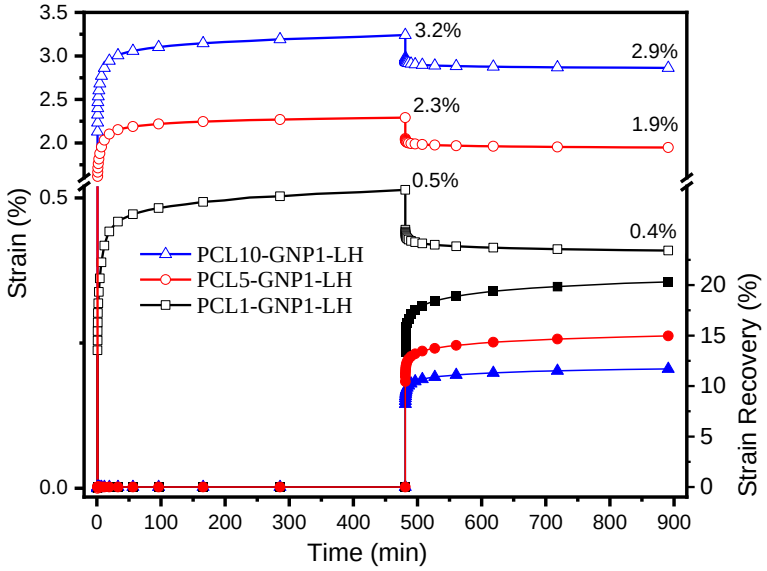


Figure 4.14 Strain (empty symbols) and Strain Recovery (solid symbols) plots from creep tests at 120 °C, 5 MPa stress on selected nanopapers.

The influence of PCL molecule chains on the load-bearing capability of GNPs was further investigated by creep tests. Creep test was carried out at 120 °C under 5 MPa stress, which is representative of operating conditions for low temperature heat exchanger, and result are reported in Figure 4.14. Upon application of the constant stress, PCL10-GNP1-LH nanopaper immediately deformed to a strain of ca. 2.5% for PCL10-GNP1-LH, followed by a further increase in strain, typical of phase I and II in creep tests, leading to strain of 3.2% after 8 hours creep at 120 °C. After the release of stress, the immediate strain recovery is around 9% of the strain after creep and the final value after 8 hours recovery is close to 12%. Expectedly, creep resistance is even higher for PCL5-GNP1-LH and PCL1-GNP1-LH, owing to the lower PCL content, leading to 2.3 and 0.5% deformation after 8 hours, respectively, which is partially recovered, leading to a final deformation of approx. 1.9 and 0.4%, respectively. These results evidence for outstanding creep resistance of GNP/PCL nanopapers, at temperature far above

the melting of PCL, further supporting for the polymer confinement and strong adhesion to GNP.

Envisaging application of these flexible PCL/GNP nanopapers as heat spreaders, thermal diffusivity (α) of the nanopapers was measured and reported in Table 4-5. Pristine GNP nanopapers has a thermal diffusivity in the range of 140 $mm^2/s$, which may be competitive with traditional metal foils[68, 69]. Diffusivity values for the GNP/PCL nanopapers was found in the range 110-140 $mm^2/s$, with a generally decreasing trend with increasing content of PCL, according with the inclusion of a poorly conductive polymer.[70]

Table 4-5 The calculated $C_p$ and in-plane thermal conductivity of all the nanopapers at 25°C.

| Sample | $\Phi_{PCL}$ (wt.%) | $C_p$ ($Jg^{-1}K^{-1}$) | Density ($gm^{-3}$) | α ($mm^2s^{-1}$) | K ($Wm^{-1}K^{-1}$) |
|---|---|---|---|---|---|
| Pristine GNP-SC | 0 | 0.71 | 1.00 | 150 ± 3 | 106.5 ± 2.1 |
| PCL10-GNP1-SC | 17 ± 3 | 0.93 | 0.58 | 116 ± 1 | 62.6 ± 0.5 |
| PCL10-GNP1-LH | 20 ± 3 | 0.97 | 1.31 | 138 ± 5 | 175.4 ± 6.7 |
| PCL5-GNP1-SC | 10 ± 1 | 0.84 | 0.64 | 130 ± 3 | 69.9 ± 1.6 |
| PCL5-GNP1-LH | 15 ± 3 | 0.90 | 1.39 | 127 ± 1 | 158.8 ± 1.3 |
| PCL1-GNP1-SC | 6.3 ± 0.5 | 0.79 | 0.96 | 138 ± 2 | 106.0 ± 1.5 |
| PCL1-GNP1-LH | 7.6 ± 1 | 0.81 | 1.41 | 146 ± 2 | 166.7 ± 2.3 |
| PCL1-GNP2-SC | 6.0 ± 0.6 | 0.79 | 1.06 | 145 ± 1 | 121.4 ± 0.8 |

While thermal diffusivity represent the efficiency of heat spreading onto a surface, the heat flux obtained in a heat exchanger, given a certain temperature gradient, is quantified by the thermal conductivity. Thermal conductivity values (Table 4-5) are strongly dependent on the nanopaper density, which lowest for the highly porous GNP nanopaper and increased in the presence of PCL, acting as a binder between GNP flakes. Furthermore, hot pressing allows to obtain a significantly higher density compared to cold pressed counterparts, yielding a straightforward enhancement in the thermal conductivity of nanopapers, up to around 166 $W(mK)^{-1}$ for PCL1-GNP1-LH. It is relevant to underline that, due to the existence of continuous

GNPs networks, the thermal conductivities of our nanopapers are much higher than that of reported for conventional GRM nanocomposites with very limited loading of the thermal conductive nanofillers.[71-74] Instead, nanopapers developed in this work target superior thermal conductivity properties coupled with high thermomechanical properties, which effectively bridge the property domains of polymeric materials and conductive ceramics. A comparison between our material and other highly filled nanostructured materials is reported in Table 4-6, further supporting both high thermal conductivity and stable thermomechanical properties of the obtained nanopapers.

Table 4-6 The TC values at room temperature for different flexible composite materials.

| Material | Nano-filler loading ca. | TC ($Wm^{-1}K^{-1}$) ca. | G'(GPa) ca. |
|---|---|---|---|
| **LCP/Graphite[75]** | 70 wt.% | 28.3 | 15 |
| **PVDF/AIN[76]** | 60 vol.% | 11.5 | 15 |
| **PBz/BN[77]** | 78 vol.% | 32.5 | 10 |
| **PPS/BN/CNT[78]** | 51 wt.% | 1.7 | - |
| **PDMS/VAGF[79]** | 92 wt.% | 614.8 | 0.5 |
| **CNFG[80]** | 50 wt. % | 164.7 | 2.6 |
| **NFC/GNs[81]** | 90 wt.% | 240.5 | 2.0 |
| **CNF/rGO[82]** | 50 wt.% | 7.3 | 7.5 |
| **NFC/BN[83]** | 50 wt.% | 145.7 | - |
| **NFC/GNP[84]** | 75 wt.% | 59.5 | 5.0 |
| **PI/h-BN[85]** | 60 wt.% | 7.0 | - |
| **PVA/BN[86]** | 50 vol.% | 30.0 | - |
| **PCL/GNP (in this work)** | **90 wt.%** | **166.0** | **15** |

*LCP, liquid crystal polymer; PVDF, polyvinylidene fluoride; AIN, aluminum nitride; PBz, polybenzoxazine; BN, boron nitride; PPS, polyphenylene sulfide; CNT, carbon nanotube; PDMS, polydimethylsiloxane; VAGF, vertically aligned graphene film; CNFG, flexible graphene/cellulose nanofiber; GNs, graphene nanosheets; NFC, nano-fibrillated cellulose; PI, polyimide; h-BN, hexagonal BN; PVA, poly(vinyl alcohol); "-", not reported.*

## 4.4 Conclusion

In this work, following the simple solution blending, sonication, filtration, drying and pressing procedures, the preparation of PCL/GNP nanopapers was carried out to combine thermal and mechanical properties of graphite nanoplates with a soft, tough and crystalline polymer, acting

as an efficient binder between nanoplates. Nanopaper characterization evidenced crystallization of PCL is dramatically affected when confined between GNP. Indeed, in addition of the main melting peak, corresponding to pristine PCL, higher temperature transitions were observed, possibly corresponding to higher stability crystals and order-disorder transitions in the organization of PCL chains between GNP. Superior thermal and thermomechanical properties were obtained for PCL/GNP nanopapers, in terms of high viscoelastic moduli, retained up to temperatures well above the melting point of PCL, as well as thermal conductivities above 160 $Wm^{-1}K^{-1}$, thus proving prepared materials to bridge the property domains of polymeric materials and conductive ceramics.

# References

1. Huang, W., *Nanopapers: From Nanochemistry and Nanomanufacturing to Advanced Applications*. 2017; p 1-255.

2. Barhoum, A.; Samyn, P.; Ohlund, T.; Dufresne, A., Review of recent research on flexible multifunctional nanopapers. *Nanoscale* **2017,** *9* (40), 15181-15205.

3. Benítez, A. J.; Walther, A., Cellulose nanofibril nanopapers and bioinspired nanocomposites: a review to understand the mechanical property space. *Journal of Materials Chemistry A* **2017,** *5* (31), 16003-16024.

4. Liu, A.; Walther, A.; Ikkala, O.; Belova, L.; Berglund, L. A., Clay Nanopaper with Tough Cellulose Nanofiber Matrix for Fire Retardancy and Gas Barrier Functions. *Biomacromolecules* **2011,** *12* (3), 633-641.

5. Ouyang, X.; Huang, W.; Cabrera, E.; Castro, J.; Lee, L. J., Graphene-graphene oxide-graphene hybrid nanopapers with superior mechanical, gas barrier and electrical properties. *AIP Advances* **2015,** *5* (1).

6. Carosio, F.; Kochumalayil, J.; Cuttica, F.; Camino, G.; Berglund, L., Oriented Clay Nanopaper from Biobased Components - Mechanisms for Superior Fire Protection Properties. *ACS Applied Materials and Interfaces* **2015,** *7* (10), 5847-5856.

7. Lagerwall, J. P. F.; Schütz, C.; Salajkova, M.; Noh, J.; Hyun Park, J.; Scalia, G.; Bergström, L., Cellulose nanocrystal-based materials: from liquid crystal self-assembly and glass formation to multifunctional thin films. *NPG Asia Materials* **2014,** *6* (1), e80-e80.

8. Yang, M.; Hou, Y.; Kotov, N. A., Graphene-based multilayers: Critical evaluation of materials assembly techniques. *Nano Today* **2012,** *7* (5), 430-447.

9. Tang, Z.; Kotov, N. A.; Magonov, S.; Ozturk, B., Nanostructured artificial nacre. *Nature Materials* **2003,** *2* (6), 413-418.

10. Yao, H.-B.; Tan, Z.-H.; Fang, H.-Y.; Yu, S.-H., Artificial Nacre-like Bionanocomposite Films from the Self-Assembly of Chitosan–Montmorillonite Hybrid Building Blocks. *Angewandte Chemie International Edition* **2010,** *49* (52), 10127-10131.

11. Zeng, X.; Ye, L.; Yu, S.; Li, H.; Sun, R.; Xu, J.; Wong, C.-P., Artificial nacre-like papers based on noncovalent functionalized boron nitride nanosheets with excellent mechanical and thermally conductive properties. *Nanoscale* **2015,** *7* (15), 6774-6781.

12. Fulvio, P. F.; Mayes, R. T.; Wang, X.; Mahurin, S. M.; Bauer, J. C.; Presser, V.; McDonough, J.; Gogotsi, Y.; Dai, S., "Brick-and-Mortar" Self-Assembly Approach to Graphitic Mesoporous Carbon Nanocomposites. *Advanced Functional Materials* **2011,** *21* (12), 2208-2215.

13. Huang, C.; Cheng, Q., Learning from nacre: Constructing polymer nanocomposites. *Composites Science and Technology* **2017,** *150*, 141-166.

14. Zhang, Y.; Gong, S.; Zhang, Q.; Ming, P.; Wan, S.; Peng, J.; Jiang, L.; Cheng, Q., Graphene-based artificial nacre nanocomposites. *Chemical Society Reviews* **2016,** *45* (9), 2378-2395.

15. Paliotta, L.; De Bellis, G.; Tamburrano, A.; Marra, F.; Rinaldi, A.; Balijepalli, S. K.; Kaciulis, S.; Sarto, M. S., Highly conductive multilayer-graphene paper as a flexible lightweight electromagnetic shield.

*Carbon* **2015,** *89*, 260-271.

16. Chen, H.; Müller, M. B.; Gilmore, K. J.; Wallace, G. G.; Li, D., Mechanically Strong, Electrically Conductive, and Biocompatible Graphene Paper. *Advanced Materials* **2008,** *20* (18), 3557-3561.

17. Huang, W.; Ouyang, X.; Lee, L. J., High-performance nanopapers based on benzenesulfonic functionalized graphenes. *ACS Nano* **2012,** *6* (11), 10178-85.

18. Xin, G.; Sun, H.; Hu, T.; Fard, H. R.; Sun, X.; Koratkar, N.; Borca-Tasciuc, T.; Lian, J., Large-area freestanding graphene paper for superior thermal management. *Adv Mater* **2014,** *26* (26), 4521-6.

19. Santagiuliana, G.; Picot, O. T.; Crespo, M.; Porwal, H.; Zhang, H.; Li, Y.; Rubini, L.; Colonna, S.; Fina, A.; Barbieri, E.; Spoelstra, A. B.; Mirabello, G.; Patterson, J. P.; Botto, L.; Pugno, N. M.; Peijs, T.; Bilotti, E., Breaking the Nanoparticle Loading–Dispersion Dichotomy in Polymer Nanocomposites with the Art of Croissant-Making. *ACS Nano* **2018,** *12* (9), 9040-9050.

20. Ramanathan, T.; Abdala, A. A.; Stankovich, S.; Dikin, D. A.; Herrera-Alonso, M.; Piner, R. D.; Adamson, D. H.; Schniepp, H. C.; Chen, X.; Ruoff, R. S.; Nguyen, S. T.; Aksay, I. A.; Prud'Homme, R. K.; Brinson, L. C., Functionalized graphene sheets for polymer nanocomposites. *Nat Nanotechnol* **2008,** *3* (6), 327-31.

21. Yang, H.; Li, F.; Shan, C.; Han, D.; Zhang, Q.; Niu, L.; Ivaska, A., Covalent functionalization of chemically converted graphene sheets via silane and its reinforcement. *Journal of Materials Chemistry* **2009,** *19* (26).

22. Hsiao, M. C.; Liao, S. H.; Yen, M. Y.; Liu, P. I.; Pu, N. W.; Wang, C. A.; Ma, C. C., Preparation of covalently functionalized graphene using residual oxygen-containing functional groups. *ACS Appl Mater Interfaces* **2010,** *2* (11), 3092-9.

23. Sun, Z.; Kohama, S.-i.; Zhang, Z.; Lomeda, J. R.; Tour, J. M., Soluble graphene through edge-selective functionalization. *Nano Research* **2010,** *3* (2), 117-125.

24. Backes, C.; Abdelkader, A. M.; Alonso, C.; Andrieux-Ledier, A.; Arenal, R.; Azpeitia, J.; Balakrishnan, N.; Banszerus, L.; Barjon, J.; Bartali, R.; Bellani, S.; Berger, C.; Berger, R.; Ortega, M. M. B.; Bernard, C.; Beton, P. H.; Beyer, A.; Bianco, A.; Bøggild, P.; Bonaccorso, F.; Barin, G. B.; Botas, C.; Bueno, R. A.; Carriazo, D.; Castellanos-Gomez, A.; Christian, M.; Ciesielski, A.; Ciuk, T.; Cole, M. T.; Coleman, J.; Coletti, C.; Crema, L.; Cun, H.; Dasler, D.; De Fazio, D.; Díez, N.; Drieschner, S.; Duesberg, G. S.; Fasel, R.; Feng, X.; Fina, A.; Forti, S.; Galiotis, C.; Garberoglio, G.; García, J. M.; Garrido, J. A.; Gibertini, M.; Gölzhäuser, A.; Gómez, J.; Greber, T.; Hauke, F.; Hemmi, A.; Hernandez-Rodriguez, I.; Hirsch, A.; Hodge, S. A.; Huttel, Y.; Jepsen, P. U.; Jimenez, I.; Kaiser, U.; Kaplas, T.; Kim, H.; Kis, A.; Papagelis, K.; Kostarelos, K.; Krajewska, A.; Lee, K.; Li, C.; Lipsanen, H.; Liscio, A.; Lohe, M. R.; Loiseau, A.; Lombardi, L.; Francisca López, M.; Martin, O.; Martín, C.; Martínez, L.; Martin-Gago, J. A.; Ignacio Martínez, J.; Marzari, N.; Mayoral, Á.; McManus, J.; Melucci, M.; Méndez, J.; Merino, C.; Merino, P.; Meyer, A. P.; Miniussi, E.; Miseikis, V.; Mishra, N.; Morandi, V.; Munuera, C.; Muñoz, R.; Nolan, H.; Ortolani, L.; Ott, A. K.; Palacio, I.; Palermo, V.; Parthenios, J.; Pasternak, I.; Patane, A.; Prato, M.; Prevost,

H.; Prudkovskiy, V.; Pugno, N.; Rojo, T.; Rossi, A.; Ruffieux, P.; Samorì, P.; Schué, L.; Setijadi, E.; Seyller, T.; Speranza, G.; Stampfer, C.; Stenger, I.; Strupinski, W.; Svirko, Y.; Taioli, S.; Teo, K. B. K.; Testi, M.; Tomarchio, F.; Tortello, M.; Treossi, E.; Turchanin, A.; Vazquez, E.; Villaro, E.; Whelan, P. R.; Xia, Z.; Yakimova, R.; Yang, S.; Yazdi, G. R.; Yim, C.; Yoon, D.; Zhang, X.; Zhuang, X.; Colombo, L.; Ferrari, A. C.; Garcia-Hernandez, M., Production and processing of graphene and related materials. *2D Materials* **2020,** *7* (2), 022001.

25. Korkut, S.; Roy-Mayhew, J. D.; Dabbs, D. M.; Milius, D. L.; Aksay, I. A., High surface area tapes produced with functionalized graphene. *ACS Nano* **2011,** *5* (6), 5214-22.

26. Lerf, A.; He, H.; Forster, M.; Klinowski, J., Structure of Graphite Oxide Revisited‖. *The Journal of Physical Chemistry B* **1998,** *102* (23), 4477-4482.

27. Chen, D.; Feng, H.; Li, J., Graphene oxide: preparation, functionalization, and electrochemical applications. *Chem Rev* **2012,** *112* (11), 6027-53.

28. Konkena, B.; Vasudevan, S., Understanding Aqueous Dispersibility of Graphene Oxide and Reduced Graphene Oxide through pKa Measurements. *J Phys Chem Lett* **2012,** *3* (7), 867-72.

29. Dai, J.; Wang, G.; Ma, L.; Wu, C., Study on the surface energies and dispersibility of graphene oxide and its derivatives. *Journal of Materials Science* **2015,** *50* (11), 3895-3907.

30. Rani, S.; Kumar, M.; Kumar, R.; Kumar, D.; Sharma, S.; Singh, G., Characterization and dispersibility of improved thermally stable amide functionalized graphene oxide. *Materials Research Bulletin* **2014,** *60*, 143-149.

31. Yan, J.-A.; Chou, M. Y., Oxidation functional groups on graphene: Structural and electronic properties. *Physical Review B* **2010,** *82* (12).

32. Islam, A. E.; Kim, S. S.; Rao, R.; Ngo, Y.; Jiang, J.; Nikolaev, P.; Naik, R.; Pachter, R.; Boeckl, J.; Maruyama, B., Photo-thermal oxidation of single layer graphene. *RSC Advances* **2016,** *6* (48), 42545-42553.

33. Liaros, N.; Tucek, J.; Dimos, K.; Bakandritsos, A.; Andrikopoulos, K. S.; Gournis, D.; Zboril, R.; Couris, S., The effect of the degree of oxidation on broadband nonlinear absorption and ferromagnetic ordering in graphene oxide. *Nanoscale* **2016,** *8* (5), 2908-17.

34. Gotterbarm, K.; Zhao, W.; Hofert, O.; Gleichweit, C.; Papp, C.; Steinruck, H. P., Growth and oxidation of graphene on Rh(111). *Phys Chem Chem Phys* **2013,** *15* (45), 19625-31.

35. Gomez, C. V.; Robalino, E.; Haro, D.; Tene, T.; Escudero, P.; Haro, A.; Orbe, J., Structural and Electronic Properties of Graphene Oxide for Different Degree of Oxidation1. *Materials Today: Proceedings* **2016,** *3* (3), 796-802.

36. Wu, H.; Drzal, L. T., Graphene nanoplatelet paper as a light-weight composite with excellent electrical and thermal conductivity and good gas barrier properties. *Carbon* **2012,** *50* (3), 1135-1145.

37. Xu, Y.; Kraemer, D.; Song, B.; Jiang, Z.; Zhou, J.; Loomis, J.; Wang, J.; Li, M.; Ghasemi, H.; Huang, X.; Li, X.; Chen, G., Nanostructured polymer films with metal-like thermal conductivity. *Nature Communications* **2019,** *10* (1), 1771.

38. Hansen, D.; Bernier, G. A., Thermal conductivity of polyethylene: The effects of crystal size, density and orientation on the thermal conductivity. *Polymer Engineering and Science* **1972,** *12* (3), 204-208.

39. Choy, C. L., Thermal conductivity of polymers. *Polymer* **1977,** *18* (10), 984-1004.

40. Bai, L.; Zhao, X.; Bao, R.-Y.; Liu, Z.-Y.; Yang, M.-B.; Yang, W., Effect of temperature, crystallinity and molecular chain orientation on the thermal conductivity of polymers: a case study of PLLA. *Journal of Materials Science* **2018,** *53* (14), 10543-10553.

41. Borhani zarandi, M.; Amrollahi Bioki, H.; Mirbagheri, Z. A.; Tabbakh, F.; Mirjalili, G., Effect of crystallinity and irradiation on thermal properties and specific heat capacity of LDPE & LDPE/EVA. *Appl Radiat Isot* **2012,** *70* (1), 1-5.

42. Huang, C.; Qian, X.; Yang, R., Thermal conductivity of polymers and polymer nanocomposites. *Materials Science and Engineering: R: Reports* **2018,** *132*, 1-22.

43. Yu, J.; Sundqvist, B.; Tonpheng, B.; Andersson, O., Thermal conductivity of highly crystallized polyethylene. *Polymer* **2014,** *55* (1), 195-200.

44. Noamani, S.; Niroomand, S.; Rastgar, M.; Sadrzadeh, M., Carbon-based polymer nanocomposite membranes for oily wastewater treatment. *npj Clean Water* **2019,** *2* (1).

45. Trujillo, M.; Arnal, M. L.; Müller, A. J.; Mujica, M. A.; Urbina de Navarro, C.; Ruelle, B.; Dubois, P., Supernucleation and crystallization regime change provoked by MWNT addition to poly(ε-caprolactone). *Polymer* **2012,** *53* (3), 832-841.

46. Wang, Y.; Li, Z.; Wang, J.; Li, J.; Lin, Y., Graphene and graphene oxide: biofunctionalization and applications in biotechnology. *Trends Biotechnol* **2011,** *29* (5), 205-12.

47. Jiang, H., Chemical preparation of graphene-based nanomaterials and their applications in chemical and biological sensors. *Small* **2011,** *7* (17), 2413-27.

48. Feng, L.; Liu, Z., Graphene in biomedicine: opportunities and challenges. *Nanomedicine (Lond)* **2011,** *6* (2), 317-24.

49. Moore, A. L.; Shi, L., Emerging challenges and materials for thermal management of electronics. *Materials Today* **2014,** *17* (4), 163-174.

50. Tang, Z.; Yao, D.; Du, D.; Ouyang, J., Highly machine-washable e-textiles with high strain sensitivity and high thermal conduction. *Journal of Materials Chemistry C* **2020,** *8* (8), 2741-2748.

51. Dharmasena, R. D. I. G.; Jayawardena, K. D. G. I.; Saadi, Z.; Yao, X.; Bandara, R. M. I.; Zhao, Y.; Silva, S. R. P., Energy Scavenging and Powering E-Skin Functional Devices. *Proceedings of the IEEE* **2019,** *107* (10), 2118-2136.

52. Colonna, S.; Bernal, M. M.; Gavoci, G.; Gomez, J.; Novara, C.; Saracco, G.; Fina, A., Effect of processing conditions on the thermal and electrical conductivity of poly (butylene terephthalate) nanocomposites prepared via ring-opening polymerization. *Materials & Design* **2017,** *119*, 124-132.

53. Picard, S.; Burns, D. T.; Roger, P., Determination of the specific heat capacity of a graphite sample using absolute and differential methods. *Metrologia* **2007,** *44* (5), 294-302.

54. Skoglund, P.; Fransson, k., Continuous cooling and isothermal crystallization of polycaprolactone. *Journal*

*of Applied Polymer Science* **1996,** *61* (13), 2455-2465.

55. Michell, R. M.; Blaszczyk-Lezak, I.; Mijangos, C.; Müller, A. J., Confinement effects on polymer crystallization: From droplets to alumina nanopores. *Polymer* **2013,** *54* (16), 4059-4077.

56. Martin, J.; Scaccabarozzi, A. D.; Nogales, A.; Li, R.; Smilgies, D.-M.; Stingelin, N., Confinement effects on the crystalline features of poly(9,9-dioctylfluorene). *European Polymer Journal* **2016,** *81*, 650-660.

57. Colonna, S.; Perez-Camargo, R. A.; Chen, H.; Liu, G.; Wang, D.; Muller, A. J.; Saracco, G.; Fina, A., Supernucleation and Orientation of Poly(butylene terephthalate) Crystals in Nanocomposites Containing Highly Reduced Graphene Oxide. *Macromolecules* **2017,** *50* (23), 9380-9393.

58. Wang, G.-s.; Wei, Z.-y.; Sang, L.; Chen, G.-y.; Zhang, W.-x.; Dong, X.-f.; Qi, M., Morphology, crystallization and mechanical properties of poly(ε-caprolactone)/graphene oxide nanocomposites. *Chinese Journal of Polymer Science* **2013,** *31* (8), 1148-1160.

59. Wang, B.; Li, Y.; Weng, G.; Jiang, Z.; Chen, P.; Wang, Z.; Gu, Q., Reduced graphene oxide enhances the crystallization and orientation of poly(ε-caprolactone). *Composites Science and Technology* **2014,** *96*, 63-70.

60. Tang, D.; Li, S.; Yang, J.; Su, J.; Yang, Q.; Kong, M.; Huang, Y.; Liao, X., Nonisothermal and isothermal crystallization behavior of isotactic polypropylene/chemically reduced graphene nanocomposites. *Polymer Composites* **2017,** *38*, E342-E350.

61. Ahmed, J.; Luciano, G.; Schizzi, I.; Arfat, Y. A.; Maggiore, S.; Arockia Thai, T. L., Non-isothermal crystallization behavior, rheological properties and morphology of poly(ε-caprolactone)/graphene oxide nanosheets composite films. *Thermochimica Acta* **2018,** *659*, 96-104.

62. Zhang, J.; Qiu, Z., Morphology, Crystallization Behavior, and Dynamic Mechanical Properties of Biodegradable Poly(ε-caprolactone)/Thermally Reduced Graphene Nanocomposites. *Industrial & Engineering Chemistry Research* **2011,** *50* (24), 13885-13891.

63. Wang, M.; Deng, X.-Y.; Du, A.-K.; Zhao, T.-H.; Zeng, J.-B., Poly(sodium 4-styrenesulfonate) modified graphene for reinforced biodegradable poly(ε-caprolactone) nanocomposites. *RSC Advances* **2015,** *5* (89), 73146-73154.

64. Kai, W.; Hirota, Y.; Hua, L.; Inoue, Y., Thermal and mechanical properties of a poly(ε-caprolactone)/graphite oxide composite. *Journal of Applied Polymer Science* **2008,** *107* (3), 1395-1400.

65. Avella, M.; Errico, M. E.; Laurienzo, P.; Martuscelli, E.; Raimo, M.; Rimedio, R., Preparation and characterisation of compatibilised polycaprolactone/starch composites. *Polymer* **2000,** *41* (10), 3875-3881.

66. Guo, Q.; Groeninckx, G., Crystallization kinetics of poly(ε-caprolactone) in miscible thermosetting polymer blends of epoxy resin and poly(ε-caprolactone). *Polymer* **2001,** *42* (21), 8647-8655.

67. Xu, G.; Du, L.; Wang, H.; Xia, R.; Meng, X.; Zhu, Q., Nonisothermal crystallization kinetics and thermomechanical properties of multiwalled carbon nanotube-reinforced poly(ε-caprolactone) composites. *Polymer International* **2008,** *57* (9), 1052-1066.

68. Gong, F.; Li, H.; Wang, W.; Xia, D.; Liu, Q.; Papavassiliou, D. V.; Xu, Z., Recent Advances in Graphene-Based Free-Standing Films for Thermal Management: Synthesis, Properties, and Applications.

*Coatings* **2018,** *8* (2).

69. Fina, G. F. M. B. F. C. C. N. M. T. S. R. F. G. A., Bispyrene functionalization drives self-assembly of graphite nanoplates into highly efficient heat spreader foils. **submitted**.

70. Nunes dos Santos, W.; Mummery, P.; Wallwork, A., Thermal diffusivity of polymers by the laser flash technique. *Polymer Testing* **2005,** *24* (5), 628-634.

71. Colonna, S.; Battegazzore, D.; Eleuteri, M.; Arrigo, R.; Fina, A., Properties of Graphene-Related Materials Controlling the Thermal Conductivity of Their Polymer Nanocomposites. *Nanomaterials (Basel)* **2020,** *10* (11).

72. Fang, H.; Bai, S.-L.; Wong, C. P., Microstructure engineering of graphene towards highly thermal conductive composites. *Composites Part A: Applied Science and Manufacturing* **2018,** *112*, 216-238.

73. Chen, H.; Ginzburg, V. V.; Yang, J.; Yang, Y.; Liu, W.; Huang, Y.; Du, L.; Chen, B., Thermal conductivity of polymer-based composites: Fundamentals and applications. *Progress in Polymer Science* **2016,** *59*, 41-85.

74. Burger, N.; Laachachi, A.; Ferriol, M.; Lutz, M.; Toniazzo, V.; Ruch, D., Review of thermal conductivity in composites: Mechanisms, parameters and theory. *Progress in Polymer Science* **2016,** *61*, 1-28.

75. Ha, S. M.; Lee, H. L.; Lee, S.-G.; Kim, B. G.; Kim, Y. S.; Won, J. C.; Choi, W. J.; Lee, D. C.; Kim, J.; Yoo, Y., Thermal conductivity of graphite filled liquid crystal polymer composites and theoretical predictions. *Composites Science and Technology* **2013,** *88*, 113-119.

76. Xu, Y.; Chung, D. D. L.; Mroz, C., Thermally conducting aluminum nitride polymer-matrix composites. *Composites Part A: Applied Science and Manufacturing* **2001,** *32* (12), 1749-1757.

77. Ishida, H.; Rimdusit, S., Very high thermal conductivity obtained by boron nitride-filled polybenzoxazine. *Thermochimica Acta* **1998,** *320* (1-2), 177-186.

78. Pak, S. Y.; Kim, H. M.; Kim, S. Y.; Youn, J. R., Synergistic improvement of thermal conductivity of thermoplastic composites with mixed boron nitride and multi-walled carbon nanotube fillers. *Carbon* **2012,** *50* (13), 4830-4838.

79. Zhang, Y.-F.; Han, D.; Zhao, Y.-H.; Bai, S.-L., High-performance thermal interface materials consisting of vertically aligned graphene film and polymer. *Carbon* **2016,** *109*, 552-557.

80. Chen, Y.; Hou, X.; Kang, R.; Liang, Y.; Guo, L.; Dai, W.; Nishimura, K.; Lin, C.-T.; Jiang, N.; Yu, J., Highly flexible biodegradable cellulose nanofiber/graphene heat-spreader films with improved mechanical properties and enhanced thermal conductivity. *Journal of Materials Chemistry C* **2018,** *6* (46), 12739-12745.

81. Yang, W.; Zhang, Y.; Liu, T.; Huang, R.; Chai, S.; Chen, F.; Fu, Q., Completely Green Approach for the Preparation of Strong and Highly Conductive Graphene Composite Film by Using Nanocellulose as Dispersing Agent and Mechanical Compression. *ACS Sustainable Chemistry & Engineering* **2017,** *5* (10), 9102-9113.

82. Yang, W.; Zhao, Z.; Wu, K.; Huang, R.; Liu, T.; Jiang, H.; Chen, F.; Fu, Q., Ultrathin flexible reduced graphene oxide/cellulose nanofiber composite films with strongly anisotropic thermal conductivity and

efficient electromagnetic interference shielding. *Journal of Materials Chemistry C* **2017,** *5* (15), 3748-3756.

83. Zhu, H.; Li, Y.; Fang, Z.; Xu, J.; Cao, F.; Wan, J.; Preston, C.; Yang, B.; Hu, L., Highly thermally conductive papers with percolative layered boron nitride nanosheets. *ACS Nano* **2014,** *8* (4), 3606-13.

84. Li, G.; Tian, X.; Xu, X.; Zhou, C.; Wu, J.; Li, Q.; Zhang, L.; Yang, F.; Li, Y., Fabrication of robust and highly thermally conductive nanofibrillated cellulose/graphite nanoplatelets composite papers. *Composites Science and Technology* **2017,** *138*, 179-185.

85. Sato, K.; Horibe, H.; Shirai, T.; Hotta, Y.; Nakano, H.; Nagai, H.; Mitsuishi, K.; Watari, K., Thermally conductive composite films of hexagonal boron nitride and polyimide with affinity-enhanced interfaces. *Journal of Materials Chemistry* **2010,** *20* (14).

86. Song, W.-L.; Wang, P.; Cao, L.; Anderson, A.; Meziani, M. J.; Farr, A. J.; Sun, Y.-P., Polymer/Boron Nitride Nanocomposite Materials for Superior Thermal Transport Performance. *Angewandte Chemie* **2012,** *124* (26), 6604-6607.

# 5 Conclusion

## 5.1 Conclusion

During the 3 years of my PhD study, I worked on different projects related to the development of novel formulations based on biopolymers. The achievements we have obtained are summarized as below:

1,Poly(L-lactide) (PLLA) films with improved resistance to the hydrolytic degradation were fabricated by the surface grafting of an amino-functionalized polyhedral oligomeric silsesquioxanes (POSS-$NH_2$) under mild conditions. The occurrence of the reaction between POSS-$NH_2$ and the PLLA chains on the surface of the films was verified by FT-IR and EDS measurements.

2, PLLA films with good oxygen barrier property, transparency and antistatic properties were developed. The proposed approach involves the Layer-by-Layer (LbL) deposition of functional coatings comprising either deposition of chitosan (CH) or branched polyethylenimine (BPEI) in combination with graphite oxide (GO). The reduction of the deposited GO layer on PLLA surface resulted in an antistatic surface of the films, making the prepared materials applicable in the antistatic packaging field.

3, Following a simple solution blending, sonication, filtration, drying and pressing procedure, composite nanopapers based on polycaprolactone (PCL) and graphite nanoplatelets (GNP) were fabricated. The resulted composite nanopapers were found to have a PCL content range of ca. 8 wt.% - 20 wt.%. The high GNP content resulted in a relatively high thermal conductivity of the composite nanopapers due to existence of the conductive GNP network. The confinement, as well as the adhesion effect of the polymer chains inside GNP galleries also endowed the nanopapers with good mechanical properties.

# Acknowledgement

Upon the completion of this thesis, I am grateful to those who have offered me encouragement and support during the three years of my PhD.

First, special acknowledgment is given to my respectable supervisor, Professor Orietta Monticelli, as well as my co-tutor, Professor Alberto Fina from Politecnico di Torino, their patient instruction and constructive suggestions have benefited me a lot.

Second, particular thanks to all the colleagues and professors in the department of chemistry and chemical industry, who have taught me and helped me for their instruction and generous support during these years. I also give my many thanks to the colleagues, teachers and professors in the lab of Alessandria, Federico Carosio, Samuele Colonna, Pepp Ferrar, Matteo Eleuteri, Lorenza Maddalena and so on, I really appreciate for their generous helps.

I also want to present my thanks to my friends in Genova, Wang Bao, Li Tao, Bai Xue, Fu Wei, Wang Yao, Qi Tianwen, Wei Wang and many other people, I am very grateful for their company during these years when I am far away from home.

Finally, I would like to express the most heartfelt gratitude to my families for their great support.

Last but not the least, the China Scholarship Council is gratefully acknowledged for the financial support during the three years of my PhD study.